UNIVERSIDADE FEDERAL DE SANTA MARIA
CENTRO DE TECNOLOGIA
PROGRAMA DE PÓS–GRADUAÇÃO EM ENGENHARIA QUÍMICA

Paola dos Reis de Souza

SOLUÇÃO NUMÉRICA DE MODELOS DE TRANSFERÊNCIA DE MASSA DIFUSIVOS EM SISTEMAS DE ADSORÇÃO

Santa Maria, RS
2017

Paola dos Reis de Souza

SOLUÇÃO NUMÉRICA DE MODELOS DE TRANSFERÊNCIA DE MASSA DIFUSIVOS EM SISTEMAS DE ADSORÇÃO

Dissertação apresentada ao Curso de Pós–Graduação em Engenharia Química, da Universidade Federal de Santa Maria (UFSM) como requisito parcial para obtenção do título de **Mestre em Engenharia Química.**

Orientadora: Profa. Dra. Nina Paula Gonçalves Salau
Co–orientador: Prof. Dr. Guilherme Luiz Dotto

Santa Maria, RS
2017

Ficha catalográfica elaborada através do Programa de Geração Automática
da Biblioteca Central da UFSM, com os dados fornecidos pelo(a) autor(a).

Souza, Paola dos Reis de
SOLUÇÃO NUMÉRICA DE MODELOS DE TRANSFERÊNCIA DE MASSA DIFUSIVOS EM SISTEMAS DE ADSORÇÃO / Paola dos Reis de Souza.- 2017.
113 p.; 30 cm

Orientadora: Nina Paula Gonçalves Salau
Coorientador: Guilherme Luiz Dotto
Dissertação (mestrado) - Universidade Federal de Santa Maria, Centro de Tecnologia, Programa de Pós-Graduação em Engenharia Química, RS, 2017

1. Modelo de transferência de massa difusional 2. Solução numérica 3. Estimação de parâmetros 4. Análise estatística 5. Adsorção I. Salau, Nina Paula Gonçalves II. Dotto, Guilherme Luiz III. Título.

Paola dos Reis de Souza

SOLUÇÃO NUMÉRICA DE MODELOS DE TRANSFERÊNCIA DE MASSA DIFUSIVOS EM SISTEMAS DE ADSORÇÃO

Dissertação apresentada ao Curso de Pós–Graduação em Engenharia Química, da Universidade Federal de Santa Maria (UFSM) como requisito parcial para obtenção do título de **Mestre em Engenharia Química.**

Aprovado em 17 de julho de 2017.

Nina Paula Gonçalves Salau, Dra. (UFSM)
Presidente (Orientadora)

Edson Luiz Foletto, Dr. (UFSM)

Luiz Antônio de Almeida Pinto, Dr. (FURG)

Santa Maria, RS
2017

AGRADECIMENTOS

À minha família que desde sempre incentivou a busca por conhecimento e me apoiou em todos os momentos;

Ao meu noivo por todo amor, amizade, compreensão e companheirismo;

À minha orientadora, Profa. Nina Paula Gonçalves Salau, pela orientação, pelos ensinamentos, pela confiança e pela oportunidade de trabalhar ao seu lado;

Ao meu co–orientador, Prof. Guilherme Luiz Dotto, pelos ensinamentos, incentivos e dedicação ao longo do desenvolvimento deste trabalho;

Aos professores membros da banca Prof. Edson Luiz Foletto e Prof. Luiz Antônio de Almeida Pinto, pela atenção, sugestões e colaboração para melhoria do texto e da análise do conteúdo do texto;

A todos os meus amigos e companheiros do laboratório, pela agradável convivência no laboratório, pela amizade e companheirismo, pelas sugestões e ajuda no desenvolvimento deste trabalho;

À CAPES pelo apoio financeiro;

À UFSM e ao PPGEQ pela estrutura física disponibilizada;

Agradeço a todos que de alguma maneira contribuíram e apoiaram para a conclusão desta dissertação.

RESUMO

SOLUÇÃO NUMÉRICA DE MODELOS DE TRANSFERÊNCIA DE MASSA DIFUSIVOS EM SISTEMAS DE ADSORÇÃO

AUTORA: Paola dos Reis de Souza
ORIENTADORA: Nina Paula Gonçalves Salau

O presente trabalho desenvolve detalhadamente a solução numérica de modelos de transferência de massa difusivos no processo de adsorção de corantes catiônicos. Os modelos difusivos são desenvolvidos com base nos fenômenos de transferência de massa em um sólido poroso: (i) transferência de massa externa, (ii) difusão intrapartícula e (iii) difusão nos sítios ativos. De modo que a difusão intrapartícula pode ocorrer por difusão do volume de poros (PVDM − *Pore Volume Diffusion Model*), difusão superficial (SDM – *Surface Diffusion Model*), ou uma combinação de ambos os mecanismos (PVSDM − *Pore Volume and Surface Diffusion Model*). O método numérico de aproximação por diferenças finitas foi empregado para a solução das equações diferenciais parciais oriundas do modelo. Para o ajuste do modelo aos dados experimentais, fez–se uso da técnica de estimação de parâmetros por mínimos quadrados não lineares. No primeiro artigo apresentado neste trabalho, os detalhes da solução numérica foram deduzidos e elucidados na modelagem do sistema de adsorção de verde malaquita em bentonita. Além disso, a caracterização da bentonita é abordada. Como resultado, a transferência de massa externa e a difusão intrapartícula atuaram simultaneamente na adsorção e o modelo PVSDM foi o mais capaz para explicar o fenômeno de adsorção. No segundo artigo, testes estatísticos foram realizados e se verificou que a média e a variância do modelo PVSDM correspondiam aos dados experimentais da adsorção de verde malaquita em bentonita. Por fim, o último artigo apresenta a modelagem e a análise estatística dos modelos difusionais para a adsorção de cristal violeta e de azul de metileno em bentonita. Como resultado, a difusão superficial foi o mecanismo controlador na adsorção de cristal violeta, sendo possível desprezar os efeitos da difusão no volume do poro. Em contrapartida, ambos os mecanismos intrapartícula são necessários para explicar o fenômeno de adsorção de azul de metileno em bentonita. Ademais os efeitos de difusão impedida foram significantes uma vez que o tamanho molecular do azul de metileno foi muito próximo ao espaço basal da bentonita. Portanto, os resultados apresentados nesta pesquisa mostraram que a técnica de aproximações por diferenças finitas aliada à técnica de estimação de parâmetros não linear é uma ferramenta adequada para a solução numérica dos modelos de transferência de massa difusivo em sistemas de adsorção.

Palavras–chave: Adsorção. Modelos difusivos. Solução numérica. Estimação de parâmetros. Análise estatística.

ABSTRACT

NUMERICAL SOLUTION OF DIFFUSION MASS TRANSFER MODELS IN ADSORPTION SYSTEMS

AUTHOR: Paola dos Reis de Souza
ADVISOR: Nina Paula Gonçalves Salau

The present work develops in detail the numerical solution of diffusion mass transfer models in the adsorption process of cationic dyes. The diffusive models are developed based on the mass transfer phenomena in a porous solid: (i) external mass transfer, (ii) intraparticle diffusion, and (iii) diffusion at the active sites. Thus, intraparticle diffusion can occur through pore volume diffusion (PVDM), surface diffusion model (SDM), or a combination of both (PVSDM – Pore Volume and Surface Diffusion Model). The numerical method of finite difference approximation was used to solve the partial differential equations derived from the model. The non–linear least squares estimation technique was used for fitting the model to the experimental data. In the first article introduced in this work, the details of the numerical solution were deduced and elucidated in the modeling of the malachite green onto bentonite adsorption system. In addition, the characterization of bentonite is addressed. As a result, the external mass transfer and the intraparticle diffusion act simultaneously in the adsorption and the PVSDM model were more able to explain the adsorption phenomenon. In the second article, statistical tests were performed and it was verified that the mean and the variance of the PVSDM model corresponded to the experimental data of the adsorption of malachite green onto bentonite. Finally, the last article presents the modeling and statistical analysis of the diffusion models for the adsorption of crystal violet and methylene blue onto bentonite. As a result, surface diffusion was the controlling mechanism in the adsorption of crystal violet, it being possible to neglect the effects of diffusion in the pore volume. In contrast, both intraparticle mechanisms are necessary to explain the phenomenon of adsorption of methylene blue onto bentonite. Further,the hindered diffusion effects were significant since the molecular size of the methylene blue was very close to the basal space of the bentonite. Therefore, the results presented in this research showed that the finite difference approximation technique within the nonlinear parameter estimation techique is a suited tool for numerical solution of the mass transfer diffusion models.

Keywords: Adsorption. Diffusion models. Numerical solution. Parameter estimation. Statistical analysis.

LISTA DE FIGURAS

CAPÍTULO 2

Figura 1 – Estrutura química dos corantes (a) verde malaquita, (b) cristal violeta e (c) azul de metileno. 20
Figura 2 – Classificação das isotermas de adsorção. 24
Figura 3 – Mecanismo de transferência de massa em um poro. **Erro! Indicador não definido.**
Figura 4 – Malha unidimensional. 32

CAPÍTULO 3

Fig. 1: FT−IR spectrum of bentonite. 44
Fig. 2: XRD of bentonite. 45
Fig. 3: SEM images of bentonite. 46
Fig. 4: EDS of bentonite. 46
Fig. 5: Redlich−Peterson isotherm of MG adsorption on bentonite at 298 K. 47
Fig. 6: Discretization of the transport of the dye molecules from the solution to the spherical particle (illustrative representation). 49
Fig. 7: Experimental dye concentration decay data and dye concentration decay curve predicted by the PVSDM with an initial dye concentration of (a) 500 mg L^{-1} and (b) 300 mg L^{-1}. 54
Fig. 8: Mass of MG adsorbed on each radial position over time to 500 mg L^{-1}. 55
Fig. 9: (a) Contribution of pore volume diffusion and (b) surface diffusion to the intraparticle diffusion at different radial positions to 500 mg L^{-1}. 56
Fig. 10: Experimental dye concentration decay data and dye concentration decay curve predicted by the PVSDM, PVDM and SDM with an initial dye concentration of (a) 500 mg L^{-1} and (b) 300 mg L^{-1}. 58

CAPÍTULO 4

Fig. 1: Experimental concentration decay data and concentration decay curve predicted by the PVSDM at initial concentration of 250 mg L^{-1}. 73

CAPÍTULO 5

Fig. 1: Redlich–Peterson isotherm for CV and MB adsorption onto bentonite. 85
Fig. 2: Fit of PVSDM, SDM and PVDM models for the adsorption decay curves of CV onto bentonite. 86
Fig. 3: (a) Contribution of pore volume diffusion and (b) surface diffusion to the intraparticle diffusion at different radial positions for CV dye.....89
Fig. 4: Fit of PVSDM, SDM and PVDM models for the adsorption decay curves of MB onto bentonite. 91
Fig. 5: Fit of PVSDM, SDM and PVDM models for the adsorption decay curves of MB onto bentonite. 92
Fig. 6: (a) Contribution of pore volume diffusion and (b) surface diffusion to the intraparticle diffusion at different radial positions for MB dye. 95
Fig. 7: Illustration of the adsorption process of (a) CV onto bentonite and (b) MB onto bentonite. 96
Fig. 8: Effect of the mass of bentonite adsorbed at equilibrium on D_s to (a) CV and (b) MB. 98

LISTA DE TABELAS

CAPÍTULO 2

Tabela 1 – Características do corante verde malaquita. 20
Tabela 2 – Características do corante cristal violeta. 21
Tabela 3 – Características do corante azul de metileno..... 22
Tabela 4 – Rotinas de mínimos-quadrados disponíveis pelo software MatLab®. 34

CAPÍTULO 3

Table 1: Experimental conditions and estimated parameters for MG concentration decay curves during adsorption on bentonite. 53

CAPÍTULO 4

Table 1: Mass transfer parameters for the adsorption of MG on bentonite at different initial dye concentrations. 70
Table 2: Estimated parameter with intervals of 95% of confidence for the adsorption of MG on bentonite. 71
Table 3: Student's *t* test for concentration of MG in aqueous solution (μ is the mean of C_A). 72
Table 4: χ^2 test for concentration of MG in aqueous solution (σ^2 is the variance of C_A) 72
Table 5: Fischer's exact test for concentration of MG in aqueous solution (Lower limit < $\sigma^2_{exp} / \sigma^2_{mod}$ < upper limit). 72

CAPÍTULO 5

Table 1: Physicochemical properties of CV and MB dyes. 83
Table 2: Constants of the Redlich–Peterson isotherm for CV and MB adsorption onto bentonite. 85
Table 3: Statistical analysis of PVSDM, SDM and PVDM models for adsorption of CV on bentonite. 87

Table 4: Experimental conditions and estimated parameters for the concentration decay curves of CV on bentonite, C_{A0} = 100 mg L^{-1}. 90
Table 5: Statistical analysis of PVSDM, SDM and PVDM models for adsorption of MB on bentonite. 93
Table 6: Experimental conditions and estimated parameters for the concentration decay curves of MB on bentonite, C_{A0} = 100 mg L^{-1} 95

LISTA DE SÍMBOLOS

ARE	Erro relativo médio, %
a_{RP}	Coeficiente de afinidade, $L^{\beta}\ mg^{-\beta}$
Bi	Número de Biot, adimensional
C_A	Concentração de adsorbato na solução aquosa, $mg\ L^{-1}$
C_{A0}	Concentração inicial de adsorbato na solução aquosa, $mg\ L^{-1}$
C_{Ar}	Concentração de adsorbato dentro da partícula à distância r, $mg\ L^{-1}$
$C_{Ar}\|_{r=0}$	Concentração de adsorbato no centro da partícula, $mg\ L^{-1}$
$C_{Ar}\|_{r=R}$	Concentração de adsorbato na superfície externa da partícula, $mg\ L^{-1}$
C_e	Concentração de adsorbato no equilíbrio, $mg\ L^{-1}$
D_{AB}	Coeficiente de difusão molecular em diluição infinita, $cm^2\ s^{-1}$
d_B	Diâmetro médio da bentonita, μm
DF	Graus de liberdade, adimensional
D_{int}	Coeficiente de difusão intrapartícula, $cm^2\ s^{-1}$
d_p	Diâmetro médio do poro, nm
D_p	Coeficiente efetivo de difusão no volume do poro, $cm^2\ s^{-1}$
D_s	Coeficiente de difusão superficial, $cm^2\ s^{-1}$
FO_{NLS}	Função objetivo de mínimos quadrados não-lineares, adimensional
h	Tamanho do passo, cm
K	Parâmetro de difusão impedida, adimensional
k_1	Constante de velocidade de pseudoprimeira ordem, min^{-1}
k_2	Constante de velocidade de pseudossegunda ordem, $g\ min^{-1}\ mg^{-1}$
k_F	Coeficiente de transferência de massa externa, $cm\ s^{-1}$
k_f	Constante de Freundlich, $((L\ mg^{-1})\ (L\ mg^{-1})^{-1/\beta})$
k_L	Constante de Langmuir, $L\ mg^{-1}$
k_{RP}	Constante de Redlich−Peterson, $L\ g^{-1}$
LL	Limite inferior, adimensional
LU	Limite superior, adimensional
m	Massa de adsorvente, g
M_B	Massa molar da água, $g\ mol^{-1}$
N	Número de pontos internos, adimensional
N_A	Fluxo mássico do soluto, $mg\ cm\ s^{-1}\ L^{-1}$
N_{AP}	Fluxo mássico do soluto no volume do poro, $mg\ cm\ s^{-1}\ L^{-1}$
N_{AS}	Fluxo mássico do soluto na superfície do poro, $mg\ cm\ s^{-1}\ L^{-1}$

NE	Número de experimentos, adimensional
NP	Número de parâmetros, adimensional
NY	Número de medições em cada experimento, adimensional
q	Capacidade de adsorção, mg g^{-1}
q_e	Capacidade de adsorção no equilíbrio, mg g^{-1}
q_t	Capacidade de adsorção no instante t, mg g^{-1}
q_m	Capacidade máxima de adsorção, mg g^{-1}
R	Raio da bentonita, μm
R^2	Coeficiente de determinação, adimensional
S	Superfície externa por massa de adsorvente, $cm^2\ g^{-1}$
S_{BET}	Superfície específica da bentonita, $m^2\ g^{-1}$
s_x	Variância amostral, adimensional
t	Tempo, min
T	Temperatura, K
V	Volume de solução, cm^3
V_A	Volume molar do ponto de bolha do corante, $cm^3\ mol^{-1}$
V_p	Volume de poro do adsorvente, $cm^3\ g^{-1}$
$\overline{X}$	Média amostral, adimensional
y_{exp}	Valor do dado experimental, adimensional
y_{mod}	Valor previsto pelo modelo, adimensional
α	Valor do parâmetro estimado, adimensional
β	Parâmetro de heterogeneidade, adimensional
ε_p	Porosidade do adsorvente, adimensional
η_B	Viscosidade da água, Cp
ρ_p	Densidade aparente do adsorvente, $g\ cm^{-3}$
ρ_s	Densidade sólida do adsorvente, $g\ cm^{-3}$
τ	Tortuosidade do adsorvente, adimensional
μ_x	Média da distribuição, adimensional
σ_x^2	Variância da distribuição, adimensional
Φ	Parâmetro de associação de água, adimensional
$\lambda_{máx}$	Comprimento de onda máximo, nm

SUMÁRIO

1 INTRODUÇÃO 15
1.1 OBJETIVOS 16
1.1.1 Objetivo geral 16
1.1.2 Objetivos específicos 16
1.2 ESTRUTURA DA DISSERTAÇÃO 16
2 REVISÃO BIBLIOGRÁFICA 19
2.1 CORANTES 19
2.1.1 Verde malaquita 20
2.1.2 Cristal violeta 21
2.1.3 Azul de metileno 21
2.1.4 Efluentes industriais 22
2.2 ADSORÇÃO 23
2.2.1 Materiais adsorventes 23
2.2.1.1 Bentonita 24
2.2.2 Isotermas de adsorção 24
2.2.3 Cinética de adsorção 26
2.2.3.1 Modelos de reação 26
2.2.3.2 Modelos difusivos 27
2.3 SOLUÇÃO NUMÉRICA DOS MODELOS DIFUSIVOS 31
2.3.1 Aproximação por diferenças finitas 31
2.3.2 Estimação de parâmetros 33
2.3.3 Análise Estatística 34
2.3.3.1 Teste t-Student 35
2.3.3.2 Teste Chi-Quadrado (χ^2) 36
2.3.3.3 Teste exato de Fischer 36
3 DETAILED NUMERICAL SOLUTION OF PORE VOLUME AND SURFACE DIFFUSION MODEL IN ADSORPTION SYSTEMS 38
1. Introduction 38
2. Mathematical model 40
3. Materials and methods 41
3.1. Adsorbate 41
3.2. Preparation and characterization of adsorbent 41
3.3. Batch adsorption experiments 42
4. Results and discussion 43
4.1. Bentonite clay characteristics 43
4.2. Adsorption isotherm 47
4.3. Numerical solution of the model 48
4.4. Estimation of mass transport parameters 51
4.5. Pore volume and surface diffusion model (PVSDM) 53
4.6. Surface diffusion model (SDM) and pore volume diffusion model (PVDM) 57
5. Conclusion 59
Acknowledgement 59
References 59
4 STATISTICAL EVALUATION OF PORE VOLUME AND SURFACE DIFFUSION MODEL IN ADSORPTION SYSTEMS 65
1. Introduction 65
2. Mathematical model 66

3. Experimental **67**
4. Model solution **68**
5. Results and discussion **69**
5.1. Concentration decay study *69*
5.2. Parameter estimation *71*
5.3. Model validation *72*
6. Conclusion **73**
Acknowledgement **74**
References **74**
5 MODELING OF HINDERED DIFFUSION OF CATIONIC DYES ADSORPTION ONTO BENTONITE **78**
1. Introduction **78**
2. Mathematical model **79**
2.1. Model development *79*
2.2. Model solution *80*
2.3. Estimation of the mass transfer parameters *81*
3. Materials and methods **82**
3.1. Adsorbent *82*
3.2. Cationic dyes *82*
3.3. Batch adsorption experiments *83*
4. Results and discussion **84**
4.1. Adsorption isotherm *84*
4.2. Case study 1: Adsorption of CV onto bentonite *86*
4.3. Case study 2: Adsorption of MB onto bentonite *90*
4.4. Comparison between CV and MB dyes *96*
5. Conclusion **99**
Acknowledgement **100**
References **100**
6 DISCUSSÃO **104**
7 CONCLUSÃO **106**
REFERÊNCIAS BIBLIOGRÁFICAS **108**
ANEXO A – APROXIMAÇÃO DE PRIMEIRA ORDEM POR DIFERENÇAS FINITAS **112**
ANEXO B – APROXIMAÇÃO DE SEGUNDA ORDEM POR DIFERENÇAS FINITAS **113**

1 INTRODUÇÃO

A poluição do meio ambiente devido ao crescimento da atividade industrial tem aumentado gradativamente nas últimas décadas, tornando-se um problema social e ambiental. Um dos maiores problemas ambientais enfrentados é a contaminação dos recursos hídricos causados pelo despejo inadequado de efluentes industriais, os quais contém uma vasta gama de contaminantes tóxicos. Dentre esses contaminantes, destacam-se os corantes sintéticos.

Os corantes sintéticos são utilizados nos mais diversos tipos de aplicações, dentre as quais podem ser citadas a coloração e o tingimento de materiais têxteis, couros, papéis, plásticos, produtos alimentares e cosméticos (BULUT et al., 2008). Estima-se a existência de mais de 10 mil diferentes corantes e pigmentos e a quantidade de corantes sintéticos produzida anualmente no mundo é cerca de 700 mil toneladas, das quais, entre 10 e 60% são perdidos nos processos de fabricação (JAURIS et al., 2016). A presença destes corantes no meio ambiente, mesmo que em pequenas quantidades, altera a cor da água, reduz a solubilidade do oxigênio, interfere no metabolismo fotossintético de plantas aquáticas e pode causar sérios riscos à saúde humana, devido a sua toxidade, efeitos carcinogênicos e mutagênicos (LIN e LEE, 2016). A fim de evitar problemas ecológicos e toxicológicos, faz-se necessário o tratamento de efluentes industriais antes do descarte.

Os métodos mais utilizados para a remoção de corantes presentes em efluentes são a sedimentação, a filtração, a oxidação, a coagulação/floculação, a coagulação eletroquímica, o tratamento biológico e a adsorção. A adsorção é uma operação unitária bastante empregada devido a sua simplicidade de operação e elevada eficiência (EL QADA et al., 2008).

A adsorção é uma operação de separação através da qual, certos componentes de uma fase fluida (adsorbato) são atraídos para a superfície de um sólido adsorvente. Devido à afinidade entre as fases, o adsorbato é atraído e ligado ao adsorvente por mecanismos físicos ou químicos, removendo, assim, o componente da fase fluída (EL QADA et al., 2008). A cinética de adsorção é de grande importância para avaliar o desempenho de um determinado adsorvente e na determinação dos mecanismos envolvidos no processo (QIU et al., 2009). O modelo de transferência de massa difusivo proposto por Leyva-Ramos e Geankoplis (1985) é a maneira mais realista de representar a cinética de adsorção, uma vez que seus pressupostos são baseados nas Leis de Fick. Entretanto, esses modelos são demasiadamente complexos e a sua solução envolve a resolução simultânea de diferentes variáveis.

O emprego de métodos numéricos se apresenta como uma ferramenta adequada para resolver os modelos de transferência de massa difusivos. Deste modo, o desenvolvimento de uma solução numérica detalhada permite o melhor entendimento das etapas de solução do modelo, possibilitando a previsão do comportamento cinético, a influência dos mecanismos de transferência de massa e a estimação dos parâmetros dos modelos difusivos.

1.1 OBJETIVOS

1.1.1 Objetivo geral

Resolver numericamente um modelo de alta-fidelidade para aumentar a capacidade de predição de modelos de transferência de massa difusivos em sistemas de adsorção.

1.1.2 Objetivos específicos

- Empregar técnicas numéricas para solução de modelos de transferência de massa difusivos;
- Desenvolver um algoritmo para a simulação dos modelos;
- Selecionar sistemas de adsorção (adsorvente/adsorbato) que justifiquem o estudo das difusões na superfície e nos poros;
- Caracterizar o material adsorvente;
- Realizar ensaios de adsorção para obtenção de dados experimentais;
- Estimar os parâmetros de transferência de massa dos sistemas de adsorção;
- Realizar análise estatística dos parâmetros estimados;
- Validar os modelos de difusão.

1.2 ESTRUTURA DA DISSERTAÇÃO

A presente dissertação está dividida em 6 capítulos, com os resultados mostrados em formato de artigos (publicados ou submetidos para publicação).

Capítulo 1 – INTRODUÇÃO

O capítulo de Introdução contextualiza o foco de pesquisa deste trabalho, abordando, brevemente, a importância da remoção de corantes sintéticos dos efluentes, as vantagens da adsorção frente a outras operações separação e a avaliação cinética a partir da utilização de modelos de transferência de massa difusivos.

Capítulo 2 – REVISÃO BILIOGRÁFICA

Este capítulo busca mostrar as principais referências utilizadas para os temas abordados na pesquisa, com uma revisão sobre a adsorção de corantes sintéticos com bentonita. O conteúdo também aborda a justificativa do uso de métodos numéricos para a solução dos modelos de transferência de massa difusivos em sistemas de adsorção.

Capítulo 3 – DETAILED NUMERICAL SOLUTION OF PORE VOLUME AND SURFACE DIFFUSION MODEL IN ADSORPTION SYSTEMS

O terceiro capítulo apresenta o desenvolvimento detalhado da solução numérica dos modelos de difusão a partir do método numérico de aproximação por diferenças finitas. Como estudo de caso, foi selecionado o sistema de adsorção de verde malaquita em bentonita. Para isso, foram realizados ensaios de adsorção em diferentes concentrações iniciais de corante e a caracterização necessária do adsorvente. Com os dados de entrada, foi possível simular e estimar os parâmetros difusionais a partir do método dos mínimos quadrados não lineares.

Artigo publicado no periódico *Chemical Engineering Research and Design*.

Capítulo 4 – STATISTICAL EVALUATION OF PORE VOLUME AND SURFACE DIFFUSION MODEL IN ADSORPTION SYSTEMS

Em sequência ao trabalho anterior, o quarto capítulo apresenta a estimação de um parâmetro global a partir do uso de método derivativo. Ademais, foram realizados os testes estatísticos: t-Student, χ^2 e Fisher e a determinação dos intervalos de confiança do parâmetro.

A validação do modelo foi realizada a partir dos dados experimentais obtidos anteriormente para a elaboração do artigo do capítulo 3.

Short Communication submetido ao periódico *Journal of Environmental Chemical Engineering.*

Capítulo 5 – MODELING OF HINDERED DIFFUSION OF CATIONIC DYES ADSORPTION ONTO BENTONITE

No quinto capítulo foram selecionados como estudo de caso, a adsorção de cristal violeta e azul de metileno em bentonita, em diferentes quantidades de adsorvente. Os parâmetros dos modelos difusivos foram estimados e avaliados por testes estatísticos. Além disso, foi estudado o efeito da difusão impedida devido à obstrução das moléculas de corante nas paredes do poro, associado ao corante azul de metileno.

Artigo submetido ao periódico *Microporous and Mesoporous Materials.*

Capítulo 6 – DISCUSSÃO

Este capítulo busca fazer uma breve discussão a respeito dos três capítulos anteriores, relacionando-os de forma a salientar os resultados encontrados para cada sistema de adsorção estudado durante o trabalho de dissertação.

Capítulo 7 – CONCLUSÃO

O capítulo final apresenta as principais conclusões da pesquisa, uma vez que as conclusões específicas foram apresentadas em cada um dos capítulos, contendo também sugestões para futuros trabalhos nesta área.

2 REVISÃO BIBLIOGRÁFICA

Para uma melhor interpretação do contexto abordado nesta dissertação, apresentam-se fundamentos teóricos dos aspectos gerais do processo de adsorção, destacando-se a aplicação de modelos de transferência de massa difusivos para análise cinética. Além disso, são abordadas técnicas para solução numérica de equações diferenciais parciais, as quais são usadas para representar os modelos de difusão em sistemas de adsorção.

2.1 CORANTES

Corantes são substâncias orgânicas coloridas ou fluorescentes, podendo ser naturais, artificiais ou sintéticos e têm a propriedade de alterar a cor de diferentes materiais.

Civilizações antigas já tinham o costume de retirar substâncias da natureza para colorir e tingir seus alimentos, tecidos, couro e papel. Porém, o emprego de corantes sintéticos iniciou em 1856 quando Willian Henry Perkin sintetizou o primeiro corante (Mauve). Desde então, diversos corantes foram desenvolvidos. Atualmente, estima-se que existam mais de dez mil tipos de corantes no mercado (JAURIS et al., 2016).

Em relação a sua aplicabilidade, corantes sintéticos são amplamente utilizados para colorir os produtos de diversas indústrias, tais como têxteis, couro, cosméticos, papel, materiais de impressão, plásticos e alimentos (YANG et al., 2016).

Corantes podem ser classificados quanto a sua aplicação (ácidos, básicos, dispersos, diretos, reativos e solventes), solubilidade (solúveis e insolúveis), classe química (trifenilmetanos, azóicos, antraquinonas, nitro, xantenos e outras) e estrutura química (aniônicos, catiônicos e não iônicos) (GUPTA e SUHAS, 2009).

Os corantes catiônicos (ou básicos) são derivados de bases orgânicas. Estes corantes apresentam uma carga positiva na sua molécula, na forma de sais de amônio, sulfônico ou oxônio, que pode estar fixa ou deslocalizada. A porção carregada positivamente da molécula do corante em solução pode facilmente interagir com superfícies de membrana de células carregadas negativamente (BAYRAMOGLU et al, 2009). Dentre os corantes catiônicos podemos destacar o verde malaquita, o cristal violeta e o azul de metileno, cujas estruturas químicas são apresentadas na Figura 1.

Figura 1 – Estrutura química dos corantes (a) verde malaquita, (b) cristal violeta e (c) azul de metileno.

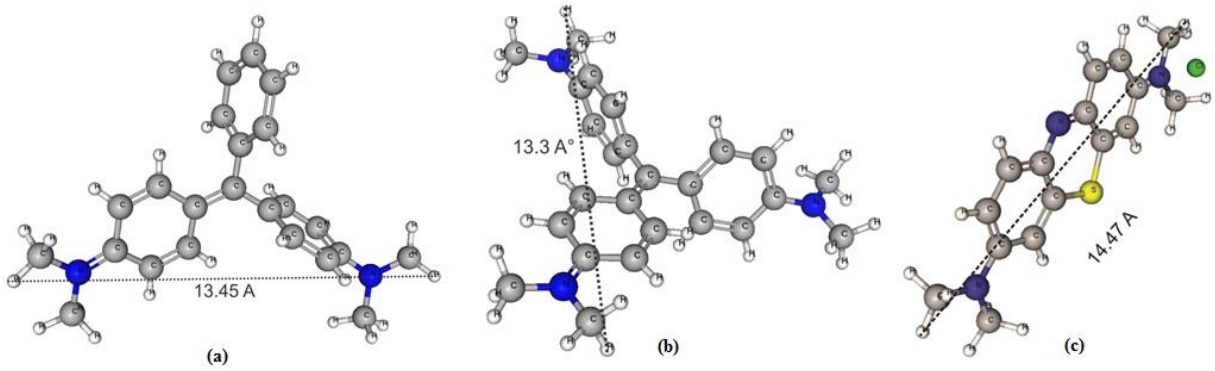

Fonte: Elaborado pelo autor.

2.1.1 Verde malaquita

O verde malaquita (MG, do inglês *Malachite Green*) é um corante catiônico pertencente à família dos trifenilmetanos, cujas características são apresentadas na Tabela 1.

Tabela 1 – Características do corante verde malaquita.

Característica	**Verde malaquita**
Nome IUPAC	4–[(4–dimetilaminofenil) –fenil–metil]–N, N–dimetil–anilina
Número no Colour Index	42.000
Fórmula molecular	$C_{23}H_{25}N_2Cl$
Massa molar	364,9 g mol^{-1}
Absorbância, $\lambda_{máx}$	618 nm

Fonte: Adaptado de BANERJEE et al, 2016 e GHASEMI et al, 2015.

O MG é bastante utilizado na indústria têxtil, no tingimento de algodão, lã, seda e couro. É também utilizado no tratamento de infecções fúngicas em ovos de peixe (aquicultura) e como agente fungicida, parasiticida e antisséptico. Entretanto, tem sido relatado que sua exposição pode causar carcinogênese, mutagênese, fraturas cromossômicas e toxicidade respiratória em alguns mamíferos. No caso dos peixes, causa efeitos prejudiciais no fígado, brânquias, rins, intestino e células gonadotrópicas pituitárias. Em humanos, pode irritar o trato respiratório ao ser inalado, causar irritação no trato gastrointestinal depois de ingerido, causar irritação,

vermelhidão, dor em contato com a pele e em contato com os olhos pode causar lesões permanentes (SRIVASTAVA et al., 2004; BULLUT et al., 2008; GHASEMI et al., 2016).

2.1.2 Cristal violeta

Outro corante catiônico é o cristal violeta (CV, do inglês *Crystal Violet*) pertencente à família dos triarilmetanos, cujas características são expostas na Tabela 2.

Tabela 2 – Características do corante cristal violeta.

Característica	**Cristal violeta**
Nome IUPAC	N–[4–[bis– (4–dimetilamino) –fenil–metileno]–2,5–ciclohexadieno –1–ilidino]–N–cloreto metilmetanamina
Número no Colour Index	42.555
Fórmula molecular	$C_{25}H_{30}N_3Cl$
Massa molar	407,98 g mol^{-1}
Absorbância, $\lambda_{máx}$	590 nm

Fonte: Adaptado de GÜZEL et al, 2014 e MITTAL et al, 2010.

O CV é um corante sintético usado para conferir cor nas indústrias de papel, têxtil e de tintas de impressão. Além disso, é utilizado na medicina como agente bactericida e antisséptico, e na veterinária como aditivo à ração de aves de capoeira para inibir a propagação de mofo, parasitas intestinais e fungos (GÜZEL et al., 2014; SABNA et al., 2015). Contudo, esse corante é altamente tóxico e carcinogênico em mamíferos. A exposição prolongada a esse corante pode causar irritação na pele e no trato digestivo, e em casos extremos, pode levar à cegueira permanente e à insuficiência renal e respiratória (FERREIRA et al., 2015; SABNA et al., 2015).

2.1.3 Azul de metileno

O corante catiônico mais comum é o azul de metileno (MB, do inglês *Methylene Blue*) pertencente à classe das fenotiazinas, cujas características são apresentadas na Tabela 3.

Tabela 3 – Características do corante azul de metileno.

Característica	**Azul de metileno**
Nome IUPAC	3,7–Bis (dimetilamino) –5–cloreto fenazatiônico
Número no Colour Index	52.015
Fórmula molecular	$C_{16}H_{18}N_3SCl$
Massa molar	319,85 g mol^{-1}
Absorbância, $\lambda_{máx}$	663 nm

Fonte: Adaptado de DARDOURI e SGHIER, 2017.

Devido as suas propriedades fotoquímicas, o MB vem sendo aplicado na inativação de bactérias e vírus, em células foto-galvânicas e no preparo de eletrodos quimicamente modificados (BORTOLUZZI, 2015). Também é antiséptico contra infecção bacteriana e é usado como antídoto para intoxicação por cianeto. Além disso, é usado na indústria para conferir cor em papel, lã, algodão e seda (DARDOURI e SGHIER, 2017). Além de causar efeitos toxicológicos em organismos aquáticos e na qualidade da água, o MB causa efeitos adversos à saúde humana, como anemia, irritação na bexiga e problemas gastrointestinais (BHATTACHARJEE et al., 2016).

2.1.4 Efluentes industriais

De acordo com Jauris et al. (2016) são produzidos anualmente 700 mil toneladas de corantes sendo que entre 10 a 60% desse total são perdidos no processo fabril, gerando uma enorme quantidade de efluentes indústrias.

Além do efeito visual, os efluentes contendo corantes são caracterizados por altos índices de alcalinidade, elevada demanda química de oxigênio e toxidade (SRINIVASAN e VIRARAGHAVAN, 2010). Ademais, os corantes são moléculas recalcitrantes (resistentes à biodegradação), o que dificulta a penetração dos raios solares e a reoxigenação das águas, prejudicando a atividade biológica dos organismos aquáticos (GUPTA e SUHAS, 2009).

A legislação aplicável no Brasil para o controle da qualidade dos efluentes lançados no meio ambiente é determinada pela Resolução 357/2005 do Conselho Nacional do Meio Ambiente (CONAMA), o qual dispõe que a quantidade de corante contida no efluente não pode alterar a cor da água do corpo hídrico receptor.

A fim de exercer o que está previsto na legislação, vários métodos foram desenvolvidos visando à remoção dos corantes dos efluentes industriais. Dentre eles, estão processos oxidativos avançados, biodegradação, degradação química, eletrofloculação, osmose reversa, precipitação e adsorção. A adsorção se destaca devido ao seu baixo custo, simplicidade de operação, elevadas taxas de remoção e possibilidade de recuperação do adsorvente (EL QADA et al., 2008).

2.2 ADSORÇÃO

A adsorção é um fenômeno de transporte que envolve a transferência de massa entre uma superfície de contato envolvendo um sólido e um fluído. Esse processo é dependente da temperatura, da natureza e da concentração da substância adsorvida (adsorbato), e da natureza e do estado de agregação do adsorvente (GHASEMI et al., 2016). Dependendo do sistema (adsorvente/adsorbato), a adsorção pode ser classificada como física ou química.

A adsorção física é caracterizada pela fraca interação entre as moléculas adsorvidas e a superfície do adsorvente. Essa energia é insuficiente para romper as ligações moleculares, tornando o processo reversível. Ao contrário, a adsorção química é um processo irreversível que envolve fortes interações moleculares. Existem dois tipos de adsorção química: a ativada, na qual a taxa de adsorção varia com a temperatura, com uma energia de ativação própria (equação de Arrhenius); e a não ativada, que ocorre rapidamente e a energia de ativação é praticamente nula (MACCABE et al., 1985.).

2.2.1 Materiais adsorventes

Os adsorventes são substâncias naturais ou sintéticas, geralmente com estrutura monocristalina, os quais são capazes de remover contaminantes de uma fase fluída. Desse modo, um bom adsorvente deve apresentar seletividade, resistência mecânica, baixo custo, resistência química, alta densidade e elevada área superficial. O adsorvente mais utilizado comercialmente é o carvão ativado, devido a sua alta área superficial. Entretanto, possui alto custo de ativação e regeneração (DEMIRBAS, 2009).

Nesse contexto, as argilas minerais se destacam devido a sua abundância na natureza e baixo custo. Geralmente são compostas por silício e oxigênio, os quais se ligam a outros

elementos tais como Al^{3+}, Fe^{3+} e Mg^{2+} (YAN et al., 2015). Ademais, possuem propriedades físicas atrativas ao processo de adsorção, tais como elevada área específica e porosidade.

2.2.1.1 Bentonita

A bentonita é uma argila mineral formada, basicamente por montmorilonita, que consiste em uma camada de alumina octaédrica entre duas camadas de sílica tetraédrica. A bentonita possui uma carga negativa permanente, causada pela substituição isomorfa de Al^{3+} por Si^{4+} na camada tetraédrica e da substituição de Mg^{2+} para Al^{3+} na camada octaédrica. A carga negativa é equilibrada pela presença de cátions permutáveis na estrutura cristalina, o que garante o seu bom desempenho em adsorver contaminantes catiônicos pela troca catiônica (YAN et al., 2015; ANIRUFHAN e RAMACHANDRAN, 2015).

Além da elevada capacidade de troca catiônica, a argila bentonita apresenta uma elevada área superficial e porosidade, as quais favorecem o processo de adsorção (MAKHOUKHI, 2015).

2.2.2 Isotermas de adsorção

A eficiência do adsorvente pode ser avaliada a partir dos dados de equilíbrio, ou seja, das isotermas de adsorção. As isotermas de adsorção expressam a relação entre a quantidade de corante adsorvido por unidade de massa de adsorvente e a concentração do corante na fase fluída, em condições fixas de temperatura e pH (BLÁZQUEZ et al., 2010).

A IUPAC (União Internacional de Química Pura e Aplicada) classifica em cinco tipos as isotermas de adsorção (Figura 2).

Figura 2 – Classificação das isotermas de adsorção.

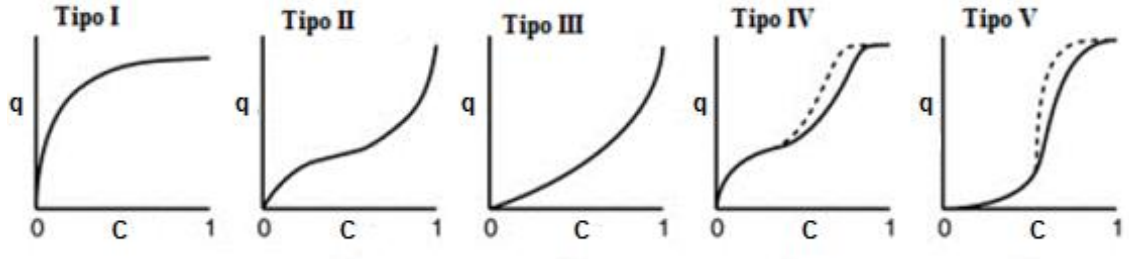

Fonte: DONOHUE e ARANOVICH, 1998.

As isotermas do tipo I apresentam um platô convexo, o qual está associado à formação de uma camada monomolecular em adsorventes não porosos ou microporosos (< 20 Å). Os tipos II e III descrevem a adsorção em multicamadas geralmente em adsorventes macroporosos (> 500 Å). Isotermas do tipo IV são relativas à adsorção em multicamadas via condensação em mesoporos (entre 20 e 500 Å). As curvas do tipo V descrevem comportamento similar ao tipo IV, considerando interações fortes e/ou fracas entre o adsorvente e o adsorbato (BLÁZQUEZ et al., 2010).

Para quantificar a capacidade de adsorção do adsorvente para corantes, várias relações podem ser adotadas, tais como Langmuir, Freundlich, Sips, Redlich–Peterson, Temkin, Dubinin– Radushkevich e BET (EL QADA et al., 2008; CRINI e BADOT, 2008; DOTTO, et al., 2011).

O modelo proposto por Langmuir (1918) assume que os sítios de ligações são distribuídos homogeneamente na superfície do adsorvente e que a adsorção ocorre em um sistema monocamada. A representação matemática do modelo é descrita pela Equação 1.

$$q_e = \frac{q_m k_L C_e}{1 + k_L C_e} \tag{1}$$

onde, q_e é a capacidade de adsorção no equilíbrio (mg g^{-1}), C_e é a concentração de adsorbato remanescente na fase fluída no equilíbrio (mg L^{-1}), q_m é a máxima capacidade de adsorção (mg g^{-1}) e k_L a constante de Langmuir (L mg^{-1}).

Freundlich (1906) propôs um modelo matemático (Equação 2) para sistemas heterogêneos, no qual a heterogeneidade é representada pelo fator β.

$$q_e = k_f C_e^{\beta} \tag{2}$$

onde k_f é a constante de Freundlich ((L mg^{-1}) (L $mg^{-1})^{-1/\beta}$) e β é o parâmetro de heterogeneidade.

A isoterma proposta por Redlich e Peterson (1959) é uma combinação entre os sistemas de Langmuir e Freundlich. Esse modelo é composto por três parâmetros e incorpora as vantagens de ambos os modelos, conforme a Equação 3.

$$q_e = \frac{k_{RP} C_e}{1 + a_{RP} C_e^{\beta}} \quad (3)$$

onde k_{RP} é a constante de Redlich–Peterson (L g^{-1}), a_{RP} é o coeficiente de afinidade (L^{β} $mg^{-\beta}$) e β é o parâmetro de heterogeneidade.

2.2.3 Cinética de adsorção

O estudo da cinética de adsorção determina a eficiência do processo, fornece informações sobre a velocidade de adsorção e sobre os fatores que influenciam a taxa de adsorção. Além disso, fornece informações sobre as interações que ocorrem na interface adsorbato/adsorvente (CRINI e BADOT, 2008).

Os modelos cinéticos mais utilizados podem ser divididos em: modelos de reação e modelos de difusão (QIU et al., 2009).

2.2.3.1 Modelos de reação

Os modelos de reação são baseados na cinética de reações químicas (QIU et al., 2009) e são muito utilizados para representar os dados de adsorção (GÜZEL et al., 2013; BANERJEE et al., 2015; PAVAN et al., 2014; DOTTO et al., 2015). Os modelos de reação usuais são o modelo de pseudoprimeira ordem e o modelo de pseudossegunda ordem.

O modelo cinético de pseudoprimeira ordem foi desenvolvido por Lagergrem (1898). Este modelo assume que a adsorção ocorre como consequência do gradiente de concentração entre a superfície do adsorvente e a fase fluída, podendo ser expresso de acordo com a Equação 4 (QIU et al., 2009).

$$q_t = q_e (1 - e^{-k_1 t}) \quad (4)$$

onde q_t é a quantidade de adsorbato retido no instante t (mg g^{-1}), q_e é a quantidade de adsorbato retido no equilíbrio (mg g^{-1}) e k_1 é a constante de velocidade de pseudoprimeira ordem (min^{-1}).

O modelo cinético de pseudossegunda ordem (Equação 5) acopla na mesma equação os mecanismos de transferência de massa interno e externo e, geralmente, é adequado em processos de adsorção química (HO & MCKAY, 1998).

$$q_t = \frac{k_2 q_e^2 t}{1 + k_2 q_e t} \tag{5}$$

onde k_2 é a constante de velocidade de pseudossegunda ordem (g min^{-1} mg^{-1}).

Apesar de que os modelos de reação fornecem resultados razoáveis, eles são incapazes de determinar os parâmetros de transferência de massa e identificar a etapa limitante da velocidade de adsorção.

2.2.3.2 Modelos difusivos

Os modelos difusivos são a maneira mais realista de interpretar a cinética de adsorção, já que nestes modelos são considerados os fenômenos de transferência de massa em um sólido poroso. Deste modo, a cinética pode ser regida por: a) Transferência de moléculas da fase fluida para a superfície externa da partícula do adsorvente através de uma camada de fluido de contorno que se encontra nos arredores da partícula (transferência de massa externa); b) Difusão de moléculas do fluído contido nos poros (difusão efetiva no poro); c) Difusão de moléculas totalmente adsorvidas ao longo da superfície dos poros (difusão de superfície) e d) interação com os sítios ativos.

Uma forma adequada de descrever o transporte de massa é considerar o fenômeno como um processo difusivo, descrito pelas Leis de Fick. A Figura 2 mostra os diferentes mecanismos envolvidos no fenômeno de adsorção em batelada em um poro, de um soluto a partir de uma solução líquida de concentração C_A.

Figura 3 - Mecanismo de transferência de massa em um poro.

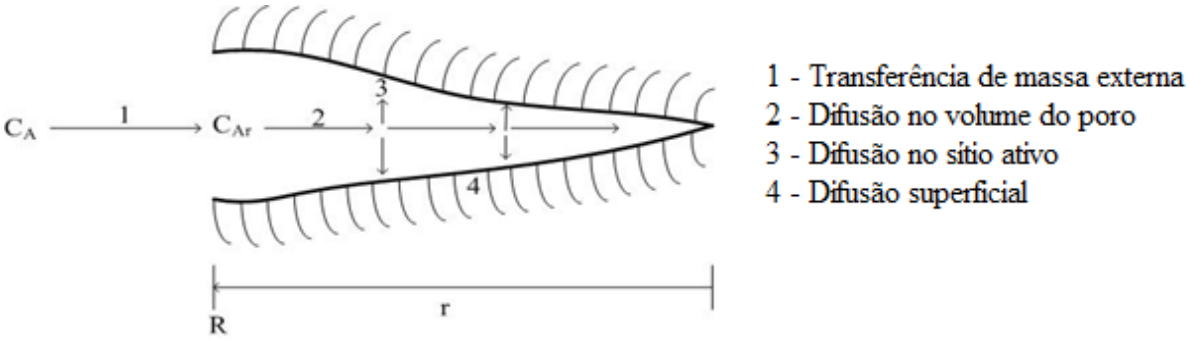

Fonte: Adaptado de LEYVA–RAMOS E GEANKOPLIS, 1985.

Na primeira etapa, o soluto é transportado de uma solução de concentração $C_{A,}$ para a abertura dos poros com concentração $C_{Ar|r=R}$, esse fenômeno ocorre através da transferência de massa convectiva, e pode ser expresso pela Lei de Fick (LEYVA–RAMOS E GEANKOPLIS, 1985).

$$N_A = k_F\left(C_A - C_{Ar}\big|_{r=R}\right) \tag{6}$$

onde k_F é o coeficiente convectivo de transferência de massa e N_A é o fluxo molar do soluto, sendo esse baseado na área externa total da partícula.

Na etapa dois, ocorre a difusão molecular no volume do poro (difusão no volume do poro), sendo descrito por:

$$N_{AP} = -\left(\frac{\varepsilon D_{AB}}{\tau}\right)\frac{\partial C_{AR}}{\partial r} = -D_p\frac{\partial C_{AR}}{\partial r} \tag{7}$$

onde N_{AP} é o fluxo molar do soluto no poro da partícula, ε é a porosidade da partícula, D_{AB} é o coeficiente de difusão, τ é o fator de tortuosidade, D_p é a difusividade efetiva do poro e C_{Ar} é a concentração do soluto dentro da partícula a uma distância r.

Na etapa três o soluto é adsorvido na superfície do poro e se assume que a concentração C_A do líquido no poro está em equilíbrio com a quantidade adsorvida q. Para correlacionar essas variáveis, faz-se o uso das isotermas de adsorção.

A etapa 4 apresenta a difusão do soluto na superfície do poro (difusão de superfície). Esse fenômeno ocorre paralelamente a etapa 2 e pode ser expressa por:

$$N_{AS} = -D_s \rho_p \frac{\partial q}{\partial r} \tag{8}$$

onde, N_{AS} é o fluxo molar do soluto na superfície do poro, ρ_p é a massa específica da partícula e D_s é a difusividade efetiva na superfície.

A partir dos conceitos dos fluxos molares, é possível determinar os balanços de massa do processo. De acordo com Suzuki, (1990), quando a transferência de massa é externa, a concentração na partícula é uniforme e o mecanismo pode ser representado pela Equação 9:

$$V \frac{dC_A}{dt} = -mSk_F \left(C_A - C_{Ar}\big|_{r=R} \right) \tag{9}$$

A Equação 9 apresenta o balanço de massa na solução de corante a qual está sujeita a condição inicial:

$$t = 0, \quad C_A = C_{A0} \tag{10}$$

No interior da partícula foi considerado que as partículas do adsorvente são esféricas; que o transporte de massa por convecção no interior dos poros é insignificante; que a difusão intrapartícula ocorre pela combinação da difusão superficial e da difusão no volume dos poros; que os valores do coeficiente de difusão efetiva no poro (D_p) e que o coeficiente de difusão superficial (D_s) são constantes e a adsorção nos sítios ativos é instantânea.

$$\varepsilon_p \frac{\partial C_{Ar}}{\partial t} + \rho_p \frac{\partial q}{\partial t} = \frac{1}{r^2} \frac{\partial}{\partial r} \left[r^2 \left(D_p \frac{\partial C_{Ar}}{\partial r} + \rho_p D_s \frac{\partial q}{\partial r} \right) \right] \tag{11}$$

A Equação 11 representa o balanço de massa dentro da partícula do adsorvente. De tal modo que, o primeiro termo do lado esquerdo da igualdade é o acúmulo de corante no volume do poro do adsorvente e o segundo termo é o acúmulo devido à adsorção de corante na superfície do adsorvente. Os termos do lado direito da igualdade são os fluxos relativos à difusão no volume do poro e à difusão na superfície do adsorvente, respectivamente. A Equação 11 fica sujeita à condição inicial:

$$C_{Ar} = 0, \quad t = 0, \quad 0 \le r \le R \tag{12}$$

Pela hipótese de que a partícula é perfeitamente esférica, consideramos que existe simetria no centro da partícula. Desse modo, a condição de contorno em *r = 0* é:

$$\left.\frac{\partial C_{Ar}}{\partial r}\right|_{r=0} = 0 \tag{13}$$

Enquanto que no limite de *r = R*, o fluxo de transferência de massa convectivo deve ser igual ao fluxo de transferência de massa da difusão intrapartícula:

$$D_p \left.\frac{\partial C_{Ar}}{\partial r}\right|_{r=R} + \rho_p D_s \left.\frac{\partial q}{\partial r}\right|_{r=R} = k_F \left(C_A - C_{Ar}\big|_{r=R}\right) \tag{14}$$

O modelo representado pelas Equações 9–14 foi proposto por Leyva–Ramos e Geankoplis (1985) e chamado de modelo de difusão na superfície e no volume do poro (PVSDM, do inglês *Pore Volume and Surface Diffusion Model*). Entretanto, esse modelo pode ser simplificado, considerando que o único mecanismo de difusão intrapartícula é a difusão no volume do poro (PVDM, do inglês *Pore Volume Diffusion Model*), no qual $Dp \neq 0$, $Ds = 0$. Ainda, pode ser simplificado considerando exclusivamente o mecanismo de difusão superficial (SDM, do inglês *Surface Diffusion Model*), no qual $Dp = 0$, e $Ds \neq 0$ (OCAMPO– PEREZ et al., 2010). Também, faz–se necessário o uso das isotermas de adsorção para relacionar a concentração de adsorbato na solução dos poros (*CAr*) e a massa de adsorbato retida na superfície dos poros (*q*).

Durante a adsorção, um processo difusivo pode ser muito mais lento que outros e, neste caso, ele determina a taxa de adsorção (RUTHVEN, 1984). Desta forma, é possível verificar a influência de cada mecanismo no processo de adsorção através do número de Biot como mostrado na Equação 15 (COONEY, 1993):

$$Bi = \frac{k_F d_B C_{A0}}{2\rho_P D_{\text{int}} q_e} \tag{15}$$

Conforme Cooney (1993), o processo é controlado pela transferência de massa externa para Bi < 0,5, enquanto que para valores de Bi> 10 existe uma dominância considerável da difusão intrapartícula.

2.3 SOLUÇÃO NUMÉRICA DOS MODELOS DIFUSIVOS

Na Engenharia Química frequentemente encontramos problemas que envolvem equações diferenciais. Equações diferenciais são equações que compreendem uma relação entre uma função desconhecida e uma ou mais de suas derivadas. Se a equação inclui apenas a derivada relativa a uma variável independente ela é chamada de Equação Diferencial Ordinária (ODE, do inglês *Ordinary Differential Equations*); se existem mais derivadas relativas a outras variáveis independentes, esta é chamada de Equação Diferencial Parcial (PDE, do inglês *Partial Differential Equations*) (DAVIS, 1984).

As Equações 9–14 constituem um problema completo de PDE. A solução desse problema é uma função que define a variável dependente como uma função da variável independente. A solução analítica compreende uma função matemática real e exata, porém são empregadas somente em PDEs mais simples, em casos mais complexos são geralmente difíceis de derivar matematicamente.

Em geral, os problemas que envolvem equações diferenciais complexas necessitam de uma variedade de ferramentas para obtenção aproximada da solução. Os principais métodos numéricos utilizados para a resolução dessas equações são: método das diferenças finitas, método dos elementos finitos, método dos elementos de contorno e método dos volumes finitos. Desse modo, não existe um método geral para solucionar numericamente PDEs, mas diferentes métodos e técnicas que podem ser aplicados para resolver equações de determinada forma ou sob algumas suposições sobre os elementos envolvidos (GRASEGGER et al., 2016).

2.3.1 Aproximação por diferenças finitas

O método de aproximações de diferenças finitas consiste em transformar uma PDE em um conjunto de ODEs de primeira ordem usando as relações de diferenças finitas para todas as derivadas espaciais (x) para, então, resolver o conjunto de ODEs ao longo do tempo (t) (SCHIESSER, 1991).

A primeira etapa para a resolução do método numérico é discretizar a região onde se procura a solução. Para a discretização, define–se uma malha, que é um conjunto finito de pontos pertencentes ao domínio, chamados nós da malha (MELO, 2011 *apud* FERREIRA e LIMA, 2010).

Figura 4 – Malha unidimensional.

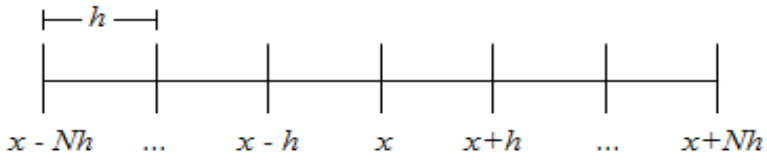

Fonte: Elaborado pelo autor.

A ferramenta básica no cálculo das aproximações das derivadas é a série de Taylor. O valor da função *f* a uma distância *h* de um ponto *x* qualquer pode ser estimado através da expansão desta série, conforme a seguir.

$$f(x+h) = f(x) + \frac{df(x)}{dx}h + \frac{1}{2}\frac{df^2(x)}{dx^2}h^2 + Oh^3 \tag{16}$$

O termo Oh^3 significa que a série continua indefinidamente, porém a soma dos termos é proporcional a h^3. Truncando a série no termo de ordem 2, tem-se:

$$\frac{df(x)}{dx} = \frac{f(x+h) - f(x)}{h} \tag{17}$$

Reescrevendo para a *i–nésima* parte de um conjunto de *N* elementos:

$$\frac{df(x_i)}{dx} = \frac{f(x_{i+1}) - f(x_i)}{h} \tag{18}$$

A Equação 18 é chamada de diferença progressiva para derivada de 1ª ordem. De forma análoga, as demais diferenças são obtidas a partir da série de Taylor. Os Anexos A e B

sumarizam as aproximações de diferenças finitas de primeira e segunda ordem, respectivamente.

2.3.2 Estimação de parâmetros

Na modelagem matemática, para a representação de um processo ou fenômeno qualquer, surgem variáveis que não podem ser medidas experimentalmente como, por exemplo, o coeficiente de difusão superficial (D_s). O valor destas variáveis pode ser determinado a partir de um conjunto de dados disponíveis através de um procedimento chamado de estimação de parâmetros. A estimação dos parâmetros consiste em ajustar os valores dos parâmetros de tal forma que as previsões do modelo sejam as mais próximas possíveis dos valores medidos experimentalmente (SCHWAAB e PINTO, 2007).

De acordo com Schwaab (2007), o procedimento de estimação de parâmetros pode ser dividido em três etapas: a escolha da função objetivo, a minimização da função objetivo através de métodos de otimização e a análise estatística dos resultados.

A função objetivo mede a distância entre os dados reais e do modelo. Uma função objetivo muito comum de ser minimizada em problemas de otimização é a função dos mínimos quadrados (LS, do inglês *Least Squares*). Contudo, métodos de solução do problema para ajuste de curvas que possuem modelos matemáticos não lineares são encontrados a partir da utilização da função dos mínimos quadrados não lineares (NLS, do inglês *Nonlinear Least Squares*):

$$FO_{NLS} = \sum \left(y_{\exp} - y_{\mathrm{mod}} \right)^2 \tag{19}$$

onde FO_{NLS} é a função objetivo de mínimos quadrados não lineares, y_{exp} os valores medidos experimentalmente e y_{mod} os valores preditos pelo modelo.

O ajuste de funções não lineares pelo método dos mínimos quadrados é feito através do processo iterativo para determinar o valor mínimo da função objetivo. Isso pode ser feito usando diferentes tipos de métodos de otimização para estimar os parâmetros do modelo, estes métodos podem ser determinísticos (derivativos ou de busca direta) ou heurísticos.

Os métodos derivativos são aqueles que utilizam derivadas para a minimização da função objetivo. O método mais simples é o método do gradiente que utiliza somente as derivadas de primeira ordem (vetor gradiente da função objetivo). Outro método derivativo muito comum é o método de Newton, o qual utiliza além do vetor gradiente, a matriz Hessiana

da função objetivo (derivadas de segunda ordem) (SCHWAAB, 2007). O método de Levenberg–Marquardt foi proposto como uma melhoria ao Método de Newton.

Os métodos de busca direta não utilizam as derivadas da função objetivo e a direção de busca é determinada a partir dos valores da função objetivo. Desse modo, a principal vantagem desse método é o fato de não utilizarem as derivadas da função objetivo, tornando as iterações deste método mais rápidas. Alguns exemplos de métodos de busca direta são os métodos de Hooke e Jeeves, Rosenbrock, Powell e Simplex (EDGAR e HIMMELBLAU, 1989).

Os métodos heurísticos são baseados em princípios evolutivos e inspirados em fenômenos da natureza. São empregados em problemas que envolvem um número grande de parâmetros ou a alta correlação entre os parâmetros e a natureza multimodal da função objetivo. Dentre os métodos heurísticos, destacam-se os métodos de Busca Aleatória, Algoritmo Genérico e o Enxame de Partículas (SCHWAAB, 2007).

A implementação dos métodos de otimização envolvem processos iterativos demasiadamente complexos e lentos, para isso se faz necessário a implementação junto a *softwares*. O software MatLab® possui rotinas de otimização próprias para cada tipo de problema de estimação de parâmetro. A Tabela 4 sumariza as funções disponíveis pelo software MatLab® para o ajuste por mínimos-quadrados.

Tabela 4 – Rotinas de mínimos-quadrados disponíveis pelo software MatLab®.

Função	Descrição
lsqlin	Resolve problemas de mínimos-quadrados lineares restritos
lsqnonlin	Resolve problemas de mínimos-quadrados não lineares
lsqnonneg	Resolve problemas não negativos de mínimos-quadrados

Fonte: Adaptado pelo Optimization Toolbox for use with MatLab, 2017.

2.3.3 Análise Estatística

Depois de minimizada a função objetivo é de fundamental importância o estabelecimento dos intervalos de confiança dos parâmetros e os testes de qualidade do ajuste do modelo aos dados experimentais. Desse modo, considerando que os desvios experimentais seguem uma distribuição normal de probabilidade, as distribuições *t*-Student, Fischer e χ^2 podem ser utilizadas como indicadores (SCHWAAB, 2007).

Para a utilização dos testes estatísticos é necessário o conceito de graus de liberdade (DF, do inglês *degrees of freedom*), definido como o número de determinações independentes menos o número de parâmetros estatísticos a serem avaliados:

$$DF = NE.NY - NP \tag{20}$$

onde *DF* é o número de graus de liberdade, *NE* é o número de experimentos, *NY* o número de medidas em cada experimento e *NP* o número de parâmetros do modelo.

2.3.3.1 Teste t-Student

A distribuição *t*-Student é uma distribuição de probabilidade estatística, publicada por um autor que se chamou de *Student*, pseudônimo de William Sealy Gosset. A distribuição *t* tem a mesma forma de sino da distribuição normal e é dependente apenas do tamanho do conjunto amostral, assim quanto maior o tamanho amostral mais estreita é a distribuição em torno do valor média.

A variável normalizada *t* é definida por:

$$t = \frac{\overline{X} - \mu_X}{\frac{s_X}{\sqrt{N}}} \tag{21}$$

onde $\overline{X}$ e s_X^2 são as médias e as variâncias amostrais, respectivamente, μ_X é a média da distribuição e *N* o número de amostragens independentes. Conforme Schwaab e Pinto (2007), a distribuição *t* tem enorme importância prática porque permite impor limites precisos sobre a região de confiança onde deve estar a média verdadeira, a partir de valores amostrados.

Além disso, a partir da distribuição *t* é possível definir os intervalos de confiança para os parâmetros do modelo (SCHWAAB e PINTO, 2007).

$$\alpha - t\sigma_\alpha < \alpha < \alpha + t\sigma \tag{22}$$

onde α é o valor estimado para o parâmetro, *t* é a probabilidade obtida com o número de graus de liberdade e grau de confiança arbitrado pelo usuário e σ_α é o desvio padrão associado à estimativa do parâmetro.

2.3.3.2 Teste Chi-Quadrado (χ^2)

Ao contrário da distribuição *t*-Student, a distribuição chi-quadrado é assimetria e positiva. Ademais, é dependente exclusivamente do tamanho do conjunto amostral e quanto maior o valor do conjunto amostral mais larga é a distribuição em torno do valor médio χ^2.

A variável normalizada χ^2 é definida por:

$$\chi^2 = \sum_{i=1}^{N} \left(\frac{x_i - \overline{X}}{\sigma_X} \right)^2 \tag{23}$$

onde x_i é a variável medida, $\overline{X}$ é a média amostral, σ_X^2 é a variância da distribuição e *N* é o número de amostragens independentes. A distribuição χ^2 tem enorme importância prática porque permite impor limites precisos sobre a região de confiança onde deve estar a variância verdadeira, a partir de valores amostrados (SCHWAAB e PINTO, 2007).

2.3.3.3 Teste exato de Fischer

De forma semelhante à distribuição chi-quadrado, a distribuição de Fischer é assimetria e positiva, porém é dependente de duas variáveis que representam os tamanhos dos conjuntos amostrais e quanto maiores os valores dos parâmetros mais estreita é a distribuição, já que as variâncias se aproximam das variâncias reais.

A variável normalizada *F* é definida por:

$$F = \frac{s_X^2 / \sigma_X^2}{s_Y^2 / \sigma_Y^2} \tag{24}$$

onde σ_X^2 e σ_Y^2 são as variâncias da distribuição, s_X^2 e s_X^2 são as variâncias amostrais obtidas. Schwaab e Pinto (2007) afirmam que distribuição *F* tem enorme importância prática, pois permite estabelecer comparações muito mais eficientes entre diferentes variâncias amostrais que aquelas obtidas com a distribuição χ^2. Quando as variâncias reais dos dois conjuntos de dados analisados são supostamente iguais, a Equação 24 pode ser simplificada:

$$F = \frac{s_X^2}{s_Y^2} \tag{25}$$

3 DETAILED NUMERICAL SOLUTION OF PORE VOLUME AND SURFACE DIFFUSION MODEL IN ADSORPTION SYSTEMS

P.R. Souza, G.L. Dotto, N.P.G. Salau

Abstract

In this work, the numerical solution of pore volume and surface diffusion model (PVSDM) was developed and presented in detail. The finite difference approximations method was employed to solve the partial differential equations of the diffusional model. The experimental adsorption of Malachite Green dye (MG) on bentonite clay was selected as case study. The equilibrium data were obtained from batch systems and, the Redlich−Peterson isotherm was suitable to represent the results. Due to non−linearity of the isotherm, the non−linear least squares technique were used to estimate the diffusional parameters. The Biot number has shown that the adsorption was simultaneously controlled by external mass transfer and intraparticle diffusion. Thus, both internal resistances (pore volume and surface) must be considered. The MG concentrations as a function of time decreases and the amount of MG mass adsorbed on bentonite clay as a function of the radial position increases until reaching equilibrium. The experimental concentration decay curve of MG was properly represented by PVDSM model. Further, the amount of MG mass adsorbed at higher radial positions was larger than at lower radial positions, within the PVSDM boundaries (particle boundaries), indicating that the method of finite difference approximations was appropriate for the numerical solution of PVSDM model.

Keywords: Diffusional mass transfer model; numerical solution; parameter estimation; adsorption rate.

1. Introduction

Adsorption is a unit operation used to separate different compounds from a fluid phase, using a solid matrix (the adsorbent). It is known that adsorption involves several mass transfer steps (Qiu et al., 2009). Despite of the importance of mass transfer in adsorption, studies involving adsorption kinetics are typically based in adsorption reaction models (Geetha et al., 2015; Zheng et al., 2015; Ghasemi et al., 2016; Lin and Lee, 2016). The adsorption reaction models (pseudo−first order and pseudo−second order) assume that the adsorption kinetics are exclusively controlled by the adsorption rate of the solute on the surface of the adsorbent, and the intraparticle diffusion and external mass transfer can be neglected (Ocampo−Pérez et al., 2012). Furthermore, it is considered that the adsorption kinetics can be represented in the same

manner as the rate of a chemical reaction (Qiu et al., 2009). Based on these models, it is not possible to obtain the mass transfer parameters and identify the rate controlling step.

The most realistic way to predict the adsorption kinetics is the use of mass transfer diffusional models (Qiu et al., 2009; Dotto et al., 2014; Largitte and Pasquier, 2016). These models are developed based on three consecutive stages: external mass transfer, intraparticle diffusion and sorption of an active site. Specifically, the intraparticle diffusion can be controlled by pore volume diffusion (Pore Volume Diffusion Model − PVDM), surface diffusion (Surface Diffusion Model − SDM), or a combination of both mechanisms (Pore Volume and Surface Diffusion Model − PVSDM) (Leyva−Ramos and Geankoplis, 1985; Ocampo−Pérez et al., 2010). However, their greater complexity makes their use mathematically more difficult, and usually the mass transfer diffusional models are simplified (Leyva−Ramos et al., 2012; Dotto et al., 2014; Podstawczyk and Witek−Krowiak, 2016) or solved with commercial software (Ocampo−Pérez et al., 2010; Ocampo−Pérez et al., 2015; Dotto et al., 2016). The commercial software cited in the literature (e,g, PDESOL and COMSOL) have graphical user interface that allow to abstract from details of the implementation of numerical methods and consider it as a "black box".

Malachite green (MG) is a cationic dye used in the textile industry for dyeing leather, silk, paper and fibers (Bulut et al., 2008). Furthermore, it is also used as a bactericidal, fungicidal and parasiticidal in aquaculture industries and livestock (Srivastava and Sinha, 2004; Geetha et al., 2015; Banerjee et al., 2016). The MG exposure is reported as carcinogenic and toxic for live organisms (Ghasemi et al., 2016; Lin and Lee, 2016) and thereby, it is essential to remove it from industrial effluents. In this way, adsorption has been widely used to remove several dyes from aqueous solutions, due to its high efficiency, simple operation and ability to separate a wide variety of compounds (El−Qada et al., 2008; Arellano−Cárdenas et al., 2013). It can be found in the literature that bentonite clay has high potential for the MG removal from aqueous solutions (Bulut et al., 2008; Arellano−Cárdenas et al., 2013), because of its high specific surface area, swelling capacity and cation exchange capacity (Yan et al., 2015).

Majority of previous works have investigated the adsorption kinetics based in adsorption reaction models. Even when the adsorption kinetics are predicted with mass transfer diffusional models, due to greater complexity, their solution requires model simplifications and commercial "black–box" softwares. To overcome this problem, the novelty of the research relies on two main issues: (1) Developing a detailed numerical solution of PVSDM model using the method of finite difference approximations; (2) Determining the diffusional parameters by

fitting the numerical solution of the non–linear model with the dye concentration decay data, using the non–linear least square technique.; (3) Comparing the PVSDM with its simplification, the SDM and PVDM models, using a case study in which any intraparticle diffusion can be neglected and both internal resistances (pore volume and surface) must be considered.

2. Mathematical model

The diffusional models deduced in this study were based on the following assumptions: batch system adsorption, the adsorption occurs at 298 K; the particles of bentonite clay are spherical; the mass transport by convection within the pores is negligible; the intraparticle diffusion can occur by pore volume diffusion and surface diffusion or both; the values of effective pore volume diffusion coefficient (D_p) and surface diffusion coefficient (D_s) are constant; and the adsorption rate on an active site is instantaneous (Leyva−Ramos and Geankoplis, 1985; Ocampo−Pérez et al., 2010).

$$V\frac{dC_A}{dt} = -mSk_F\left(C_A - C_{Ar}\big|_{r=R}\right) \tag{1}$$

$$t = 0, C_A = C_{A0} \tag{2}$$

$$\varepsilon_p \frac{\partial C_{Ar}}{\partial t} + \rho_p \frac{\partial q}{\partial t} = \frac{1}{r^2}\frac{\partial}{\partial r}\left[r^2\left(D_p \frac{\partial C_{Ar}}{\partial r} + \rho_p D_s \frac{\partial q}{\partial r}\right)\right] \tag{3}$$

$$t = 0, 0 \le r \le R, C_{Ar} = 0 \tag{4}$$

$$\left.\frac{\partial C_{Ar}}{\partial r}\right|_{r=0} = 0 \tag{5}$$

$$D_p \left.\frac{\partial C_{Ar}}{\partial r}\right|_{r=R} + \rho_p D_s \left.\frac{\partial q}{\partial r}\right|_{r=R} = k_F\left(C_A - C_{Ar}\big|_{r=R}\right) \tag{6}$$

The model represented by Eqs. (1−6) is the pore volume and surface diffusional model (PVSDM). The parameters k_F, D_s, and D_p correspond to external mass transport, surface diffusion, and pore volume diffusion mechanisms, respectively. The PVSDM model can be simplified by considering that the sole intraparticle diffusion mechanism may be either pore volume diffusion (PVDM) ($D_p \neq 0$, $D_s = 0$) or surface diffusion (SDM) ($D_p = 0$, $D_s \neq 0$).

Additionally, the dye adsorption on active sites was considered instantaneous (Ocampo−Pérez et al., 2010; Ocampo−Pérez et al., 2015; Dotto et al., 2016), representing that exists a local equilibrium between the concentration of MG in the pore solution, C_{Ar}, and the mass of MG adsorbed on the pore surface, q. This equilibrium relationship between C_{Ar} and q is represented by the adsorption isotherm:

$$q = f\left(C_{Ar}\right) \tag{7}$$

3. Materials and methods

3.1. Adsorbate

Malachite green (triphenylmethane dye; molecular weight 364.9 g mol^{-1}; C.I. 42,000; λ_{max} = 618 nm; molecular size of 8.0 Å) was supplied by Sigma−Aldrich with purity higher than 96 wt.%, and was used without further purification. Dye stock solution (1 g L^{-1}) was prepared by weighing 1.000 g of MG in analytical balance (Marte, AY220, Brazil) and dissolving in 1000 mL of distilled water. The dye solutions at different concentrations (150 − 500 mg L^{-1}) were prepared by diluting the stock solution with adequate volume of distilled water. All other reagents were of analytical grade.

3.2. Preparation and characterization of adsorbent

Natural bentonite clay from Mendoza province (Argentina) was used as adsorbent. The material was collected, oven dried at 100°C for 48 h, ground (Wiley Mill Standard, 03, USA) and sieved until the discrete particle size ranging from 45 to 250 μm. The mean diameter of Sauter was 47.4 μm.

The specific surface area, pore volume and average pore diameter were obtained by N_2 adsorption/desorption isotherms in a volumetric adsorption analyzer (Micromeritcs, ASAP 2020, USA) using the Bennett, Emmet and Teller (BET) method (Leyva−Ramos et al., 2012). The solid density of bentonite clay was related in literature (Heier et al., 2015). The apparent density, void fraction and external surface area of the sample were estimated by the following equations (Suzuki, 1990):

$$V_p = \frac{1}{\rho_p} - \frac{1}{\rho_s} \quad (8)$$

$$\varepsilon_p = 1 - \frac{\rho_p}{\rho_s} \quad (9)$$

$$S = \frac{6}{d_B \rho_p} \quad (10)$$

The bentonite clay functional groups were identified by Fourier transform infrared spectroscopy (FT−IR) (Shimadzu, Prestige 21, Japan) analysis, which was carried out in the range from 4000 to 500 cm^{-1} (Silverstein et al., 2005). X−ray diffraction (XRD) (Rigaku, Miniflex 300, Japan) was used to verify the crystalline/amorphous structure of the sample (Waseda et al., 2011). In order to visualize the bentonite clay surface and confirm its mean diameter, images were obtained from scanning electron microscopy (SEM) (Jeol, JSM−6060, Japan) (Goldstein et al., 2003); Energy dispersive X−ray spectroscopy (EDS) was also used to determine the sample composition (Goldstein et al., 2003).

3.3. Batch adsorption experiments

Erlenmeyer flasks of 125 mL were used as a batch adsorber to get the experimental data of MG. The bentonite clay (0.100 g) was added into aqueous dye solutions with initial concentrations of 150, 200, 250, 300 and 500 mg L^{-1}. The solutions were stirred at 150 rpm and 298 K in a thermostated shaker (Marconi, MA 093, Brazil). Aliquots were withdrawn at different time intervals until the equilibrium (the equilibrium was judged reached when the dye concentration in the liquid did not present difference between three consecutive measures), filtered (the filtration influence was lower than 3.5% and was considered in the calculations) through filter paper and the dye concentration was determined by UV−Visible spectrophotometer (Shimadzu, UV mini, Japan) at maximum wavelength of MG (λ_{max} = 618 nm) (Banerjee et al., 2016). For each experimental point (each time), one separate Erlenmeyer was used, to ensure that the volume used to quantify the dyes was negligible in relation to the total volume of the solution. To guarantee the experimental accuracy, reproducibility and reliability of the collect data, the adsorption experiments were performed in triplicate; blanks

were run in parallel and all dye solutions were stored in glass flasks, which were cleaned by soaking HNO_3 (1.5 mol L^{-1}) for 24 h.

4. Results and discussion

4.1. Bentonite clay characteristics

The surface area, pore volume and pore diameter of bentonite clay, determined by the N_2−BET method were S^{BET} = 172.66 $m^2\,g^{-1}$, V_p = 0.315 $cm^3\,g^{-1}$, and d_p = 7.30 nm, respectively. The solid density, reported in the literature, was ρ_s = 2.650 g cm^{-3}; the particle density, void fraction and external surface area, determined by the Eqs. (8−10) were ρ_p = 1.444 g cm^{-3}, ε_p = 0.445 and S = 877.42 $cm^2\,g^{-1}$, respectively.

The FT−IR spectrum of bentonite clay is shown in Fig. 1. The absorption band at 3629 cm^{-1} corresponds to the stretching vibrations of structural OH groups of bentonite (Zhirong et al., 2011; Caglar et al., 2015). The other hydroxyl groups can be seen at 3425 cm^{-1} (Zhirong et al., 2011). The H−O−H bending vibration of water occurs at 1653 cm^{-1} (Zhirong et al., 2011; Parolo et al., 2014). The intense band at 1035 cm^{-1} is relative to the Si−O bending vibration (Caglar et al., 2015; Tomul et al., 2016). The group Al−Al−OH is observed at 915 cm^{-1} (Zhirong et al., 2011; Caglar et al., 2015). The band at 797 cm^{-1} indicates the presence of quartz in the sample (Zhirong et al., 2011; Caglar et al., 2015). The bending vibrations of Al−O−Si and Si−O−Si can be seen at 527 and 472 cm^{-1}, respectively (Zhirong et al., 2011).

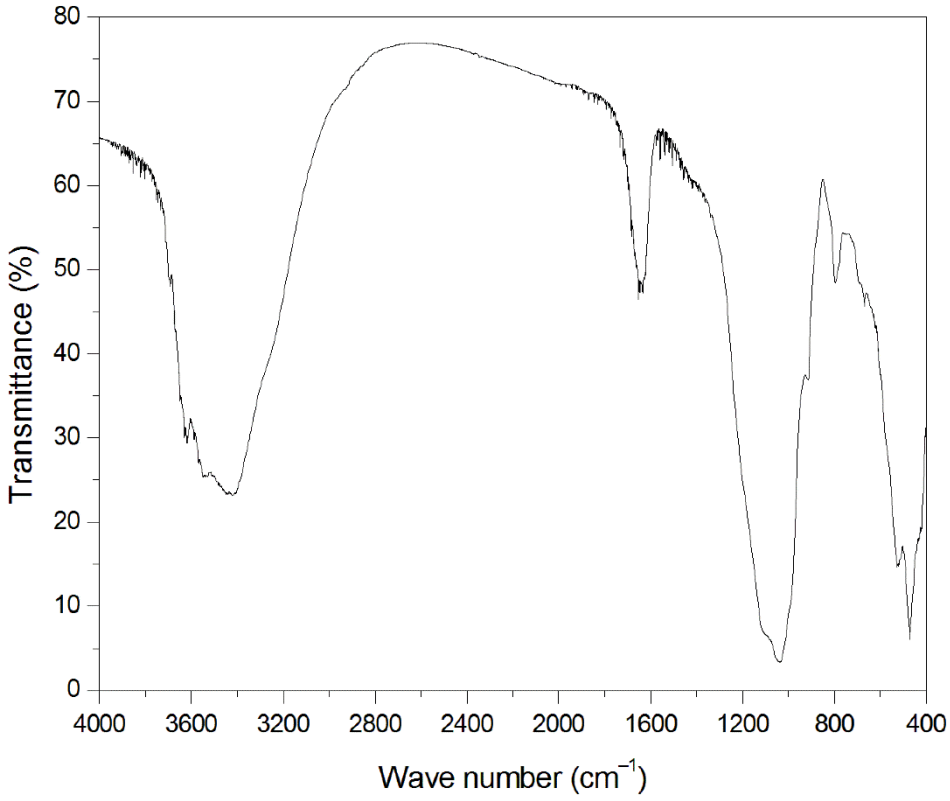

Fig. 1: FT−IR spectrum of bentonite.

The XRD patterns of bentonite clay are show in Fig. 2. It was found in this figure that the predominant component of bentonite clay is montmorillonite, but quartz and feldspar are the main impurity. The patterns indicate the montmorillonite at diffraction peaks of 5.5°, 19.8° and 34.8°; the diffraction peaks at 26.5° and 40.2° represents the quartz; and the diffraction peaks at 20.7° represents the feldspar (Kalburcu et al., 2015; Hafshejani et al., 2016). The basal space of bentonite was 15.2 Å, this value was also determined by XRD. The aforementioned compounds and functional groups can be potential adsorption sites to interact with MG dye. Furthermore, comparing the molecular size of MG dye (8.0 Å) (Guo et al., 2003) with the basal space (15.2 Å) and pore diameter (7.30 nm) of bentonite, it is possible to corroborate that the MG molecules were transferred inside the particle, supporting the existence of intraparticle diffusion control in the adsorption mechanism of this study.

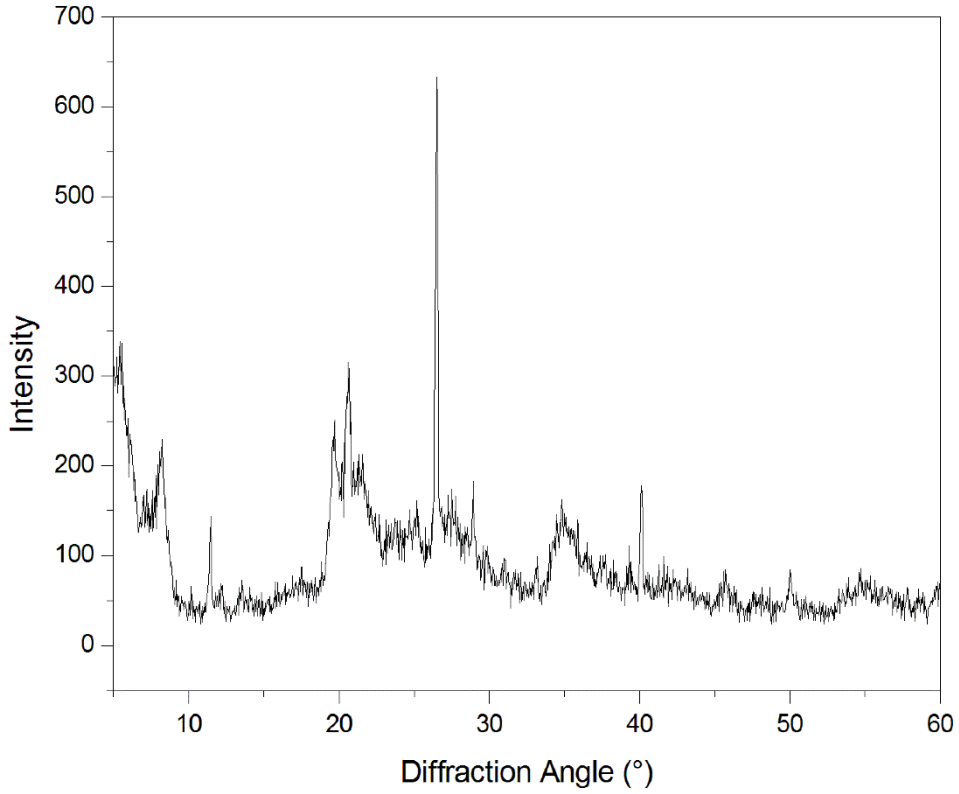

Fig. 2: XRD of bentonite.

The SEM images of bentonite clay are displayed in Fig. 3. The images show that the adsorbent geometry can be approximated to spheres and also confirms the mean diameter around 50 μm. Furthermore, the sample displays small cavities and cracks that allow the adsorption. The results from chemical analyses of the bentonite clay using EDS are show in Fig. 4. Oxygen, aluminum and silicon are the main elements found in the clay, representing an aluminosilicate material (Vhahangwele and Mugera, 2015). Carbon is also present on the sample, which may be due the decomposition of organic compounds (Masindi et al., 2015). It was also found low levels of Mg, Na, K, Ca, Ti and Fe.

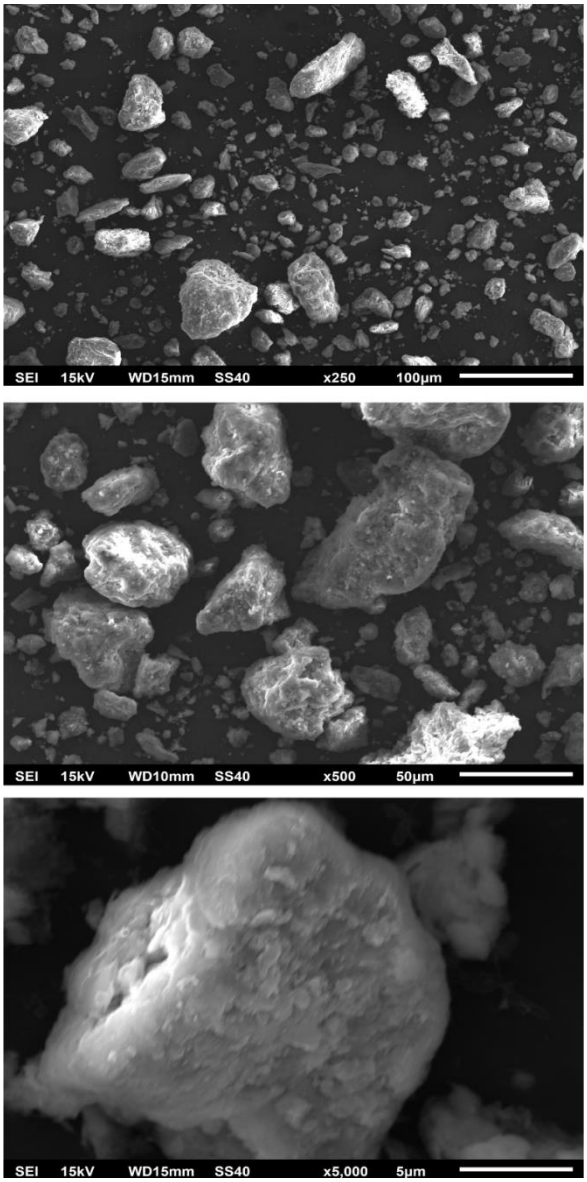

Fig. 3: SEM images of bentonite.

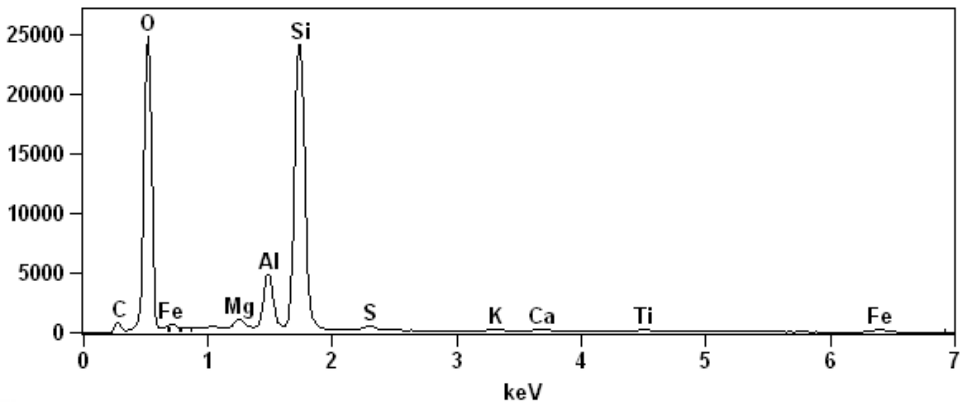

Fig. 4: EDS of bentonite.

4.2. Adsorption isotherm

Fig. 5 shows the experimental adsorption equilibrium data. The adsorption isotherm curve can be classified as type ‘‘H’’ (Giles et al., 1960), indicating a great affinity between MG and bentonite clay and numerous readily accessible sites. This behavior is favorable for adsorption since, even at high initial MG concentration in the solution, the MG concentration at equilibrium was lower than 10 mg L^{-1}, indicating an effective decolorization.

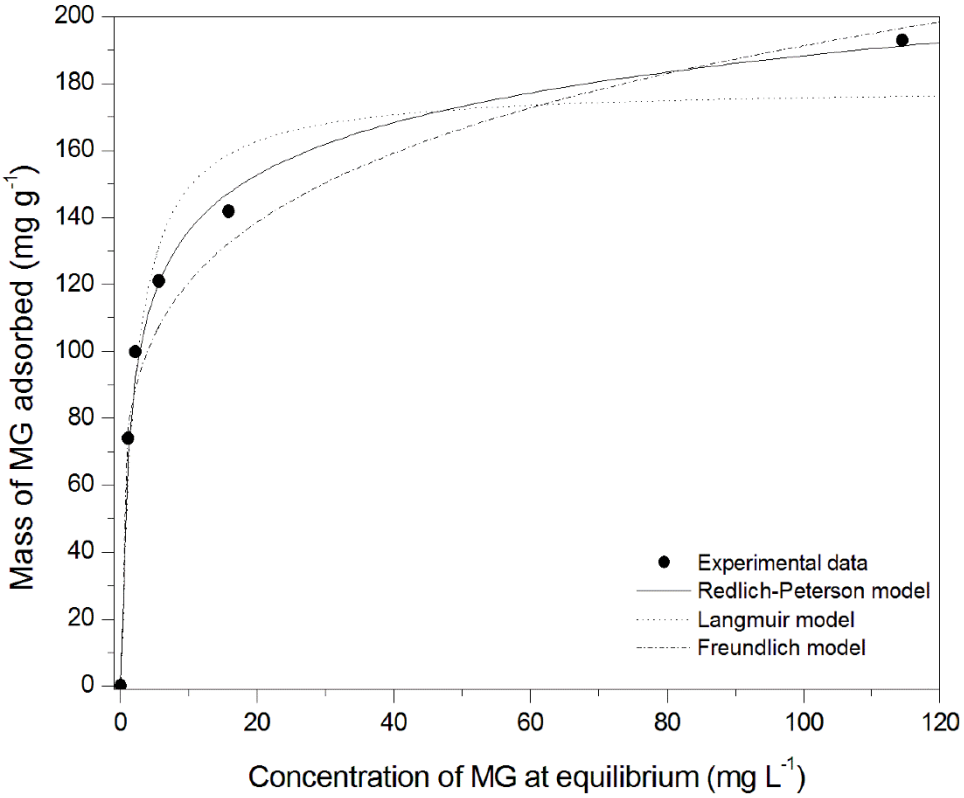

Fig. 5: Redlich−Peterson isotherm of MG adsorption on bentonite at 298 K.

The Redlich−Peterson isotherm model (Redlich and Peterson, 1959) is represented by the Eq. (11) and was compared with Langmuir (Langmuir, 1918) and Freundlich (Freundlich, 1906) isotherms to fit the experimental data:

$$q = \frac{k_{RP} C_{Ar}}{1 + a_{RP} C_{Ar}^{\beta}} \tag{11}$$

The adsorption constants were obtained by parameter optimization. The objective function to be minimized is the non−linear least square function, given by Eq. (12). It is defined as the sum of the differences between the experimental data (q) and the model data ($\hat{q}$) for all *Ny* experiments.

$$\min\left| f\left(k_{RP}, a_{RP}, \beta\right)\right| = \sum_{i=1}^{Ny}\left(q^i - \hat{q}^i\right)^2 \tag{12}$$

The Matlab® function *lsqnonlin* using the Trust−Region−Reflective algorithm (Coleman and Li, 1996) was used to solve Eq. (12). Additionally, the fit quality between the experimental data (q) and the model data ($\hat{q}$) was evaluated by the average relative error (*ARE*) (Dotto et al., 2014), by the following equation:

$$ARE = \frac{100}{Ny}\sum_{i=1}^{Ny}\left|\frac{q^i - \hat{q}^i}{q^i}\right| \tag{13}$$

The results revealed that Redlich−Peterson isotherm model presented best fit with the experimental data ($R^2 > 0.99$ and $ARE < 3.40\%$). The estimated values of a_{RP}, k_{RP} and β were, respectively, 1.27 (L mg^{-1}), 148.83 (L g^{-1}) and 0.89. In this way, this model was substituted in Eq. (7) in order to represent the local equilibrium between the concentration of MG in the pore solution, C_{Ar}, and the mass of MG adsorbed on the pore surface, q.

4.3. Numerical solution of the model

The mathematical model solution was found solving simultaneously Eqs. (1−6). Additionally, Eq. (11) represents the relationship between q and C_{Ar}. Using the chain rule, the terms involving q can be rewritten as:

$$\frac{\partial q}{\partial t} = \frac{\partial C_{Ar}}{\partial t}\frac{\partial}{\partial C_{Ar}}\left(\frac{k_{RP}C_{Ar}}{1+a_{RP}C_{Ar}^{\beta}}\right) \tag{14}$$

$$\frac{\partial q}{\partial r} = \frac{\partial C_{Ar}}{\partial r}\frac{\partial}{\partial C_{Ar}}\left(\frac{k_{RP}C_{Ar}}{1+a_{RP}C_{Ar}^{\beta}}\right) \tag{15}$$

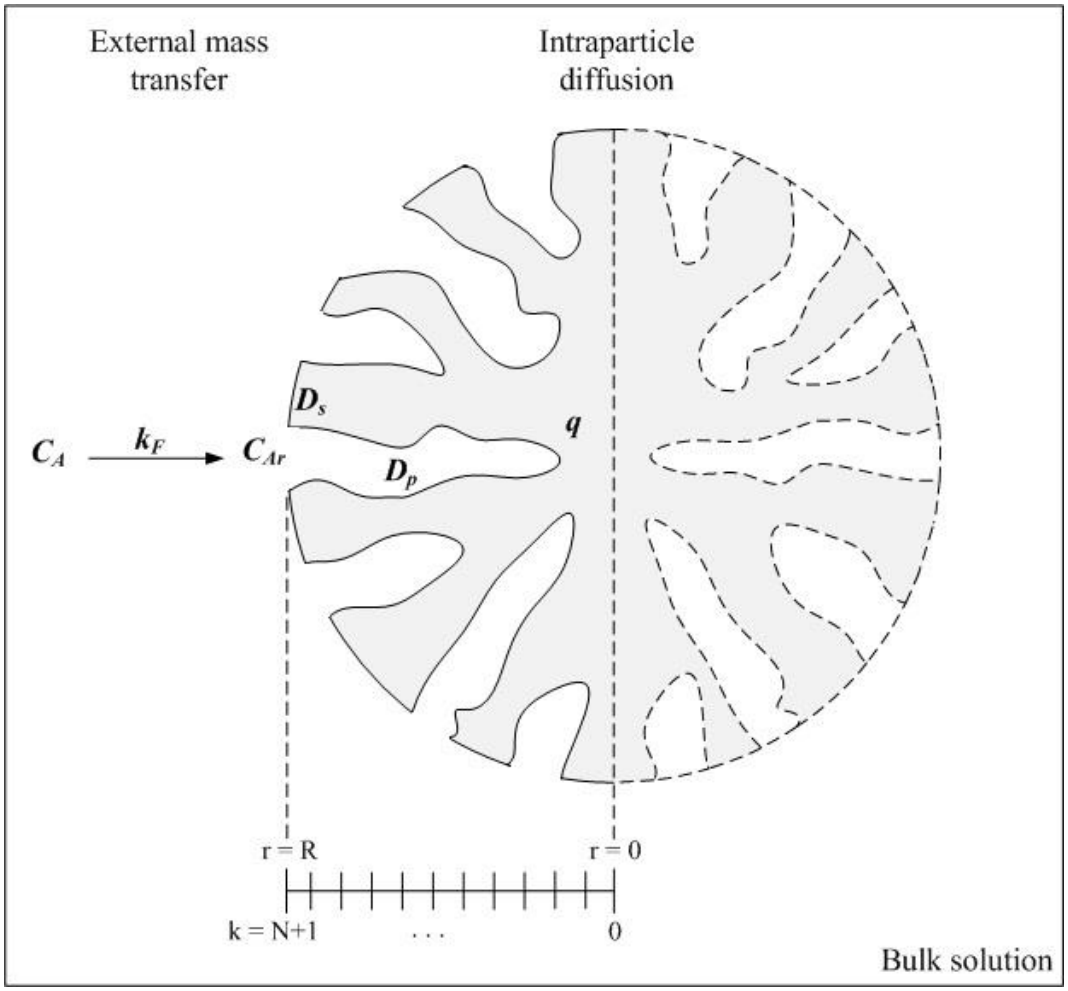

Fig. 6: Discretization of the transport of the dye molecules from the solution to the spherical particle (illustrative representation).

The method of finite difference approximations was used to solve the partial differential equations, which turns them into a set of first order ordinary differential equations using the finite difference relationships for all the spatial derivatives (r) and solves the ordinary differential equations for time (Schiesser,1991). The model has been discretized into $N+1$ points, where N is the number of internal points (Fig. 6). In this way, we have C_{Ar} in different points k, where $k = 0$ is the point at $r = 0$ and $k = N+1$ is the point at $r = R$. The points are spaced equally with the step size given by following equation:

$$h = \frac{R}{N+1} \tag{16}$$

The temporal variation of the MG concentration in aqueous solution, determined by Eq. (1) is rewritten in the discretized form, as:

$$\frac{dC_A}{dt} = -\frac{mSk_F}{V}\left(C_A - C_{Ar}^{N+1}\right) \tag{17}$$

Eq. (17) is subjected to the initial condition given by Eq. (2). The mass balance for the bentonite clay particle, Eq. (3), is rewritten using the second−order central difference approximations of the first and second derivative:

$$\varepsilon_p \frac{dC_{Ar}}{dt} + \rho_p \frac{dC_{Ar}}{dt}\frac{d}{dC_{Ar}^k}\left(\frac{k_{RP}C_{Ar}^k}{1+a_{RP}C_{Ar}^{k\ \beta}}\right) =$$
$$\frac{1}{r^2}\left\{\begin{array}{l} 2r\left[\begin{array}{l} D_p\left(\dfrac{C_{Ar}^{k+1}-C_{Ar}^{k-1}}{2h}\right)+ \\ \rho_p D_s\left(\dfrac{C_{Ar}^{k+1}-C_{Ar}^{k-1}}{2h}\right)\dfrac{d}{dC_{Ar}^k}\left(\dfrac{k_{RP}C_{Ar}^k}{1+a_{RP}C_{Ar}^{k\ \beta}}\right)\end{array}\right]+ \\ r^2\left[\begin{array}{l} D_p\left(\dfrac{C_{Ar}^{k+1}-2C_{Ar}^k+C_{Ar}^{k-1}}{h^2}\right)+ \\ \rho_p D_s\left(\dfrac{C_{Ar}^{k+1}-2C_{Ar}^k+C_{Ar}^{k-1}}{h^2}\right)\dfrac{d}{dC_{Ar}^k}\left(\dfrac{k_{RP}C_{Ar}^k}{1+a_{RP}C_{Ar}^{k\ \beta}}\right)\end{array}\right]\end{array}\right. \tag{18}$$

Isolating $\frac{dC_{Ar}}{dt}$ in Eq. (18) and making the necessary simplifications, we obtain the following equation:

$$\frac{dC_{Ar}}{dt} = -\left[r\left(-C_{Ar}^{k+1}+2C_{Ar}^k-C_{Ar}^{k-1}\right)+h\left(C_{Ar}^{k-1}-C_{Ar}^{k+1}\right)\right]$$
$$\frac{\left\{-D_p a_{RP}^2 C_{Ar}^{k\ 2\beta}+\left[\rho_p D_s k_{RP}(\beta-1)-2D_p\right]a_{RP}C_{Ar}^{k\ \beta}-D_p-\rho_p D_s k_{RP}\right\}}{h^2 r\left\{-\varepsilon_p a_{RP}^2 C_{Ar}^{k\ 2\beta}+\left[\rho_p k_{RP}(\beta-1)-2\varepsilon_p\right]a_{RP}C_{Ar}^{k\ \beta}-\varepsilon_p-\rho_p k_{RP}\right\}} \tag{19}$$

Eq. (19) is subjected to the initial condition given by Eq. (4). The second−order forward difference approximations of the first derivative were used to solve the boundary condition at *r* = 0:

$$C_{Ar}^0 = \frac{4C_{Ar}^1 - C_{Ar}^2}{3} \tag{20}$$

The second−order backward difference approximations of the first derivative were used to solve the boundary condition at r = R:

$$D_p\left(\frac{3C_{Ar}^{N+1}-4C_{Ar}^{N}+C_{Ar}^{N-1}}{2h}\right)+\rho_p D_s\left(\frac{3C_{Ar}^{N+1}-4C_{Ar}^{N}+C_{Ar}^{N-1}}{2h}\right)\frac{d}{dC_{Ar}^{N+1}}\left(\frac{k_{RP}}{1+a_{RP}C_{Ar}^{N+1\beta}}\right) \quad (21)$$
$$=k_F\left(C_A-C_{Ar}^{N+1}\right)$$

Eq. (21) has no analytical solution, i. e. it is not possible to solve explicitly the equation to obtain C_{Ar}^{N+1}. Thus, an implicit method to solve non−linear equation of Eq. (21) is required and the Matlab® function *fsolve*, using the Levenberg−Marquardt algorithm (Levenberg, 1944; Marquardt, 1963) was chosen for this purpose.

The resulting ordinary differential equations system presents high stiffness and requires a solver to stiff problems. The Matlab® function *ode15s* based on the numerical differentiation formulas (NDFs) was chosen to solve the ordinary differential equations (Shampine and Reichelt, 1997).

4.4. Estimation of mass transport parameters

The external mass transfer coefficient (k_F) was calculated by the procedure proposed by Furusawa and Smith (1973), when $t\rightarrow 0$ then $C_{Ar}\rightarrow 0$ and $C_A\rightarrow C_{A0}$. Substituting these conditions in Eq. (1), k_F can be calculated by the Eq. (22).

$$\left.\frac{d\left(C_A/C_{A0}\right)}{dt}\right|_{t=0}=-\frac{mSk_F}{V} \quad (22)$$

The term in the right of Eq. (22) is the slope of the curve C_A/C_{A0} versus t, at $t = 0$ and was calculated by the first three data points. The values of k_F calculated using Eq. (22) are shown in Table 1.

The molecular diffusivity of MG in an aqueous solution (D_{AB}) was estimated using the following equation (Wilke and Chang, 1955; Valderrama et al., 2008; Leyva–Ramos et al., 2012; Ocampo–Pérez et al.,2012):

$$D_{AB} = 7.4\times10^{-8}\left[\frac{(\varphi M_B)^{0.5} T}{\eta_B V_A^{0.6}}\right] \tag{23}$$

where φ = 2.6, M_B = 18.02 g mol^{-1}, η_B = 0.904 cp, T = 298.15 K and V_A= 196.05 cm^3 mol^{-1}. The molecular diffusivity coefficient of MG determined with Eq. (23) was 7.04×10^{-6} cm^2 s^{-1}.

The relationship between the effective pore volume diffusion coefficient, D_p, and the molecular diffusivity, D_{AB}, can be described by the model based on the tortuosity factor (τ). In this way D_p can be obtained from the following equations (Wilke and Chang, 1955; Valderrama et al., 2008)

$$D_p = \frac{D_{AB}\varepsilon_p}{\tau} \tag{24}$$

where

$$\tau = \frac{\left(2-\varepsilon_p\right)^2}{\varepsilon_p} \tag{25}$$

The effective pore volume diffusion coefficient was considered only in the cases involving pore volume diffusion (PVSDM and PVDM models) being equal in both models D_p = 6.11×10^{-7} cm^2 s^{-1} (Table 1).

The surface diffusion coefficient was also obtained by parameter estimation using the Matlab® function *lsqnonlin* with the Trust−Region−Reflective algorithm (Coleman and Li, 1996). The non−linear least squares objective function to be minimized is defined as the sum of the differences between the experimental data (C_A) and the model data ($\hat{C}_A$), given by Eq. (26).

$$\min\left|f\left(D_S\right)\right| = \sum_{i=1}^{Ny}\left(C_A^i - \hat{C}_A^i\right)^2 \tag{26}$$

The D_s evaluation is only performed in the cases of involving surface diffusion (PVSDM and SDM models).

Table 1: Experimental conditions and estimated parameters for MG concentration decay curves during adsorption on bentonite.

Exp	C_{A0} (mg L^{-1})	C_{Ae} (mg L^{-1})	q_e (mg g^{-1})	k_F x10^3 (cm s^{-1})	D_px10^7 (cm^2 s^{-1})	D_sx10^9 (cm^2 s^{-1})	*Bi*
1	500	114.55	192.92	2.89	6.11	1.15	10.67
2	300	15.86	141.93	2.65	6.11	0.79	11.61
3	250	5.61	121.10	2.44	6.11	0.76	10.85
4	200	2.21	99.79	2.16	6.11	0.74	9.58
5	150	1.09	73.94	1.99	6.11	0.68	9.72

4.5. Pore volume and surface diffusion model (PVSDM)

As previously mentioned, PVSDM model takes into account that intraparticle diffusion was due to both, pore volume and surface diffusion mechanisms. For the purpose of solve the PVSDM model, k_F and D_p were calculated from Eq. (22) and Eq. (24), respectively. Therefore, the only unknown parameter was D_s and was evaluated by fitting the numerical solution of the PVSDM model with the dye concentration decay data, using the non−linear least squares technique, according Eq. (26).

Dye concentration decay curves for initial dye concentrations of 150, 200, 250, 300 and 500 mg L^{-1} were obtained. However, dye concentration decay curves for initial dye concentrations lower than 300 mg L^{-1} have shown similar shape and thus they were omitted from the graphs for readability purposes. However, future work was developed to determine a global parameter and the confidence intervals of the parameter from statistical tests.

Fig. 7 shows the experimental dye concentration decay data and the dye concentration decay curves predicted by the PVSDM model using the optimal values of D_s (Table 1). The results revealed that PVSDM model adjust properly fit with the experimental data for 500 mg L^{-1} ($R^2 > 0.98$ and $ARE < 4.95\%$) and 300 mg L^{-1} ($R^2 > 0.99$ and $ARE < 8.35\%$).

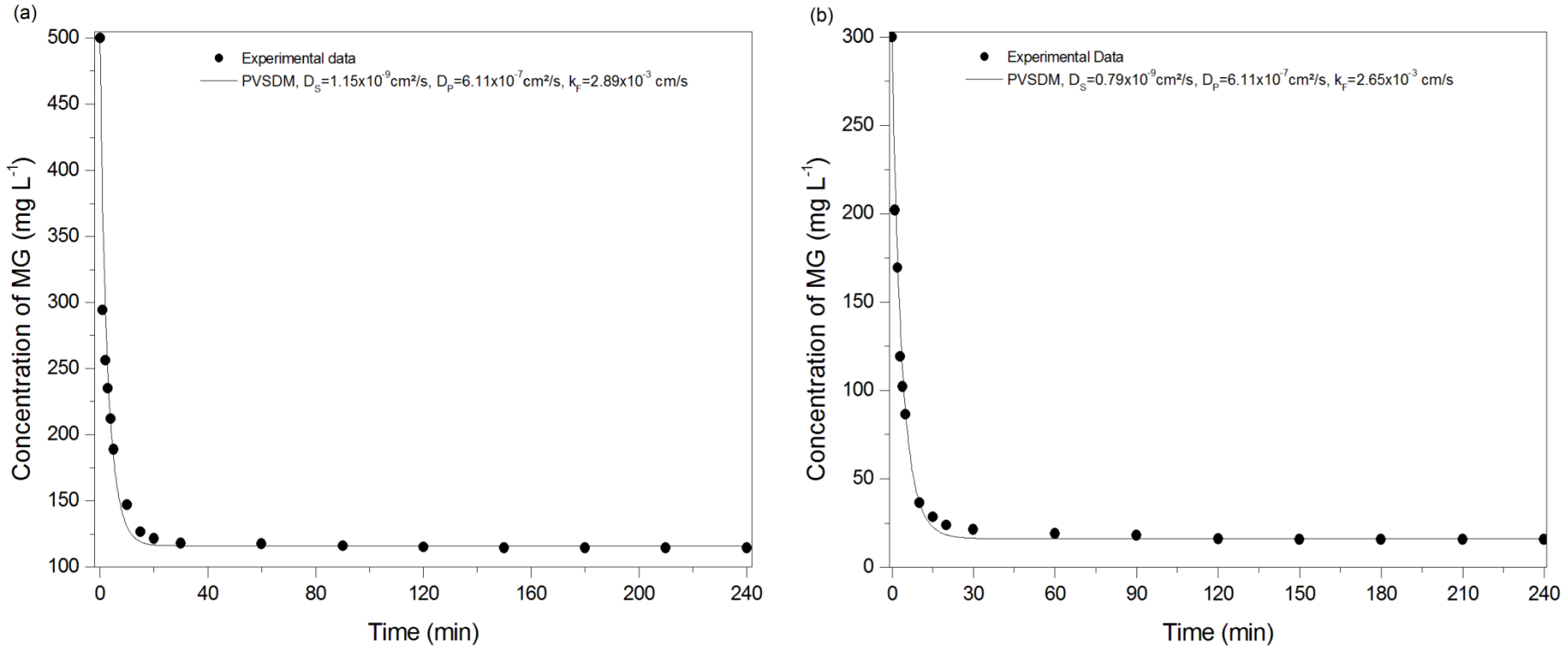

Fig. 7: Experimental dye concentration decay data and dye concentration decay curve predicted by the PVSDM with an initial dye concentration of (a) 500 mg L^{-1} and (b) 300 mg L^{-1}.

The amount of dye adsorbed on each radial position over time is depicted in Fig. 8, according to the results of Fig. 7a. The dashed lines represent the boundaries of the particle, which indicates that the finite differences approximation technique has been properly addressed in this system, since the internal points were defined by the boundary conditions. Additionally, when comparing with Fig. 7a, it can be seen that as the MG concentration decreases, the MG mass adsorbed on the solid increases until reaching equilibrium. Also in Fig. 8, it can be seen that the amount of MG mass adsorbed at higher radial positions was larger than at lower radial positions. This is because the dye is initially adsorbed on the outside of the particle ($r = R$) and takes a few minutes to reach the center of the particle ($r = 0$).

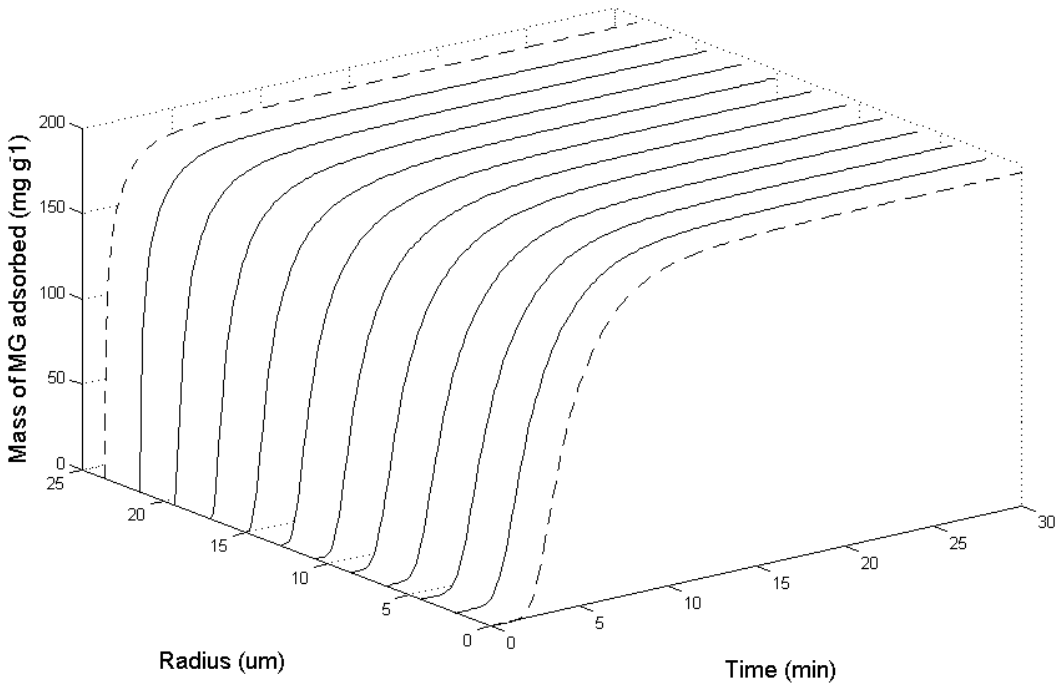

Fig. 8: Mass of MG adsorbed on each radial position over time to 500 mg L^{-1}.

The relative contribution of each diffusion mechanism to the intraparticle mass transfer of the MG was estimated by computing the mass flux due to the pore volume diffusion, N_{AP}, and surface diffusion, N_{AS}, using the following equations:

$$\frac{N_{AP}}{N_{AP}+N_{AS}} = \frac{D_p \partial C_{Ar}/\partial r}{D_p \partial C_{Ar}/\partial r + D_s \rho_p \partial q/\partial r} \tag{27}$$

$$\frac{N_{AS}}{N_{AP}+N_{AS}} = \frac{D_s \rho_p \, \partial q/\partial r}{D_p \, \partial C_{Ar}/\partial r + D_s \rho_p \, \partial q/\partial r} \tag{28}$$

The relative contribution of each diffusive mechanism during adsorption of MG on bentonite clay as a function of the particle radius and time is depicted in Fig. 9. As shown in this figure, the relative contribution of both mechanisms was dependent on the time and the radial position in the particle. For example, at around 4 min, the pore volume diffusion is the main intraparticle diffusion mechanism at the entrance of the pore; but the surface diffusion was almost the only mechanism for particle radius less than 6 μm. Only after the equilibrium, at around 22 min, the relative contribution of both mechanisms it remained constant with the particle radius and time, and the contribution of pore volume diffusion and the contribution of surface diffusion were respectively, 66 and 34% of the global intraparticle diffusion.

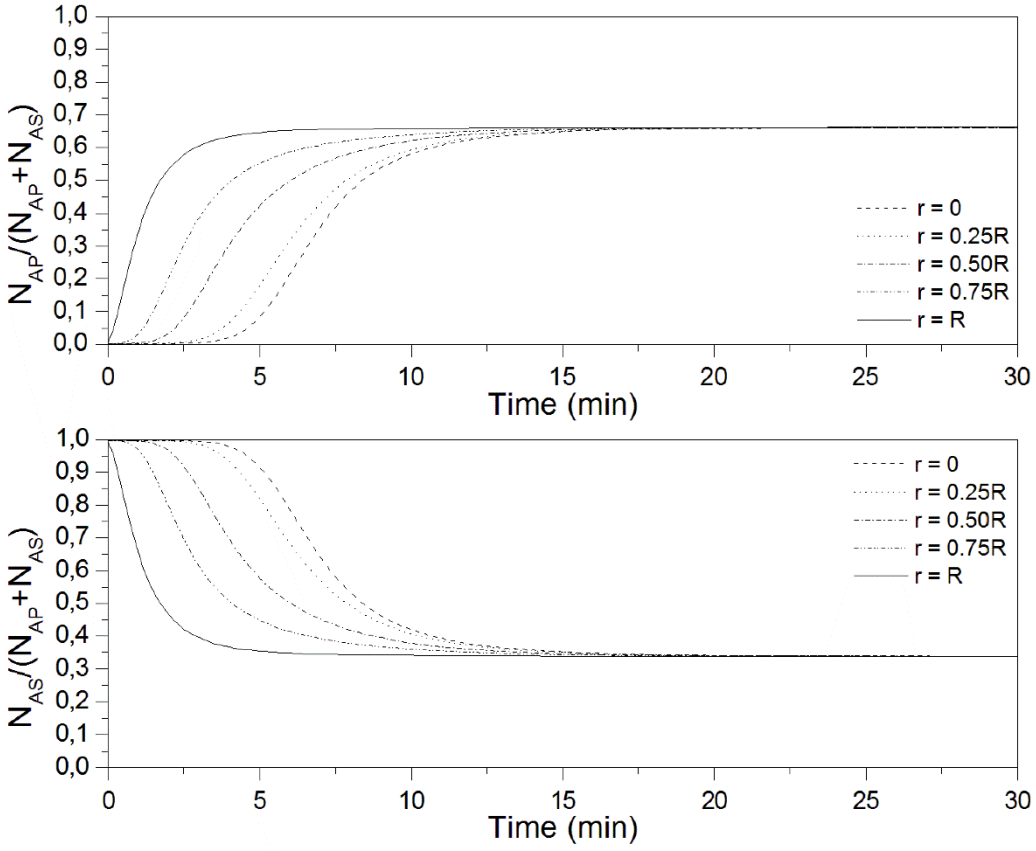

Fig. 9: (a) Contribution of pore volume diffusion and (b) surface diffusion to the intraparticle diffusion at different radial positions to 500 mg L^{-1}.

The dimensionless Biot number (*Bi*), which reflects the relative importance of external mass transfer to intraparticle diffusion, was used to verify the influence of each mass transfer step on the dye adsorption. The Biot number is defined by Eq. (29) (Cooney, 1993).

$$Bi = \frac{k_F d_B C_{A0}}{2\rho_P D_{\text{int}} q_e} \tag{29}$$

According to the literature, a complete dominance of the external mass transfer exists for $Bi < 0.5$, while a considerable dominance of the surface diffusion exists for $Bi > 10$ (Cooney, 1993). Since the *Bi* values obtained in this work range from 9.58 to 11.61 (Table 1), the adsorption of MG on bentonite was simultaneously controlled by external mass transfer and intraparticle diffusion.

4.6. Surface diffusion model (SDM) and pore volume diffusion model (PVDM)

The rate of adsorption of MG on bentonite clay also was evaluated with the PVDM and SDM models. The experimental and the predicted dye concentration decay curves for the adsorption are depicted in Fig. 10.

The PVDM model despises the surface diffusion. As it can be seen in Fig. 10, the PVDM model did not interpret the experimental data for 500 mg L^{-1} ($R^2 > 0.95$ and $ARE < 17.91\%$) and 300 mg L^{-1} ($R^2 > 0.96$ and $ARE < 56.10\%$) and clearly overestimated the dye concentration decay curve, i.e. the rate of adsorption of MG is much faster than the one predicted with the PVDM model.

According to the SDM model, the intraparticle diffusion is exclusively due to surface diffusion and pore volume diffusion can be neglected. The mass parameter D_s was evaluated by fitting the numerical solution of the model with the dye concentration decay data, using the non−linear least squares technique, according Eq. (26). The curves predicted by the SDM model using the optimal values of D_s (Fig. 10) present reasonable results for 500 mg L^{-1} ($R^2 > 0.98$ and $ARE < 6.70\%$) and 300 mg L^{-1} ($R^2 > 0.98$ and $ARE < 9.90\%$); however, analyzes already mentioned findings suggest that the MG adsorption on bentonite clay involves a combination of the mechanisms of surface and pore volume diffusion, requiring the implementation of PVSDM model.

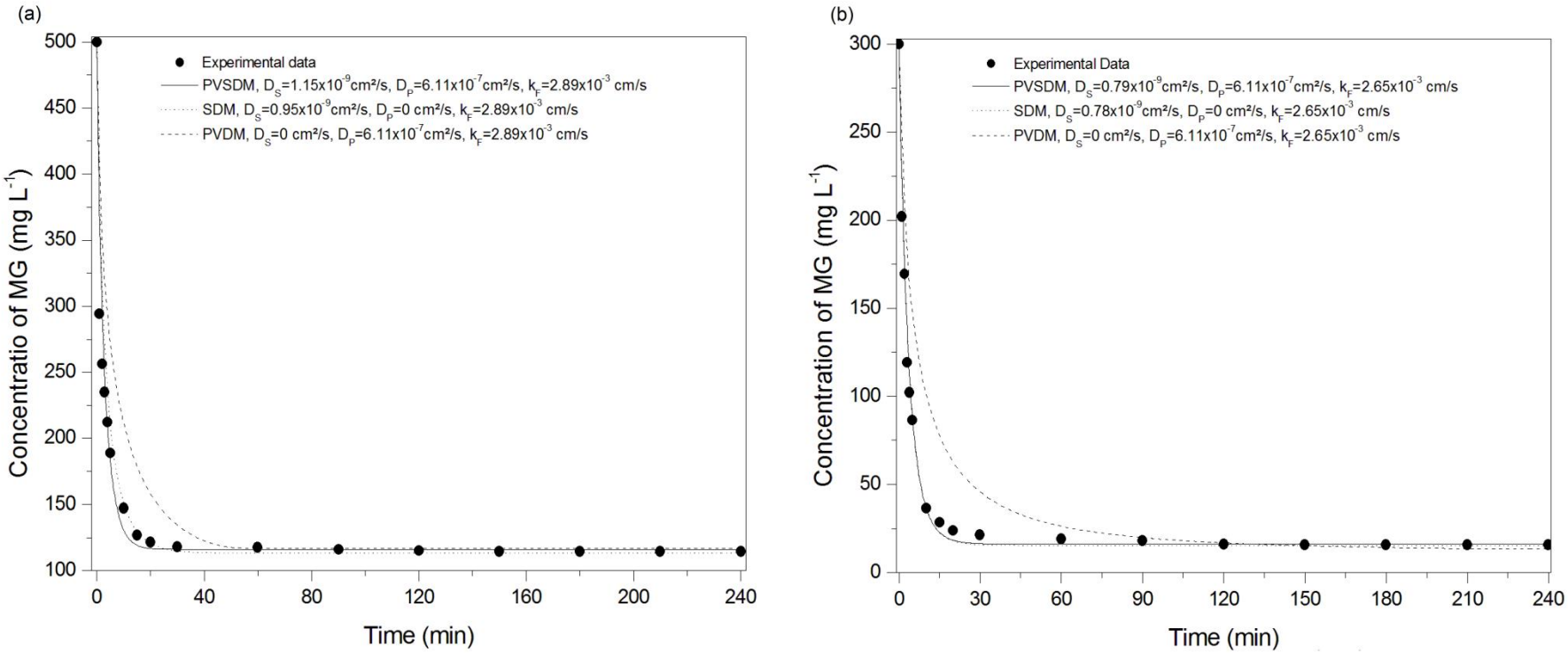

Fig. 10: Experimental dye concentration decay data and dye concentration decay curve predicted by the PVSDM, PVDM and SDM with an initial dye concentration of (a) 500 mg L^{-1} and (b) 300 mg L^{-1}.

5. Conclusion

The numerical solution of PVSDM model was developed in this work. The method of finite difference approximations was employed to solve the partial differential equations of the model and the parameters was evaluated by fitting the numerical solution of the model with the dye concentration decay data, using the non−linear least squares technique. The equilibrium, of the particular system, was well represented by the Redlich−Peterson isotherm. The experimental dye concentration decay data were well represented by the PVSDM model, indicating that this numerical solution is an appropriate tool for solving the problem.

The results indicate that the adsorption was simultaneously controlled by external mass transfer and intraparticle diffusion. In addition, both, surface diffusion and pore volume diffusion presented significant contribution to the evaluation of the PVSDM model.

Finally, the SDM and PVDM models were also tested, in order to verify the possibility of a simplification in the PVSDM model. These models were not adequate to represent the adsorption phenomena. The results demonstrated that in the MG adsorption onto bentonite, any internal resistance (pore or surface) can be neglected and the PVSDM must be implemented.

Acknowledgement

The authors are grateful to National Council for the Improvement of Higher Education (CAPES) for granting the scholarship to the first author.

References

Arellano−Cárdenas, S., López−Cortez, S., Cornejo−Mazón, M., Mares−Gutiérrez, J.C., 2013. Study of malachite green adsorption by organically modified clay using a batch method. Appl. Surf. Sci. 280, 74−78.

Banerjee, S., Sharma, G.C., Gautma, R.K., Chattopadhyaya, M.C., Upadhyay, S.N., Sharma, Y.C., 2016. Removal of Malachite Green, a hazardous dye from aqueous solutions using Avena Sativa (oat) hull as a potential adsorbent. J. Mol. Liq. 213, 162−172.

Bulut, E., Özacar, M., Şengil, I.A., 2008. Adsorption of malachite green onto bentonite: Equilibrium and kinetic studies and process design. Microporous. Mesoporous. Mater. 115, 234−246.

Caglar, B., Cubuk, O., Demir, E., Coldur, F., Catir, M., Topcu, C., Tabak, A., 2015. Characterization of AlFe−pillared Unye bentonite: A study of the surface acidity and catalytic property. J. Mol. Struct. 1089, 59−65.

Coleman, T.F., Li, Y., 1996. An Interior, Trust Region Approach for Nonlinear Minimization Subject to Bounds. SIAM. J. Optimiz. 6, 418−445.

Cooney, D.O., 1993. Comparison of simple adsorber breakthrough curve method with exact solution, Am. Inst. Chem. Eng. J. 39, 355–358.

Dotto, G.L., Buriol, C., Pinto, L.A.A., 2014. Diffusional mass transfer model for the adsorption of food dyes on chitosan films. Chem. Eng. Res. Des. 92, 2324−2332.

Dotto, G.L., Ocampo−Pérez, R., Moura, J.N., Cadaval Jr., T.R.S., Pinto, L.A.A., 2016. Adsorption rate of Reactive Black 5 on chitosan based materials: geometry and swelling effects. Adsorption. In press, 1−11, DOI 10.1007/s10450−016−9804−y.

El−Qada, E.N., Allen, S.J., Walker, G.M., 2008. Adsorption of basic dyes from aqueous solutions onto activated carbon. Chem. Eng. J. 135, 174−184.

Freundlich, H., 1906. Over the adsorption in solution. Z. Phys. Chem. A. 57, 358−471.

Furusawa, T., Smith, J.M., 1973. Fluid−particle and intraparticle mass transport rates in slurries. Ind. Eng. Chem. Fund. 12, 197−203.

Geetha, P., Latha, M.S., Koshy, M., 2015. Biosorption of malachite green dye from aqueous solution by calcium alginate nanoparticles: Equilibrium study. J. Mol. Liq. 212, 723−730.

Ghasemi, M., Mashhadi, S., Asif, M., Tyagi, I., Agarwal, S., Gupta, V.K., 2016. Microwave−assisted synthesis of tetraethylenepentamine functionalizes active carbon with high adsorption capacity for Malachite green dye. J. Mol. Liq. 213, 317−325.

Giles, C.H., MacEwan, T.H., Nakhwa, S.N., Smith, D., 1960. Studies in adsorption part XI: A system of classification of solution adsorption isotherms and its use in diagnosis of adsorption mechanisms and in measurement of specific surface areas of solids. J. Chem. Soc. 3973−3993.

Goldstein, J.I., Newbury, D.E., Echil, P., Joy, D.C., Romig Jr., A.D., Lyman, C.E., Fiori, C., Lifshin, E., 1992. Scanning electron microscopy and X−ray microanalysis, Plenum Press, New York.

Guo, Y., Yang, S., Fu, W., Qi, J., Li, R., Wang, Z., Xu, H., 2003. Adsorption of malachite green on micro– and mesoporous rice husk–based active carbon. Dyes Pigm. 56, 219–229

Hafshejani, K.S., Moslemizadeh, A., Shahbazi, K., 2016. A novel bio−based deflocculant of bentonite drilling mud. Appl. Clay. Sci. 127−128, 23−34.

Heier, D., Blackstock, T., Stack, K., Richardson, D., Lewis, T., 2015. Adsorption of wood extractives and model compounds onto bentonite. Colloid. Surf. A. 482, 213−221.

Kalburcu, T., Tabak, A., Ozturk, N., Tuzmen, N., Akgol, S., Caglar, B., Denizli, A., 2015. Adsorption of lysozyme from aqueous solutions by a novel bentonite−tyrptophane (Bent−Trp) microcomposite affinity sorbent. J. Mol. Struct. 1083, 156−162.

Langmuir, I., 1918. The adsorption of gases on plane surfaces of glass, mica and platinum. J. Am. Chem. Soc. 40, 1361−1403.

Largitte, L., Pasquier, R., 2016. A review of the kinetics adsorption models and their application to the adsorption of lead by an activated carbon. Chem. Eng. Res. Des. 109, 495−504.

Levenberg, K., 1944. A method for the solution of certain nonlinear problems in least squares. Q. Appl. Math. 2, 164−168.

Leyva−Ramos, R., Geankoplis, C.J., 1985. Model simulation and analysis of surface diffusion of liquids in porous solids. Chem. Eng. Sci. 40, 799−807.

Leyva−Ramos, R., Ocampo−Perez, R., Mendoza−Barron, J., 2012. External mass transfer and hindered diffusion of organic compounds in the adsorption on activated carbon cloth. Chem. Eng. J. 183, 141−151.

Lin, K.A., Lee, W., 2016. Highly efficient removal of Malachite green from water by magnetic reduced grapheme oxide/zeolitic imidazolate framework self−assembled nanocomposite. Appl. Surf. Sci. 361, 114−121.

Marquardt, D., 1963. An algorithm for least−squares estimation of nonlinear parameters. SIAM. J. Appl. Math. 11, 431−441.

Masindi, V., Gitari, M.W., Tutu, H., DeBeer, M., 2015. Efficiency of ball milled South African bentonite clay for remediation of acid mine drainage. J. Water. Proc. Eng. 8, 2227−240.

Ocampo−Perez, R., Leyva−Ramos, R., Alonso−Davila, P., Rivera−Utrilla, J., Sánchez−Polo, M., 2010. Modeling adsorption rate of pyridine onto granular activated carbon. Chem. Eng. J. 165, 133−141.

Ocampo−Pérez, R., Leyva−Ramos, R., Rivera−Utrilla, J., Flores−Cano, J.V., Sánchez−Polo, M., 2015. Modeling adsorption rate of tetracyclines on activated carbons from aqueous phase. Chem. Eng. Res. Des. 104, 579−588.

Ocampo−Pérez, R., Rivera−Utrilla, J., Gómez−Pacheco, C., Sánchez−Polo, M., López−Peñalver, J.J., 2012. Kinetic study of tetracycline adsorption on sludge−derived adsorbents in aqueous phase. Chem. Eng. J. 213, 88−96.

Ocampo−Pérez, R., daiem, M.M.A.; Rivera−Utrilla, J., Méndez–Díaz, J.D., Sánchez−Polo, M., 2012. Modeling adsorption rate of organic micropollutants present in landfill leachates onto granular activated carbon. J. Colloid Interf. Sci. 385(1), 174−182.

Parolo, M.E., Pettinari, G.R., Musso, T.B., Sánchez−Izquierdo, M.P., Fernández, L.G., 2014. Characterization of organo−modified bentonite sorbents: The effect of modification conditions on adsorption performance. Appl. Surf. Sci. 320, 356−363.

Podstawczyk, D., Witek−Krowiak, A., 2016. Novel nanoparticles modified composite eco−adsorbents—A deep insight into kinetics modelling using numerical surface diffusion and artificial neural network models. Chem. Eng. Res. Des. 109, 1−17.

Qiu, H., Pan, L.L., Zhang, Q.J., Zhang, W., Zhang, Q., 2009. Critical review in adsorption kinetic models. J. Zhejiang Univ. Sci. A 10, 716−724.

Redlich, O., Peterson, D.L., 1959. A useful adsorption isotherm. J. Chem. Phys. 63, 1024−1027.

Schiesser, W.E., 1991. The Numerical Method of Lines: Integration of Partial Differential Equations, Academic Press, Inc., San Diego.

Shampine, L.F., Reichelt, M.W., 1997. The MATLAB ODE Suite. SIAM J. Sci. Comput. 18, 1−22.

Silverstein, R.M., Webster, X.F., Kiemle, D.J., 2005. Spectrometric Identification of Organic Compounds, John Wiley & Sons, Danvers.

Srivastava, S., Sinha, R., Roy, D., 2004. Toxicological effects of malachite green, Aquat. Toxicol. 66, 319−329.

Suzuki, M., 1990. Adsorption Engineering, Kodansha, Tokyo.

Tomul, F., Basoglu, F.T., Canbay, H., 2016. Determination of adsorptive and catalytic properties of cooper, silver and iron contain titanium−pillared bentonite for the removal bisphenol A from aqueous solution. Appl. Surf. Sci. 360, 579−593.

Valderrama, C., Gamisans, X., de las Heras, X., Farrán, A.M., Cortina, J.L., 2008. Sorption kinetics of polycyclic aromatic hydrocarbons removal using granular activated carbon: Intraparticle diffusion coefficients. J. Hazard. Mater. 157, 386−396.

Vhahangwele, M., Mugera, G.W., 2015. The potential of ball−milled South African bentonite clay for attenuation of heavy metal from acidic wastewaters: Simultaneous sorption of Co^{2+}, Cu^{2+}, Ni^{2+}, Pb^{2+} and Zn^{2+} ions. J. Environ. Chem. Eng. 3, 2416−2425.

Waseda, Y., Matsubara, E., Shinoda, K., 2011. X−ray Diffraction Crystallography, Springer−Verlag, Berlin.

Wilke, C.R., Chang, P., 1955. Correlation of diffusion coefficients in dilute solutions. AIChE J. 1, 264−268.

Yan, L., Qin, L., Yu, H., Li, S., Shan, R., Du, B., 2015. Adsorption of acids dyes from aqueous solution by CTMAB modified bentonite: Kinetic and isotherm modeling. J. Mol. Liq. 211, 1074−1081.

Zheng, H., Qi, J., Jiang, R., Gao, Y., Li, X., 2015. Adsorption of malachite green by magnetic litchi pericarps: A response surface methodology investigation. J. Environ. Manage. 162, 232−239.

Zhirong, L., Uddin, M.A., Zhanxue, S., 2011. FT−IR and XRD analysis on natural Na−bentonite and Cu(II)−loaded Na−bentonite. Spectrochim. Acta A. 79, 1013−1016.

4 STATISTICAL EVALUATION OF PORE VOLUME AND SURFACE DIFFUSION MODEL IN ADSORPTION SYSTEMS

P.R. Souza, G.L. Dotto, N.P.G. Salau

Abstract

The Pore Volume and Surface Diffusion Model (PVSDM) was applied to represent the adsorption of malachite green on bentonite. A detailed analysis of the diffusion parameters was performed and was conclude that the external mass transfer coefficient (k_F) was dependent on the operating conditions and ranged from 1.99×10^{-3} to 2.65×10^{-3} cm s^{-1}; the pore volume diffusion coefficient (D_p) was independent on the initial dye concentration and was 6.11×10^{-7} cm^2 s^{-1}; and the surface diffusion coefficient values (D_s) increased with the initial dye concentration and ranged from 6.83×10^{-10} to 7.92×10^{-10} cm^2 s^{-1}. Also, the relative contribution of superficial diffusion mechanism was increased with the initial dye concentration. Was determinate an optimal global parameter $D_s = 7.73\times10^{-10}$ cm^2 s^{-1} was determinate and statically suitable with the Student's t test, χ^2 test and the Fisher's exact test. The model was validated using the optimal value of D_s which is valid for the whole initial MG concentration range.

Keywords: Adsorption; Diffusional model; Mass transfer parameters; Parameter estimation; Statistical analysis

1. Introduction

Malachite green (MG) is a cationic dye used in textile industry for dyeing purposes, and in aquaculture industry as a fungicide, antiseptic and parasiticidal [1−3]. The removal of MG in effluents is necessary, because the MG prolonged exposure is considered toxic and carcinogen to aquatic and human life [4, 5].

The most common methods for removal of MG are chemical oxidation [6], coagulation/flocculation [7], biodegradation [8] and adsorption [1−5]. Adsorption has been widely used to remove several dyes from aqueous solutions due to its high efficiency, simple operation and ability to separate a wide variety of compounds [9, 10]. It has been shown in the literature that bentonite has high potential for the MG dye removal from aqueous solutions, because of its high specific surface area, swelling capacity and cation exchange capacity [11].

It is well documented that the diffusional models are the most realistic way to predict the adsorption in porous solids, because includes the three simultaneous steps: external mass transport, intraparticle diffusion and adsorption on an active site. Specifically, the intraparticle diffusion may be due to pore volume diffusion, surface diffusion, or a combination of both mechanisms [12, 13]. In previous work, PVSDM model were used to suitable represent the adsorption of MG in bentonite at different initial concentrations of dye [14]. It should be highlighted that, in the study, D_s was computed for each experimental condition. Otherwise, in this work, a general value of D_s is proposed to represent the adsorption phenomenon under the whole range of experimental conditions.

This work aimed to use a PVSDM model to represent the adsorption of MG on bentonite. The diffusive parameters were accurately estimated using the non−linear least squares; and the Student's t test, χ^2 test and the Fisher's exact test were performed in order to verify if the means and the variances of the model correspond to the experimental data.

2. Mathematical model

In this work, the overall rate of adsorption was interpreted with a PVSDM model previously advanced by Souza et al. [14]. This model was developed considering: batch system adsorption, ambient temperature; the particles of bentonite are spherical; the intraparticle diffusion can occur by pore volume and surface diffusion; the values of effective pore volume diffusion coefficient (D_p) and surface diffusion coefficient (D_s) are constant; and the adsorption rate on an active site is instantaneous. The model equations and the initial and boundary conditions are as follows:

$$V\frac{dC_A}{dt} = -mSk_F\left(C_A - C_{Ar}\big|_{r=R}\right) \tag{1}$$

$$t = 0, C_A = C_{A0} \tag{2}$$

$$\varepsilon_p\frac{\partial C_{Ar}}{\partial t} + \rho_p\frac{\partial q}{\partial t} = \frac{1}{r^2}\frac{\partial}{\partial r}\left[r^2\left(D_p\frac{\partial C_{Ar}}{\partial r} + \rho_p D_s\frac{\partial q}{\partial r}\right)\right] \tag{3}$$

$$t = 0, 0 \le r \le R, C_{Ar} = 0 \tag{4}$$

$$\left.\frac{\partial C_{Ar}}{\partial r}\right|_{r=0} = 0 \tag{5}$$

$$D_p \left.\frac{\partial C_{Ar}}{\partial r}\right|_{r=R} + \rho_p D_s \left.\frac{\partial q}{\partial r}\right|_{r=R} = k_F \left(C_A - C_{Ar}\big|_{r=R}\right) \quad (6)$$

In addition, the assumption that the adsorption on active sites is instantaneous implies that exists a local equilibrium between the MG concentration in the pore solution, C_{Ar}, and the mass of MG adsorbed on the pore surface, q [13]. This equilibrium relationship is represented by the adsorption isotherm. In a previous work, the isotherm models of Langmuir [15], Freundlich [16] and Redlich−Peterson [17] was fitted to the experimental adsorption equilibrium data and the results show that the Redlich−Peterson isotherm was the one that best interprets the data [14]. Consequently, the Redlich−Peterson isotherm was chosen to describe the equilibrium data of MG in bentonite at a distance r.

$$q = f\left(C_{Ar}\right) = \frac{k_{RP} C_{Ar}}{1 + a_{RP} C_{Ar}^{\beta}} \quad (7)$$

The estimated values of a_{RP}, k_{RP} and β were, respectively, 1.27 (L mg^{-1}), 148.83 (L g^{-1}) and 0.89 [14].

3. Experimental

Detailed information concerning adsorbate and characterization of the adsorbent can be obtained in the work of Souza et al. [14]. Briefly, the bentonite was collected and oven dried at 100°C for 48 h, ground (Wiley Mill Standard, 03, USA) and sieved until the mean diameter of Sauter from 47.4 μm.

The surface area, pore volume and pore diameter of bentonite, determined by the N_2−BET method [18] using a volumetric adsorption analyzer (Micromeritcs, ASAP 2020, USA), were S^{BET} = 172.66 m^2 g^{-1}, V_p = 0.315 cm^3 g^{-1}, and d_p = 7.30 nm, respectively. The solid density, reported in the literature [19] was ρ_s = 2.650 g cm^{-3}; the particle density, void fraction and external surface area, were ρ_p = 1.444 g cm^{-3}, ε_p = 0.445 and S = 877.42 cm^2 g^{-1}, respectively.

The batch adsorption tests were carried out in Erlenmeyer flasks of 125 mL, which were stirred in a thermostated shaker (Marconi, MA 093, Brazil) at different initial dye concentrations (150, 200, 250, 300 and 500 mg L^{-1}). 100 mg of bentonite were added in 50 mL

of the dye solutions and stirred at 150 rpm and 298 K. Aliquots were collected in preset time intervals (1, 2, 3, 4, 5, 10, 15, 20, 30, 60, 90, 120, 150, 180, 210 and 240 min) and also at equilibrium (the equilibrium was considered attained when the dye concentration in the liquid phase did not present difference between three consecutive measures). The aliquots were filtered through filter paper and the dye concentration was determined by UV−Visible spectrophotometer (Shimadzu, UV mini, Japan) at maximum wavelength of MG (λ_{max} = 618 nm) [1].

4. Model solution

The PVSDM model was fitted to the experimental concentration decay curves obtained. The model equations were solved numerically using a computer code developed and run in the MatLab® software. For this purpose, the partial differential equation of diffusional model can be rewritten using the second−order central difference approximations of the first and second derivative in Eq. (3). The second−order forward difference approximations of the first derivative can be used to solve the boundary condition at $r = 0$ in Eq. (5) and the second−order backward difference approximations of the first derivative can be used to solve the boundary condition at $r = R$ in Eq. (6) [14].

The resulting implicit algebraic equation of Eq. (6) can be solved by the MatLab® built−in routine *fsolve* [20] using the Levenberg−Marquardt algorithm [21, 22].

Discretized partial differential equations yield ordinary differential equation systems that are very stiff; therefore, can be solved by the MatLab® built−in routine *ode15s* that is a variable order solver based on the numerical differentiation formulas (NDFs) [23].

However, the values of the external mass transfer coefficient (k_F) and of the diffusion coefficients (D_p and D_s) are needed for solving the PVSDM model.

The external mass transfer coefficient (k_F) was estimated by the method proposed by Furusawa and Smith [24]. This method is based upon evaluating Eq. (1) at the initial conditions; $t = 0$, $C_A = C_{A0}$ and $C_{Ar} = 0$, and the following equation is obtained:

$$\left.\frac{d\left(C_A/C_{A0}\right)}{dt}\right|_{t=0} = -\frac{mSk_F}{V} \tag{8}$$

The term in the right of Eq. (8) is the slope of the curve C_A/C_{A0} versus t, at $t = 0$ and was estimated by using the first three data points.

The pore volume diffusion coefficient (D_p) can be described by the model based on the tortuosity factor, using the Eq. (9) [25, 26]:

$$D_p = \frac{D_{AB}\varepsilon_p}{\tau} \tag{9}$$

The pore volume coefficient calculated by Souza et al. [14] was $D_p = 6.11\times10^{-7}$ cm^2 s^{-1}.

Non−linear least square optimization can be used to estimate the surface diffusion coefficient (D_s). The non−linear least squares objective function to be minimized is defined as the sum of the differences between the experimental data (C_A) and model data ($\hat{C}_A$) of adsorbate concentration, Eq. (10), and the MatLab® built−in routine *lsqnonlin* can be used to solve it. By default, *lsqnonlin* chooses the Trust−Region−Reflective algorithm that is a subspace trust−region method and is based on the interior−reflective Newton method [27].

$$\min\left| f\left(D_S\right)\right| = \sum_{j=1}^{NE}\sum_{i=1}^{NY-1}\left[C_A(j,i) - \hat{C}_A(j,i)\right]^2 \tag{10}$$

The computer used to perform the model simulation and the parametric estimation was an IntelVR CoreTM i7−3770 with 3.40 GHz processor and 12 Gb of RAM memory and it is running with the Windows 7 64 bits Operating System.

5. Results and discussion

5.1. Concentration decay study

In the previous work, it was possible to conclude that both diffusive mechanisms (pore volume and surface) contribute to the adsorption of MG on bentonite; therefore, the implementation of the PVSDM model is necessary [14]. The experimental conditions and the mass transfer parameters for the adsorption of MG on bentonite was determined by Souza et al. [14] and are shown in Table 1. Moreover, the relative contribution of each diffusion mechanism

to the intraparticle mass transfer of the MG was estimated by computing the mass flux due to the pore volume diffusion, N_{AP}, and surface diffusion, N_{AS}, using the following equations:

$$\frac{N_{AP}}{N_{AP}+N_{AS}} = \frac{D_p\,\partial C_{Ar}/\partial r}{D_p\,\partial C_{Ar}/\partial r + D_s\rho_p\,\partial q/\partial r} \tag{11}$$

$$\frac{N_{AS}}{N_{AP}+N_{AS}} = \frac{D_s\rho_p\,\partial q/\partial r}{D_p\,\partial C_{Ar}/\partial r + D_s\rho_p\,\partial q/\partial r} \tag{12}$$

Table 1: Mass transfer parameters for the adsorption of MG on bentonite at different initial dye concentrations.

Exp.	C_{A0} (mg L^{-1})	C_{Ae} (mg L^{-1})	q_e (mg g^{-1})	k_F x 10^3 (cm s^{-1})	D_s x 10^{10} (cm^2 s^{-1})	$\frac{N_{AP}}{N_{AP}+N_{AS}0}$(%)	$\frac{N_{AS}}{N_{AP}+N_{AS}}$(%)
1	500	114.55	192.92	2.89	11.55	65.40	34.60
2	300	15.86	141.93	2.65	7.92	26.75	73.25
3	250	5.61	121.10	2.44	7.59	12.24	87.76
4	200	2.21	99.79	2.16	7.38	5.03	94.97
5	150	1.09	73.94	1.99	6.83	2.55	97.45

It was verified that the initial dye concentration increase caused an increase in the k_F values. This shows that at higher initial dye concentrations, the external mass transfer resistance was decreased. Similar dependences on the k_F in relation to C_{A0} were found in the phenol adsorption on organobentonite [28].

Other important physical trends can be seen in Table 1: (i) D_s values increased with the initial MG concentration; (ii) the relative contribution of surface diffusion (N_{AS}) decreased with the increase in the initial MG concentration, and consequently the, N_{AP} increased. The first fact can be explained as follows: the initial dye concentration (C_{A0}) increase caused an increase in the q_e values and, consequently, the D_s values increased [29, 30]. The MG dye molecules are adsorbed on the high energy sites and so few of the adsorbed molecules had enough energy to move along the surface from one site to another. Since the high energy sites have been occupied, the dye molecules would be adsorbed on the low−energy sites. Therefore, a greater number of molecules had enough energy to move from one site to the other [28, 30]. The second fact is consequence of the first. The same dependence on D_s with the C_{A0} was verified by others authors [28, 31].

5.2. Parameter estimation

Table 1 shows the mass transfer parameters for initial dye concentrations of 150, 200, 250, 300 and 500 mg L^{-1}. However, the results for initial dye concentrations lower than 300 mg L^{-1} have shown similar results for D_s. For this reason, the curve of 500 mg L^{-1} was neglected, and was determinate a D_s global parameter. The curve of 250 mg L^{-1} was used to validate the results. Thus, 1 parameter was estimated, for 3 experimental data set at 17 different time units. According to Eq. (13), 50 degrees of freedom were available for the statistical tests.

$$DF = NE.NY - NP \tag{13}$$

where *DF* is the degrees of freedom of the system, *NE* the number of experiments, *NY* the number of measures for each experiment, and *NP* the number of parameters.

The PVSDM model parameter, estimated with intervals of 95% of confidence, are given in Table 2. Simulations were performed using the model with the estimated parameter to compare to each set of experimental data and, hence, to check the fit accuracy. The Student's t−test was performed to find out if the means of the concentration decay curve experimental and concentration decay curve predicted by the model are significantly different. Further, the χ^2 and Fisher's exact test were also performed to verify if variances of the experimental and model data of concentration differ in any interesting way [32].

Table 2: Estimated parameter with intervals of 95% of confidence for the adsorption of MG on bentonite.

Parameter	Value
D_s (cm^2 s^{-1})	$7.73x10^{-10}$±1.94 $x10^{-10}$

Table 3 present the Student's t−test results, where μ is the mean value of the concentration of MG in aqueous solution. It can be seen that intervals of experimental and model data intercept each other, i. e. the means of all experimental data sets are equivalent to those found through the model prediction.

Table 3: Student's *t* test for concentration of MG in aqueous solution (μ is the mean of C_A).

	Exp. 2	Exp. 4	Exp. 5
Experimental	$60.61 < \mu < 81.31$	$38.37 < \mu < 53.84$	$29.14 < \mu < 40.82$
Model	$62.33 < \mu < 85.67$	$38.47 < \mu < 55.56$	$29.48 < \mu < 42.59$

Table 4 shows the χ^2 test results, where all variances of experimental and model data are contained into the intervals. Table 5 presents the Fisher's exact test results, where the variances ratios of experimental and model data are into the lower and upper limits, i. e. the model variances are also equivalent to experimental variances.

Table 4: χ^2 test for concentration of MG in aqueous solution (σ^2 is the variance of C_A)

	Exp. 2	Exp. 4	Exp. 5
Experimental	$2763.13 < \sigma^2 < 11028.51$	$1544.37 < \sigma^2 < 6164.07$	$880.36 < \sigma^2 < 3513.78$
Model	$2957.24 < \sigma^2 < 12348.96$	$1585.56 < \sigma^2 < 6621.04$	$933.26 < \sigma^2 < 3897.13$

Table 5: Fischer's exact test for concentration of MG in aqueous solution (Lower limit < $\sigma^2_{\text{exp}} / \sigma^2_{\text{mod}}$ < upper limit).

Exp. 2	Exp. 4	Exp. 5
$0.37 < 0.90 < 2.70$	$0.37 < 0.94 < 2.70$	$0.37 < 0.91 < 2.70$

In general, it can be asserted that the PVSDM model was statically suitable to represent the experimental data of the adsorption of MG onto bentonite. From the statistical viewpoint, the optimal parameter $D_s = 7.73 \times 10^{-10}$ cm^2 s^{-1} was significant (95% of confidence) and consistent with the three experimental data set, allowing the correct physical interpretation of the mass transfer phenomena that occurs in the adsorption of MG onto bentonite.

5.3. Model validation

In order to verify the reliability of the optimal value of $D_s = 7.73 \times 10^{-10}$ cm^2 s^{-1}, a new simulation was performed using a data set with an initial concentration different from the ones used to the parametric estimation. Fig. 1 shows the decay curve of the MG concentration at an initial concentration of 250 mg L^{-1}.

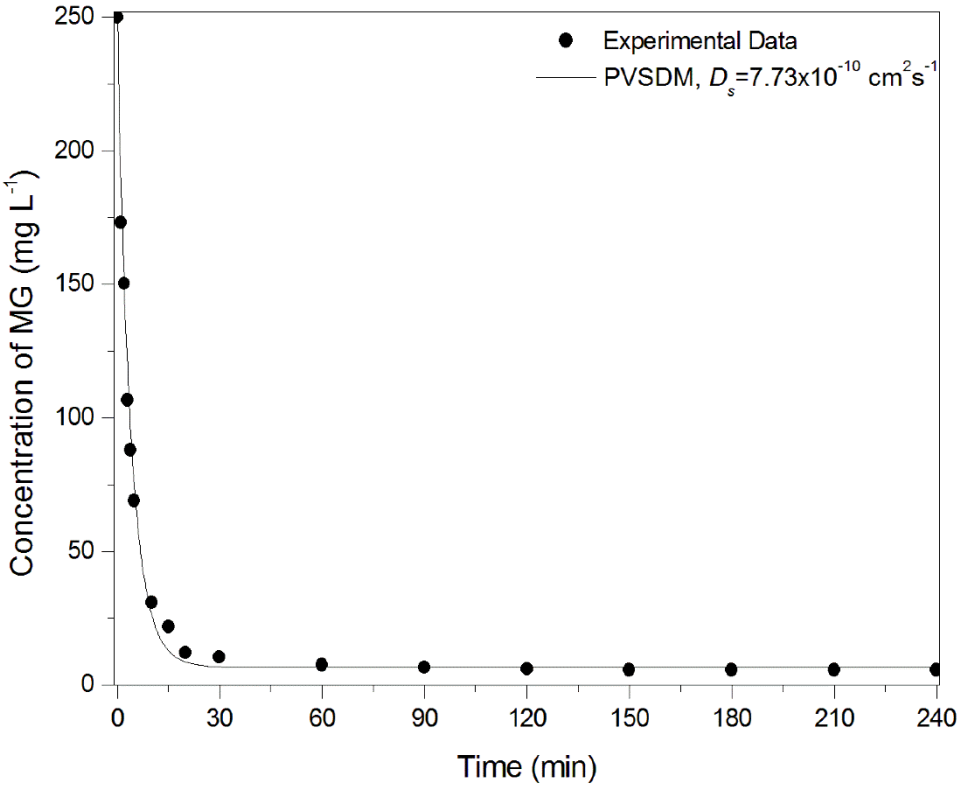

Fig. 1: Experimental concentration decay data and concentration decay curve predicted by the PVSDM at initial concentration of 250 mg L^{-1}.

According to the results of Fig. 1, it can be concluded that the estimated parameter, D_s, is capable of predicting adsorption kinetics of MG on bentonite at any initial concentration of MG ranging from 150 to 300 mg L^{-1}.

6. Conclusion

In this work, the PVSDM model was used to represent the adsorption data of the MG on bentonite at different initial concentrations. The parameter estimation problem was solved by the non−linear least squares method, and the confidence intervals showed that the estimated parameters were significant. In addition, the statistical analysis of Student's *t*−test, χ^2 test and Fisher's exact test showed that the model is equivalent to the experimental data of the process in a 95% confidence interval.

Due to the contribution of the surface diffusion and the pore volume diffusion mechanisms, the PVSDM model is the most adequate to interpret the adsorption of MG on bentonite. The values of D_s ranged from $6.83x10^{-10}$ to $7.92x10^{-10}$. In addition, a general value of $D_s = 7.73x10^{-10}$ was found to represent the adsorption phenomenon of the dye MG onto bentonite at initial dye concentration ranging from 150 to 300 mg L^{-1}.

Acknowledgement

The authors are grateful to National Council for the Improvement of Higher Education (CAPES) for granting the scholarship to the first author.

References

[1] S. Banerjee, G.C. Sharma, R.K. Gautma, M.C. Chattopadhyaya, S.N. Upadhyay, Y.C. Sharma, Removal of Malachite Green, a hazardous dye from aqueous solutions using Avena Sativa (oat) hull as a potential adsorbent, J. Mol. Liq. 213 (2016) 162−172.

[2] P. Geetha, M.S. Latha, M. Koshy, Biosorption of malachite green dye from aqueous solution by calcium alginate nanoparticles: Equilibrium study, J. Mol. Liq. 212 (2015) 723−730.

[3] S. Srivastava, R. Sinha, D. Roy, Toxicological effects of malachite green, Aquat. Toxicol. 66 (2004) 319−329.

[4] A.A. Zahhar, N.S. Awwad, Removal of malachite green dye from aqueous solutions using organically modified hydroxyapatite, J. Environ. Chem. Eng. 4 (2016) 633−638.

[5] K.A. Lin, W. Lee, Highly efficient removal of Malachite green from water by magnetic reduced grapheme oxide/zeolitic imidazolate framework self−assembled nanocomposite, Appl. Surf. Sci. 361 (2016) 114−121.

[6] J.A. Bañuelos, O. García−Rodríguez, A. El−Ghenymy, F.J. Rodríguez−Valadez, L.A. Godínez, E. Brillas, Advanced oxidation treatment of malachite green dye using a low cost carbon−felt air−diffusion cathode, J. Environ. Chem. Eng. 4 (2016) 2066−2075.

[7] L.W. Man, P. Kumar, T.T. Teng, K.L. Wasewar, Design of experiments for Malachite Green dye removal from wastewater using thermolysis – coagulation – flocculation, Des. Water. Treat. 40 (2012) 260–271.

[8] L. Du, M. Zhao, G. Li, F. Xu, W. Chen, Y. Zhao, Biodegradation of malachite green by Micrococcus sp. strain BD15: Biodegradation pathway and enzyme analysis, Int. Biodet. Biodeg. 78 (2013) 108−116.

[9] S. Arellano−Cárdenas, S. López−Cortez, M. Cornejo−Mazón, J.C. Mares−Gutiérrez, Study of malachite green adsorption by organically modified clay using a batch method, Appl. Surf. Sci. 280 (2013) 74−78.

[10] E.N. El−Qada, S.J. Allen, G.M. Walker, Adsorption of basic dyes from aqueous solutions onto activated carbon, Chem. Eng. J. 135 (2008) 174−184.

[11] L. Yan, L. Qin, H. Yu, S. Li, R. Shan, B. Du, Adsorption of acids dyes from aqueous solution by CTMAB modified bentonite: Kinetic and isotherm modeling, J. Mol. Liq. 211 (2015) 1074−1081.

[12] R. Leyva−Ramos, C.J. Geankoplis, Model simulation and analysis of surface diffusion of liquids in porous solids, Chem. Eng. Sci. 40 (1985) 799−807.

[13] R. Ocampo−Pérez, R. Leyva−Ramos, P. Alonso−Davila, J. Rivera−Utrilla, M. Sánchez−Polo, Modeling adsorption rate of pyridine onto granular activated carbon, Chem. Eng. J. 165 (2010) 133−141.

[14] P.R. Souza, G.L. Dotto, N.P.G. Salau, Detailed numerical solution of pore volume and surface diffusion model in adsorption systems, Chem. Eng. Res. Des. 122 (2017) 298–307.

[15] I. Langmuir, The adsorption of gases on plane surfaces of glass, mica and platinum, J. Am. Chem. Soc. 40 (1918) 1361−1403.

[16] H. Freundlich, Over the adsorption in solution, Z. Phys. Chem. A. 57 (1906) 358−471.

[17] O. Redlich, D.L. Peterson, A useful adsorption isotherm, J. Chem. Phys. 63 (1959) 1024−1027.

[18] R. Leyva−Ramos, R., Ocampo−Perez, J. Mendoza−Barron, External mass transfer and hindered diffusion of organic compounds in the adsorption on activated carbon cloth, Chem. Eng. J. 183 (2012) 141−151.

[19] D. Heier, T. Blackstock, K. Stack, D. Richardson, T. Lewis, Adsorption of wood extractives and model compounds onto bentonite, Colloid. Surf. A. 482 (2015) 213−221.

[20] K.F. Beers, Numerical Methods for Chemical Engineering, Cambridge University Press, New York, 2007.

[21] L. Levenberg, A method for the solution of certain nonlinear problems in least squares, Q. Appl. Math. 2 (1944) 164−168.

[22] D. Marquardt, An algorithm for least−squares estimation of nonlinear parameters, SIAM. J. Appl. Math. 11 (1963) 431−441.

[23] L.F. Shampine, M.W. Reichelt, The MATLAB ODE Suite, SIAM J. Sci. Comput. 18 (1997) 1−22.

[24] T. Furusawa, J.M. Smith, Fluid−particle and intraparticle mass transport rates in slurries, Ind. Eng. Chem. Fund. 12 (1973) 197−203.

[25] C.R. Wilke, P. Chang, Correlation of diffusion coefficients in dilute solutions, AIChE J. 1 (1955) 264−268.

[26] C. Valderrama, X. Gamisans, X. de las Heras, A.M. Farrán, J.L. Cortina, Sorption kinetics of polycyclic aromatic hydrocarbons removal using granular activated carbon: Intraparticle diffusion coefficients, J. Hazard. Mater. 157 (2008) 386−396.

[27] T.F. Coleman, Y. Li, An Interior, Trust Region Approach for Nonlinear Minimization Subject to Bounds, SIAM. J. Optimiz. 6 (1996) 418−445.

[28] R. Ocampo−Pérez, R. Leyva−Ramos, J. Mendonza−Barron, R.M. Guerrerro−Coronado, Adsorption rate of phenol from aqueous solution onto organobentonite: surface diffusion and kinetic models, J. Colloid. Interface Sci. 364 (2011) 195–204.

[29] D.M. Ruthven, Principles of Adsorption and Adsorption Processes, John Wiley & Sons, New York, 1984.

[30] M. Suzuki, Adsorption Engineering, Kodansha, Tokyo, 1990.

[31] G.L. Dotto, R. Ocampo−Pérez, J.N. Moura, T.R.S. Cadaval Jr., L.A.A. Pinto, Adsorption rate of Reactive Black 5 on chitosan based materials: geometry and swelling effects, Adsorption. 22 (2016) 973−983.

[32] M. Schwaab, J.C. Pinto, Experimental Data Analysis I. Fundamentals of Statistics and Parameter Estimation, E−papers, Rio de Janeiro, 2007.

5 MODELING OF HINDERED DIFFUSION OF CATIONIC DYES ADSORPTION ONTO BENTONITE

P.R. Souza, G.L. Dotto, N.P.G. Salau

Abstract

Mass transfer models considering the hindered diffusion were solved and applied for the adsorption crystal violet (CV) and methylene blue (MB) onto bentonite. The adsorption decay curves were obtained in batch system using different adsorbent dosages. Pore volume and surface diffusion model (PVSDM), surface diffusion model (SDM) and pore volume diffusion model (PVDM) were used to interpret the experimental data as well the hindered diffusion effect was taking into account. Results have shown that the adsorption of CV onto bentonite can be represented by both PVSDM and SDM models because the surface diffusion represented more than 92.5% of total intraparticle diffusion. The MB adsorption onto bentonite was represented by PVSDM model, but, in this case, the hindered diffusion effect was significant, since the size of MB molecules is similar to the basal space of the adsorbent. The values of surface diffusion coefficient increased with the mass of the dyes adsorbed at equilibrium. The Biot number confirmed that the intraparticle diffusion was the rate limiting step in the adsorption of CV and MB onto bentonite.

Keywords: Adsorption rate; Diffusional mass transfer model; Porosity; Hindered diffusion; Parameter estimation; Statistical analysis.

1. Introduction

The environmental contamination due the release of dye containing effluents, from paper, textile, food and paint industries has become a serious issue in recent years. It is estimated the existence of more than 10,000 dyes with different chemical structures available commercially [1]. In this study, crystal violet (CV) and methylene blue (MB) dyes were chosen. Crystal violet is a cationic dye used in dyeing textiles and coloring in paper, moreover, it is used as a biological stain, a dermatological agent, a veterinary medicine, and an additive to poultry feed to inhibit propagation of fungus [1–3]. Methylene blue is also a cationic dye used in textile industries and in color of paper, furthermore is an antiseptic against bacterial infection and antidote for cyanide poisoning [4,5]. Both dye molecules are highly toxic, potentially carcinogenic, mutagenic and allergenic on exposed organisms [6–8]. For these reasons, the treatment of industrial wastewaters with these two dyes is of significant concern.

Several scientific studies have shown that popular processes such as electrochemical degradation, biological treatments [10,11], oxidation [12,13] and adsorption [1–4] can be used

for the removal of different dyes from aqueous phase. Among these processes, adsorption stands out in relation to other techniques, in terms of cost, simplicity of design and ability to separate a wide variety of compounds [14,15]. It has been demonstrated in the literature that bentonite has high potential for removal of cationic dyes in aqueous solutions, due to its high specific surface area, swelling capacity and cation exchange capacity [16].

It is well known that diffusional models are the most realistic way to predict adsorption in porous solids, because they include three simultaneous steps: external mass transport, intraparticle diffusion and active site adsorption. Particularly, intraparticle diffusion may be due to pore volume diffusion (PVDM), surface diffusion (SDM), or a combination of both mechanisms (PVSDM) [17]. In previous works, PVSDM model was used to represent the adsorption of malachite green onto bentonite at different initial concentrations of dye [18,19]. However, it can be found in the literature the significance of the hindered diffusion in the adsorption of MB onto activated carbon. Such diffusion consists of steric exclusion, drag effects and obstruction due to molecules adsorbed on the pore walls [20].

This work aimed to elucidate in detail the overall adsorption rate of cationic dyes onto bentonite. The experimental adsorption of crystal violet (CV) and methylene blue (MB) were chosen as case studies. PVSDM, SDM and PVDM models were solved and used to interpret the experimental adsorption decay curves. The diffusive parameters were accurately estimated using the non−linear least squares; and Student's t−test, χ^2 test and Fisher's exact test were performed in order to verify if the means and the variances of each diffusional model corresponds to the experimental data. Besides, the effect of hindered diffusion in the adsorption was carefully inspected.

2. Mathematical model

2.1. Model development

Generally, in solid–liquid adsorption systems it is considered that the mass transfer can occur in three steps: external mass transfer, intraparticle diffusion and adsorption on active sites. The intraparticle diffusion may be controlled by pore volume diffusion, surface diffusion or a combination of both mechanisms [17,21–23]. Furthermore, the following preliminary assumptions were made for the considered system: batch system adsorption, ambient

temperature; the particles of bentonite are spherical; the intraparticle diffusion can occur by pore volume and surface diffusion; the values of effective pore volume diffusion coefficient (D_p) and surface diffusion coefficient (D_s) are constant. Based on the above assumptions, the model equations and the initial and boundary conditions are as follows [17]:

$$V\frac{dC_A}{dt} = -mSk_F\left(C_A - C_{Ar}\big|_{r=R}\right) \tag{1}$$

$$t = 0, C_A = C_{A0} \tag{2}$$

$$\varepsilon_p\frac{\partial C_{Ar}}{\partial t} + \rho_p\frac{\partial q}{\partial t} = \frac{1}{r^2}\frac{\partial}{\partial r}\left[r^2\left(D_p\frac{\partial C_{Ar}}{\partial r} + \rho_p D_s\frac{\partial q}{\partial r}\right)\right] \tag{3}$$

$$t = 0, 0 \le r \le R, C_{Ar} = 0 \tag{4}$$

$$\left.\frac{\partial C_{Ar}}{\partial r}\right|_{r=0} = 0 \tag{5}$$

$$D_p\left.\frac{\partial C_{Ar}}{\partial r}\right|_{r=R} + \rho_p D_s\left.\frac{\partial q}{\partial r}\right|_{r=R} = k_F\left(C_A - C_{Ar}\big|_{r=R}\right) \tag{6}$$

The model represented by Eqs. (1) – (6) is the pore volume and surface diffusion (PVSDM). PVSDM model can be simplified by considering that the sole intraparticle diffusion mechanism may be either pore volume diffusion (PVDM) or surface diffusion (SDM). In this work, the adsorption of dyes in active sites was considered instantaneous [23], and there is a local equilibrium between the concentration of dyes in the solution of pores, C_{Ar}, and the mass of dyes adsorbed on the pore surface, q [24]. This equilibrium relationship is represented by the adsorption isotherm:

$$q = f\left(C_{Ar}\right) \tag{7}$$

2.2. Model solution

PVSDM model was solved according to the numerical solution proposed by Souza et al. [18]. In brief, the model equations were numerically solved using a computer code developed and run in the MatLab® software. For this purpose, the partial differential equations of the diffusional model were expressed as a system of simultaneous ordinary differential equations

by the application of the method of finite difference approximations. The resulting system of ordinary differential equations are very stiff; therefore, to avoid a very small time step, an implicit method was chosen and, hence, the system was solved with the MatLab® built−in routine *ode15s*, a variable order solver based on the numerical differentiation formulas (NDFs).

2.3. Estimation of the mass transfer parameters

The external mass transfer coefficient (k_F) was estimated by the method proposed by Furusawa and Smith [25]. This method is based upon evaluating Eq. (1) at the initial conditions; $t = 0$, $C_A = C_{A0}$ and $C_{Ar} = 0$ and the following equation is obtained:

$$\left.\frac{d\left(C_A/C_{A0}\right)}{dt}\right|_{t=0} = -\frac{mSk_F}{V} \tag{8}$$

The term in the right of Eq. (8) is the slope of the curve C_A/C_{A0} versus t, at $t = 0$ and was estimated by using the first two data points.

Many relations have been developed to estimate D_p, and some of the relations are based on the molecular diffusivity of the solute and in the porous structure of the solid. The simplest empirical model is based upon the tortuosity factor and is represented by the following equation [26,27]:

$$D_p = \frac{D_{AB}\varepsilon_p}{\tau} \tag{9}$$

In a previous work, the tortuosity factor of bentonite was mentioned equal to 5.24 [18]. The molecular diffusivities were estimated with the Wilke and Chang correlation [26,27]:

$$D_{AB} = 7.4\times10^{-8}\left[\frac{(\varphi M_B)^{0.5}T}{\eta_B V_A^{0.6}}\right] \tag{10}$$

Non−linear least square optimization was used to estimate the surface diffusion coefficient (D_s). The non−linear least squares objective function to be minimized is defined as the sum of the differences between the experimental data (C_A) and model data ($\hat{C}_A$) of adsorbate

concentration, as given by Eq. (11). This objective function was minimized with the MatLab® built−in routine *lsqnonlin* using the Trust−Region−Reflective algorithm [28].

$$\min\left| f\left(D_S\right)\right| = \sum_{j=1}^{NE} \sum_{i=1}^{NY-1} \left[C_A(j,i) - \hat{C}_A(j,i)\right]^2 \tag{11}$$

The computer used to perform the model simulation and the parametric estimation was an IntelVR CoreTM i7−3770 with 3.40 GHz processor and 12 Gb of RAM memory and it is running with the Windows 7 64 bits Operating System.

3. Materials and methods

3.1. Adsorbent

The bentonite used in this study was collected in province of Mendoza (Argentina), oven dried at 100°C for 48 h, ground (Wiley Mill Standard, 03, USA) and sieved until the discrete particle size ranging from 45 to 250 μm. The mean diameter of Sauter was 47.4 μm.

The surface area, pore volume and pore diameter of bentonite, determined by the N_2−BET method [20] using a volumetric adsorption analyzer (Micromeritcs, ASAP 2020, USA), were S^{BET} = 172.66 $m^2\,g^{-1}$, V_p = 0.315 $cm^3\,g^{-1}$, and d_p = 7.30 nm, respectively. The solid density, reported in the literature [29] was ρ_s = 2.650 g cm^{-3}; the particle density, void fraction and external surface area, were ρ_p = 1.444 g cm^{-3}, ε_p = 0.445 and S = 877.42 $cm^2\,g^{-1}$, respectively. More detailed characterization was published elsewhere [18].

3.2. Cationic dyes

Distilled water was used to prepare all solutions. All reagents were of analytical grade. The crystal violet (CV) (maximum wavelength of 590 nm) and methylene blue (MB) (maximum wavelength of 664 nm) were supplied by Inlab with purity higher than 96 wt. %, and was used without further purification. The molecular structure and physical properties of these dyes are listed in Table 1. The molecular structures were obtained from MarvinSketch software, version 14.9.22.0.

Table 1: Physicochemical properties of CV and MB dyes.

Dye	Molecular structure	Molecular formula	Molecular weight (g mol^{-1})	Molar volume (cm^3 mol^{-1})
CV	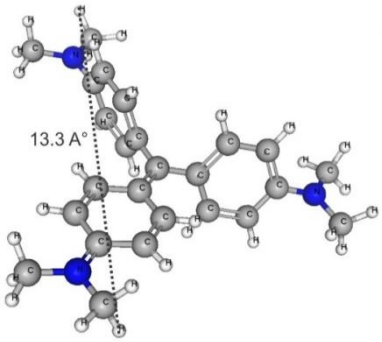	$C_{25}H_{30}N_3Cl$	407.98	223.93
MB	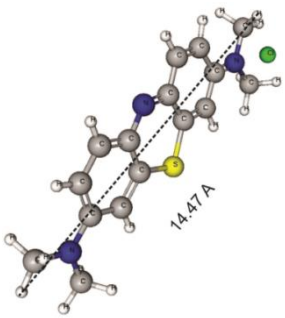	$C_{16}H_{18}N_3SCl$	319.85	157.18

3.3. Batch adsorption experiments

Erlenmeyer flasks of 125.0 mL were used as a batch adsorber to get the experimental data of cationic dyes. The experiments were performed with 50.0 mL of dye solution with initial concentration of 100.0 mg L^{-1} at different adsorbent dosages (0.0125, 0.0250, 0.0375, 0.0500 g) weighing in analytical balance (Marte, AY220, Brazil). The solutions were stirred at 300 rpm and 298 K in a thermostatic shaker (Solab, SL 222, Brazil). Aliquots were withdrawn at different time intervals until the equilibrium (the equilibrium was judged reached when the dye concentration in the liquid did not present difference between three consecutive measures), filtered through filter paper (the filter paper presented no significant interference in the dyes quantification) and the dye concentration was determined by UV−Visible spectrophotometer (Shimadzu, UV mini, Japan) at maximum wavelength of each dye. For each experimental point (each time), one separate Erlenmeyer was used, to ensure that the volume used to quantify the

dyes was negligible in relation to the total volume of the solution. To guarantee the experimental accuracy, reproducibility and reliability of the collect data, the adsorption experiments were performed in triplicate; blanks were run in parallel and all dye solutions were stored in glass flasks, which were cleaned by soaking HNO_3 (1.5 mol L^{-1}) for 24 h.

4. Results and discussion

4.1. Adsorption isotherm

The adsorption isotherms are primordial to determine the mathematical relation between the dye concentration in the solution within the pore of the adsorbent and the mass of dye adsorbed on the pore surface. This relation is substituted in Eq. (7) and the diffusional model can be solved. The experimental equilibrium curves for the adsorption of CV and MB onto bentonite are graphed in Fig. 1. It can be observed in Fig. 1 that at low equilibrium concentrations, the isotherms presented an inclined portion, followed by a plateau at high concentrations. Thus, both isotherms have shown the type I behavior according to the IUPAC classification [30], confirming the high affinity among the adsorbate molecules and adsorbent surface. The adsorption isotherm of Redlich–Peterson [31] was fitted to the adsorption equilibrium data of both dyes. This adsorption isotherm can be represented by the following equation:

$$q = \frac{k_{RP} C_{Ar}}{1 + a_{RP} C_{Ar}^{\beta}} \tag{12}$$

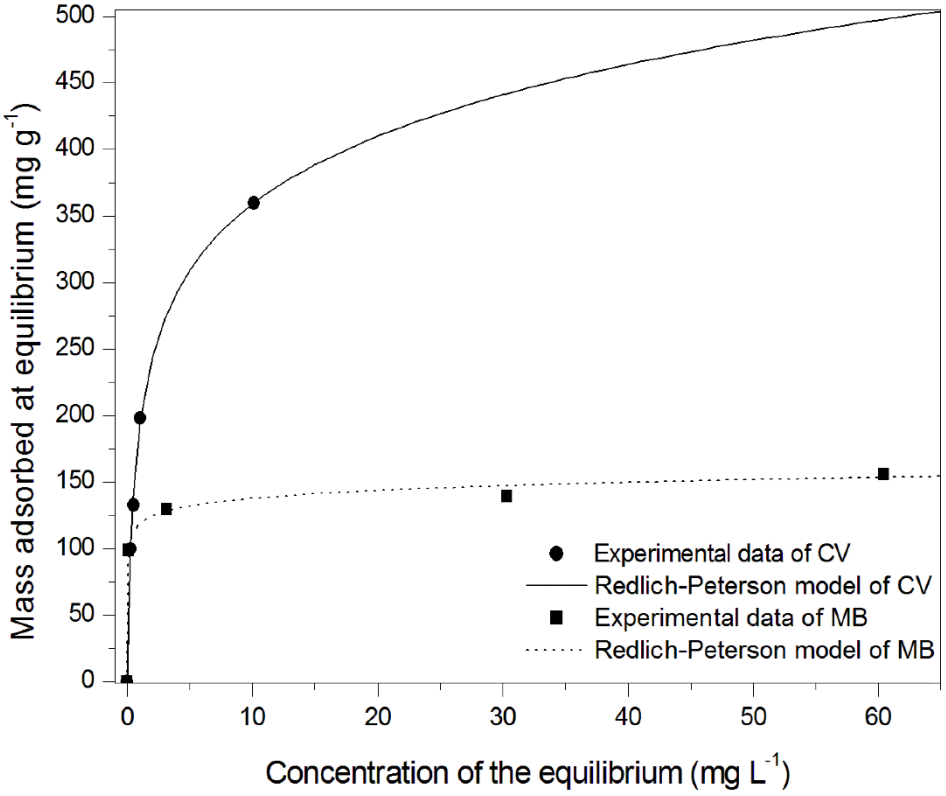

Fig. 1: Redlich–Peterson isotherm for CV and MB adsorption onto bentonite.

The values of the isotherm constants were obtained by parameter optimization of the non–linear least square function. The parameter optimization was solved by the MatLab® function *lsqnonlin* using the Trust–Region–Reflective algorithm [28] and the values of the estimated constants are displayed in Table 2.

Table 2: Constants of the Redlich–Peterson isotherm for CV and MB adsorption onto bentonite.

Dye	k_{RP} (L g^{-1})	a_{RP} (L^{β} $mg^{-\beta}$)	β	R^2
CV	731.24	2.80	0.84	0.999
MB	13747.32	114.51	0.94	0.998

Based on the high values of the coefficient of determination (R^2) presented in Table 2, it can be seen that the Redlich–Peterson model was able to explain the equilibrium adsorption of CV and MB onto bentonite.

4.2. Case study 1: Adsorption of CV onto bentonite

The diffusional models (PVSDM, SDM and PVDM) were used to represent the experimental data of the adsorption decay curves of CV at different adsorbent dosages. Fig. 2 shows the experimental and modeled data for the adsorption of CV onto bentonite. It was found that the experimental data presented a typical behavior, with C_A starting from C_{A0} and tending to C_e. As it can be seen in Fig. 2, PVDM model was not able to interpret the experimental data and overestimated the dye concentration decay curve, i.e. the rate of adsorption of CV onto bentonite was much faster than the one predicted with PVDM model. However, both PVSDM and SDM models agreed very well with the experimental data, once that the modeled curves were overlapped.

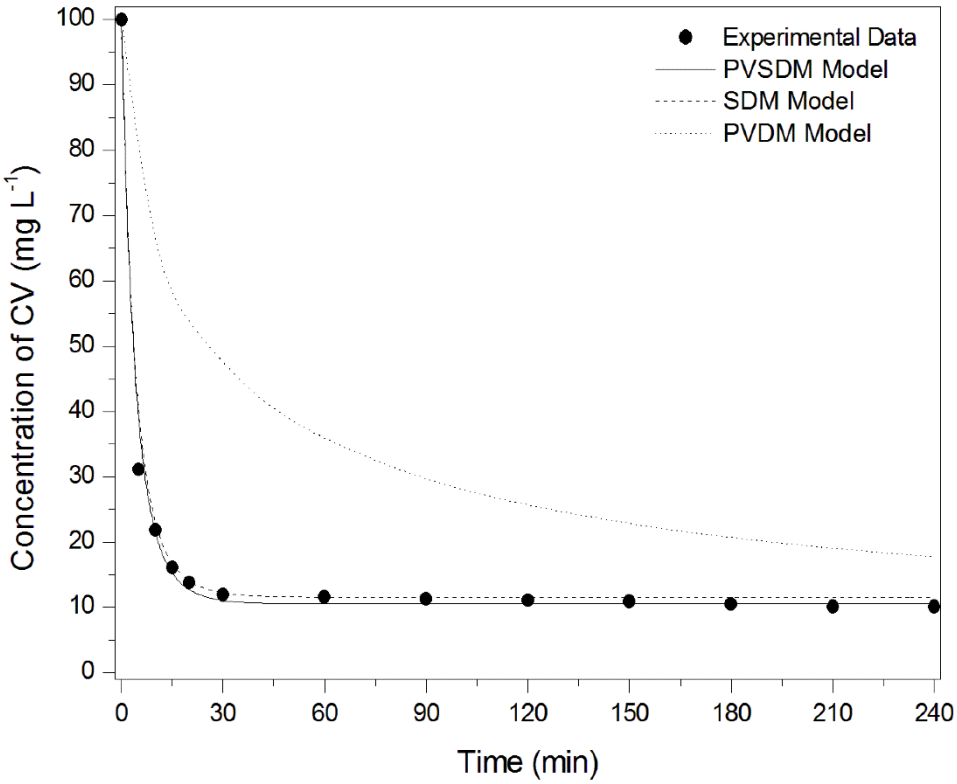

Fig. 2: Fit of PVSDM, SDM and PVDM models for the adsorption decay curves of CV onto bentonite.

The Student's t−test was performed to find out if the means of the concentration decay curve experimental and concentration decay curve predicted by the models are significantly different. Further, the χ^2 and Fisher's exact test were also performed to verify if variances of the experimental and models data of concentration differ in any interesting way [32]. The results of the statistical tests at 95% of confidence are presented in Table 3.

Table 3: Statistical analysis of PVSDM, SDM and PVDM models for adsorption of CV on bentonite.

	Student's t test	**χ^2 test**	**Fischer's exact**	**Objective Function value**	**R^2**
Experiment 1	$4.117 < \mu_{exp} < 13.27$	$389.78 < \sigma^2_{exp} < 2065.54$	$LL < \sigma^2_{exp}/\sigma^2_{mod} < UL$		
PVSDM	$3.62 < \mu_{mod} < 13.61$	$380.42 < \sigma^2_{mod} < 2185.37$	$0.32 < 1.00 < 3.15$	0.998	0.999
SDM	$3.62 < \mu_{mod} < 13.62$	$380.40 < \sigma^2_{mod} < 2185.23$	$0.32 < 1.00 < 3.15$	0.989	0.999
PVDM	$10.82 < \mu_{mod} < 21.22$	$411.69 < \sigma^2_{mod} < 2365.02$	$0.32 < 0.92 < 3.15$	2324.87	0.923
Experiment 2	$4.98 < \mu_{exp} < 14.10$	$386.94 < \sigma^2_{exp} < 2050.46$	$LL < \sigma^2_{exp}/\sigma^2_{mod} < UL$		
PVSDM	$4.33 < \mu_{mod} < 14.31$	$378.33 < \sigma^2_{mod} < 2173.38$	$0.32 < 0.99 < 3.15$	2.882	0.999
SDM	$4.34 < \mu_{mod} < 14.31$	$378.28 < \sigma^2_{mod} < 2173.08$	$0.32 < 0.99 < 3.15$	2.814	0.999
PVDM	$14.38 < \mu_{mod} < 24.96$	$425.72 < \sigma^2_{mod} < 2445.59$	$0.32 < 0.89 < 3.15$	3462.74	0.900
Experiment 3	$7.02 < \mu_{exp} < 16.10$	$383.40 < \sigma^2_{exp} < 2031.73$	$LL < \sigma^2_{exp}/\sigma^2_{mod} < UL$		
PVSDM	$6.20 < \mu_{mod} < 16.14$	$375.97 < \sigma^2_{mod} < 2159.80$	$0.32 < 0.99 < 3.15$	10.505	0.998
SDM	$6.23 < \mu_{mod} < 16.17$	$375.78 < \sigma^2_{mod} < 2158.70$	$0.32 < 0.99 < 3.15$	10.116	0.998
PVDM	$21.37 < \mu_{mod} < 32.08$	$436.96 < \sigma^2_{mod} < 2510.20$	$0.32 < 0.86 < 3.15$	5663.100	0.878
Experiment 4	$16.70 < \mu_{exp} < 24.86$	$310.00 < \sigma^2_{exp} < 1642.74$	$LL < \sigma^2_{exp}/\sigma^2_{mod} < UL$		
PVSDM	$16.49 < \mu_{mod} < 25.59$	$314.96 < \sigma^2_{mod} < 1809.32$	$0.32 < 0.96 < 3.15$	68.966	0.988
SDM	$17.58 < \mu_{mod} < 26.58$	$308.56 < \sigma^2_{mod} < 1772.35$	$0.32 < 0.98 < 3.15$	94.456	0.990
PVDM	$39.78 < \mu_{mod} < 49.29$	$344.28 < \sigma^2_{mod} < 1977.78$	$0.32 < 0.88 < 3.15$	10689.257	0.877

In Table 3, for all models, the χ^2 and Fisher's exact test results have shown that the variances are contained into the intervals, meaning that models variances are also equivalent to experimental variances. Furthermore, it can be observed that both PVSDM and SDM models have intercepted the experimental intervals for the Student's t–test for all the experiments. Differently, PVDM model has not intercepted the experimental intervals, i. e. the means of the experimental data for all experiments are not equivalent to those found through the models simulated data. Thus, PVDM model cannot be considered equivalent to the process data, showing that this model is not good enough when compared to PVSDM and SDM models.

To accurately quantify the residuals of all experiments, Table 3 presents a comparison of the objective function values (Eq. 13) for the three models tested. It can be seen that PVDM model has presented the highest value for the objective function and, therefore, it is not able to accurately explain the adsorption phenomenon.

The relative contribution of each diffusion mechanism to the intraparticle mass transfer of the CV was estimated by computing the mass flux due to the pore volume diffusion, N_{AP}, and surface diffusion, N_{AS}, [17,20] using the following equations:

$$\frac{N_{AP}}{N_{AP}+N_{AS}} = \frac{D_p\,\partial C_{Ar}/\partial r}{D_p\,\partial C_{Ar}/\partial r + D_s\rho_p\,\partial q/\partial r} \tag{13}$$

$$\frac{N_{AS}}{N_{AP}+N_{AS}} = \frac{D_s\rho_p\,\partial q/\partial r}{D_p\,\partial C_{Ar}/\partial r + D_s\rho_p\,\partial q/\partial r} \tag{14}$$

It is depicted in Fig. 3 the relative contribution of each diffusive mechanism during adsorption of CV onto bentonite as a function of the particle radius and time. The results have indicated that the contribution of surface diffusion represented over 92.5% of the total intraparticle diffusion on CV, regardless of radial position and time. Consequently, the intraparticle diffusion was predominantly due to surface diffusion.

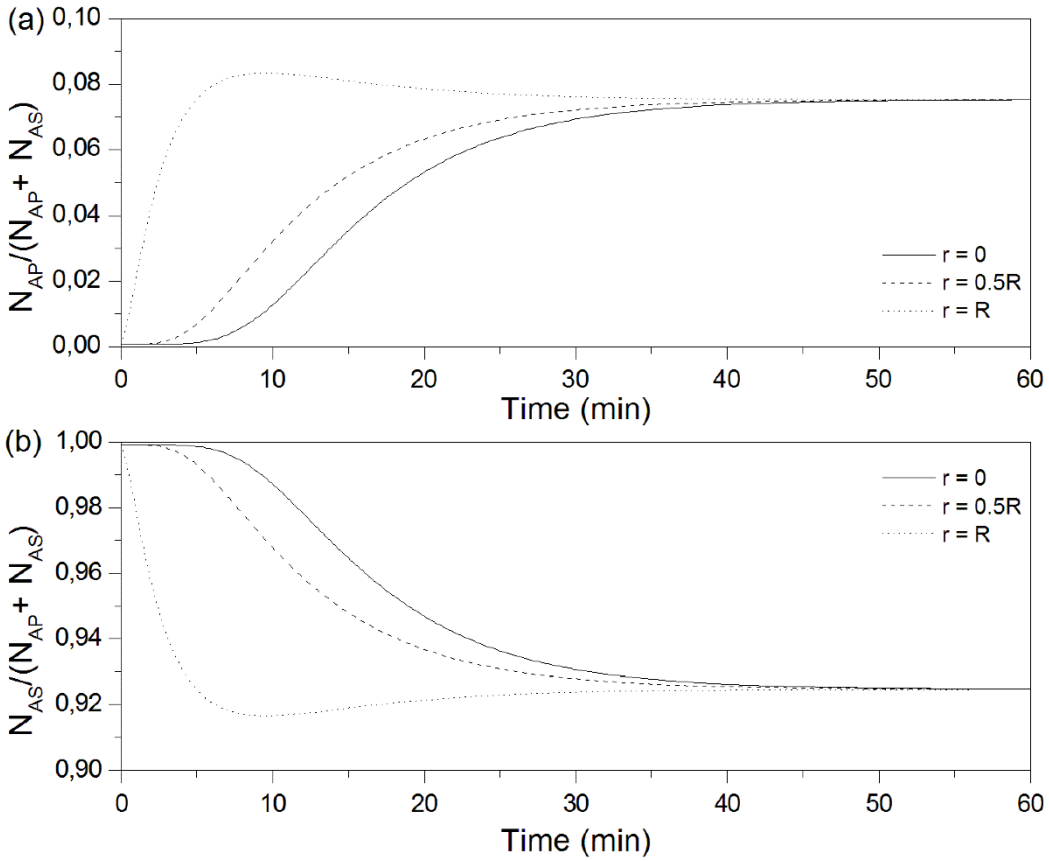

Fig. 3: (a) Contribution of pore volume diffusion and (b) surface diffusion to the intraparticle diffusion at different radial positions for CV dye.

As a result, both, the general PVSDM model and the simplified SDM model can be used to interpret the adsorption process of CV onto bentonite. In Table 4, it is possible to verify the conditions and estimated parameters of both models for all the experiments. From Table 4, it is possible corroborate that PVSDM and SDM are adequate, since the D_s values estimated from both models were similar. Consequently, it is possible to confirm that the surface diffusion is the main intraparticle mechanism involved onto the CV adsorption onto bentonite.

Table 4: Experimental conditions and estimated parameters for the concentration decay curves of CV on bentonite, C_{A0} = 100 mg L^{-1}.

Exp	m (g)	C_{Ae} (mg L^{-1})	q_e (mg g^{-1})	$k_F \times 10^3$ (cm s^{-1})	$D_s^{PVSDM} \times 10^{10}$ (cm^2 s^{-1})	$D_s^{SDM} \times 10^{10}$ (cm^2 s^{-1})	*Bi*
1	0.0500	0.24	99.76	9.27	6.21	6.19	24.62
2	0.0375	0.48	132.69	9.97	6.37	6.30	19.57
3	0.0250	1.03	197.94	10.93	6.47	6.37	14.22
4	0.0125	10.12	359.53	17.76	7.01	6.49	12.48

4.3. Case study 2: Adsorption of MB onto bentonite

The concentration decay curves predicted with PVSDM, SDM and PVDM models were plotted in Fig. 4 to elucidate the experimental data of the MB adsorption onto bentonite, at different adsorbent dosages. It is observed in Fig. 4 that SDM model satisfactorily interpreted the MB adsorption data onto bentonite using the optimal value of D_s = 1.66×10^{-10} cm^2 s^{-1}. PVDM model using the value of D_p = 6.98×10^{-7} cm^2 s^{-1} could not interpret the experimental data of concentration decay; the time to achieve the predicted PVDM equilibrium was 90 min, but the experimental value was 240 min (Fig. 4). Startling, PVSDM model using the values of D_p = 6.98×10^{-7} cm^2 s^{-1} and the estimated value of D_s = 3.46×10^{-10} cm^2 s^{-1} could not interpret the experimental data from the decay curves of MB onto bentonite. It was expected that PVSDM model would present the best result because it considers both surface and pore volume diffusion effects. Thus, a possible explanation is that the molecular diameter of MB (14.47 A°) is very close to the basal space of bentonite (15.2 A°) and thereby, the diffusion is restricted.

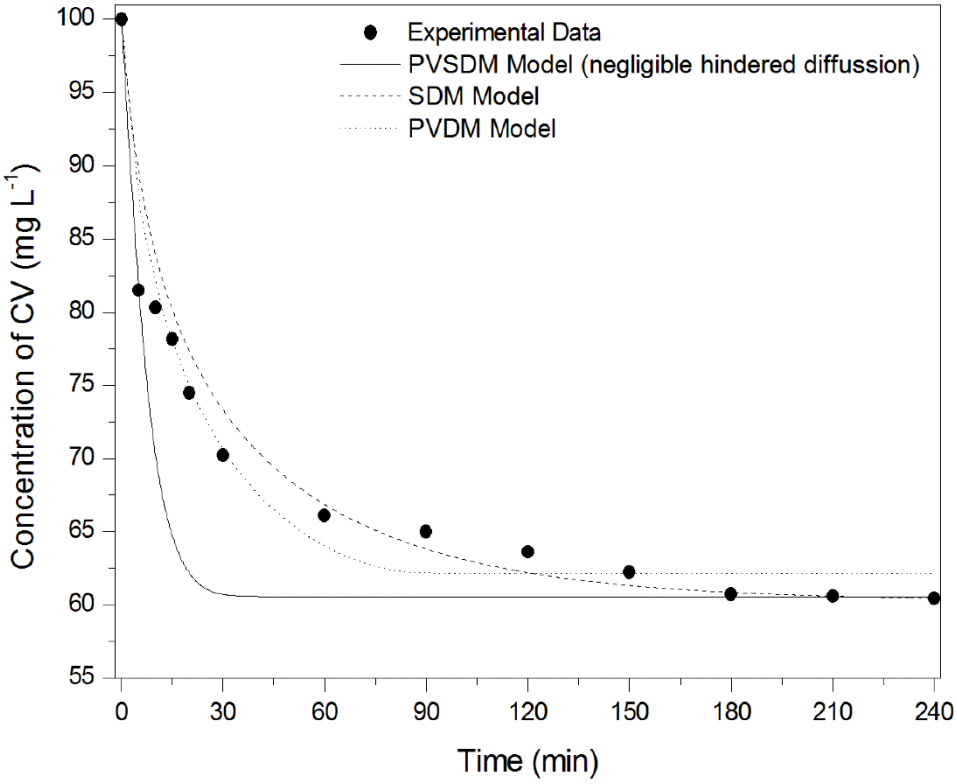

Fig. 4: Fit of PVSDM, SDM and PVDM models for the adsorption decay curves of MB onto bentonite.

Satterfield et al. [33] have upgraded the Eq. (9) to include the effect due to restricted diffusion and suggested the following equation:

$$D_p = \frac{K_p K_r D_{AB} \varepsilon_p}{\tau} \tag{15}$$

where K_p are K_r are the hindrance factors for the steric exclusion and wall drag effects, respectively. Various correlations have been proposed to estimate K_p and K_r, when the correlations are dependent on the ratio of the molecular diameter (*dm*) to the average pore diameter (*dp*) [20,34–40]. However, these models are polynomials of order other than zero, i. e. the values of K_p and K_r have different roots. Hence, in this work, a new parameter *K* was used to estimate the hindrance factors. This new parameter *K* encompasses the both steric exclusion and wall drag effects.

$$K = K_p K_r \tag{16}$$

In this case, the non−linear least squares objective function to be minimized is represented by the following equation:

$$\min\left| f\left(K, D_S\right)\right| = \sum_{j=1}^{NE} \sum_{i=1}^{NY-1} \left[C_A(j,i) - \hat{C}_A(j,i)\right]^2 \tag{17}$$

New simulations were performed and compared with each set of experimental data. Fig. 5 shows the experimental and modeled data for the adsorption of MB onto bentonite. It was observed that PVSDM model using the optimal values of D_s = 1.91 ×10^{-10} cm^2 s^{-1}and K = 0.014 has agreed very well with the experimental data of adsorption decay. Comparing Figs. 4 and 5, it can be noticed that PVSDM model only agree with the experimental data if the hindered diffusion effect is considered.

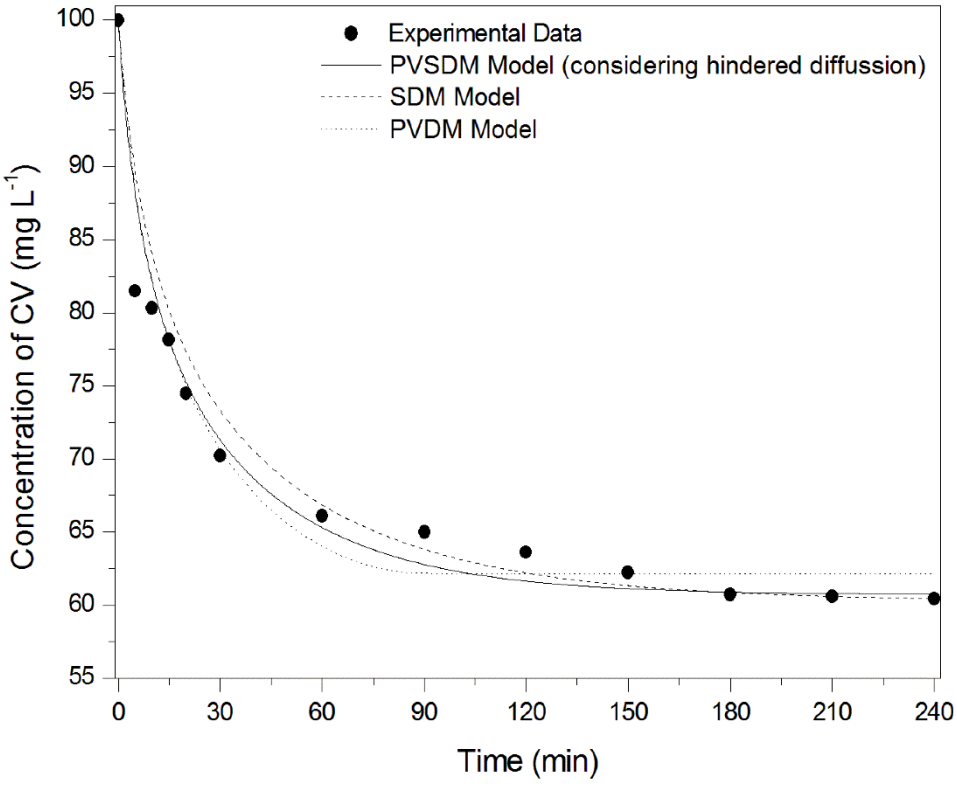

Fig. 5: Fit of PVSDM, SDM and PVDM models for the adsorption decay curves of MB onto bentonite.

To corroborate with the graphical analysis, statistical tests were also performed and are presented in Table 5.

Table 5: Statistical analysis of PVSDM, SDM and PVDM models for adsorption of MB on bentonite.

	Student's t test	**χ^2 test**	**Fischer's exact**	**Objective Function value**	**R^2**
Experiment 1	$12.22 < \mu_{exp} < 22.27$	$470.44 < \sigma^2_{exp} < 2492.97$	$LL < \sigma^2_{exp}/\sigma^2_{mod} < UL$		
PVSDM	$10.64 < \mu_{mod} < 21.18$	$423.11 < \sigma^2_{mod} < 2430.63$	$0.32 < 1.09 < 3.15$	19.985	0.999
SDM	$10.24 < \mu_{mod} < 20.64$	$411.95 < \sigma^2_{mod} < 2366.51$	$0.32 < 1.11 < 3.15$	39.856	0.999
PVDM	$20.39 < \mu_{mod} < 31.62$	$479.39 < \sigma^2_{mod} < 2753.93$	$0.32 < 0.96 < 3.15$	1775.434	0.974
Experiment 2	$17.25 < \mu_{exp} < 27.17$	$458.50 < \sigma^2_{exp} < 2429.67$	$LL < \sigma^2_{exp}/\sigma^2_{mod} < UL$		
PVSDM	$16.63 < \mu_{mod} < 27.22$	$427.19 < \sigma^2_{mod} < 2454.04$	$0.32 < 1.05 < 3.15$	26.932	0.998
SDM	$15.87 < \mu_{mod} < 26.13$	$399.94 < \sigma^2_{mod} < 2297.51$	$0.32 < 1.12 < 3.15$	162.545	0.998
PVDM	$27.36 < \mu_{mod} < 38.26$	$451.93 < \sigma^2_{mod} < 2596.16$	$0.32 < 0.99 < 3.15$	2217.465	0.967
Experiment 3	$42.61 < \mu_{exp} < 49.57$	$225.01 < \sigma^2_{exp} < 1192.36$	$LL < \sigma^2_{exp}/\sigma^2_{mod} < UL$		
PVSDM	$42.24 < \mu_{mod} < 50.13$	$237.22 < \sigma^2_{mod} < 1362.72$	$0.32 < 0.93 < 3.15$	32.905	0.994
SDM	$43.08 < \mu_{mod} < 50.90$	$232.81 < \sigma^2_{mod} < 1337.38$	$0.32 < 0.94 < 3.15$	34.953	0.991
PVDM	$43.29 < \mu_{mod} < 51.86$	$279.29 < \sigma^2_{mod} < 1604.41$	$0.32 < 0.79 < 3.15$	271.035	0.985
Experiment 4	$68.93 < \mu_{exp} < 72.86$	$71.74 < \sigma^2_{exp} < 380.19$	$LL < \sigma^2_{exp}/\sigma^2_{mod} < UL$		
PVSDM	$69.10 < \mu_{mod} < 73.70$	$80.51 < \sigma^2_{mod} < 462.55$	$0.32 < 0.87 < 3.15$	51.017	0.987
SDM	$69.99 < \mu_{mod} < 74.71$	$84.81 < \sigma^2_{mod} < 487.19$	$0.32 < 0.83 < 3.15$	95.220	0.983
PVDM	$69.35 < \mu_{mod} < 73.88$	$77.16 < \sigma^2_{mod} < 443.27$	$0.32 < 0.891 < 3.15$	65.150	0.983

In according with Table 5, the χ^2 and Fisher's exact test results have indicated that the variances are contained into the intervals for all models, i.e. the model variances are intercept with the experimental variances. The Student's t–test has revealed that, for the experiment 2, PVDM model has not intercepted the interval, and thereby cannot be considered equivalent to the process data. However, both PVSDM and SDM models have intercepted the interval demonstrating that the means of the experimental data for all experiments are equivalent to the models simulated data with 95% of confidence.

It was added in Table 5 the objective function values for the three models simulated. It can be seen that PVSDM model has presented the smallest value for the objective function and, hence, it was much better than the other tested models for modeling of MB onto bentonite adsorption.

Fig. 6 shows the relative contribution of each diffusive mechanism as a function of the particle radius and time for the adsorption of MB onto bentonite. The graphics have indicated that the relative contribution of both mechanisms was dependent on the time and the radial position in the particle; and the contribution of surface diffusion and pore volume diffusion were respectively, 80 and 20% of the global intraparticle diffusion. This result has suggested that the adsorption of MB onto bentonite involves a combination of the both internal resistances, requiring the implementation of PVSDM model.

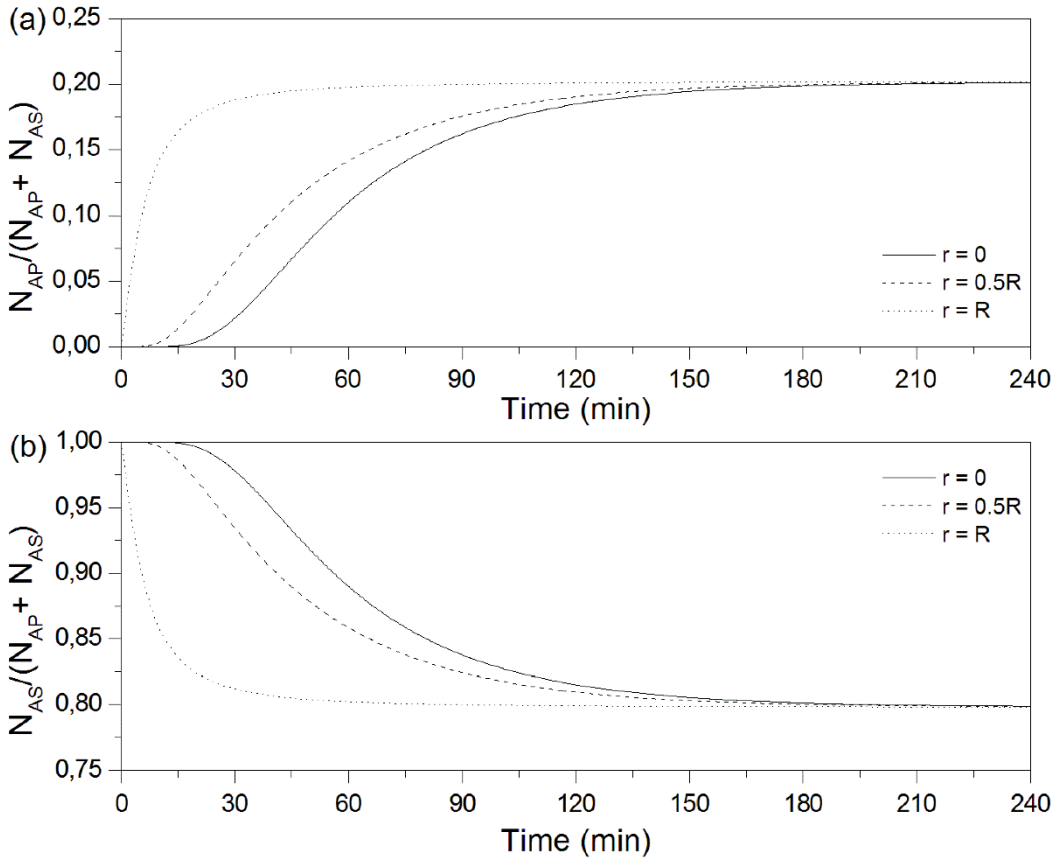

Fig. 6: (a) Contribution of pore volume diffusion and (b) surface diffusion to the intraparticle diffusion at different radial positions for MB dye.

Table 6 exhibits the operating conditions and estimated parameters by PVSDM model for all the concentration decay curves of MB.

Table 6: Experimental conditions and estimated parameters for the concentration decay curves of MB on bentonite, C_{A0} = 100 mg L^{-1}.

Exp	m (g)	C_{Ae} (mg L^{-1})	q_e (mg g^{-1})	$k_F \times 10^3$ (cm s^{-1})	$D_s \times 10^{10}$ (cm^2 s^{-1})	$K \times 10^3$	$D_p \times 10^9$ (cm^2 s^{-1})	Bi
1	0.0500	0.11	98.90	2.00	1.84	14.26	9.95	18.03
2	0.0375	3.15	129.47	2.25	1.86	14.24	9.93	15.29
3	0.0250	30.33	139.33	2.82	1.89	14.18	9.89	17.55
4	0.0125	60.43	155.77	3.11	1.91	14.13	9.86	17.11

4.4. Comparison between CV and MB dyes

Fig. 7 illustrates the adsorption of the CV and MB molecules onto bentonite. It can be observed that MB molecules are larger than CV molecules, being the molecular diameter of MB (14.47 A°) very close to the basal space of bentonite (15.2 A°). Thus, MB molecules have a greater difficulty in penetrating the pores of the adsorbent (hindered diffusion) and, therefore, a higher resistance to the mass transfer processes.

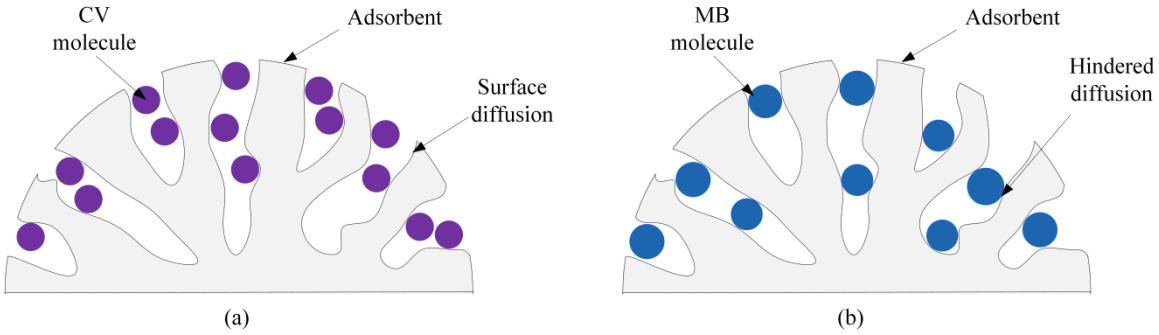

Fig. 7: Illustration of the adsorption process of (a) CV onto bentonite and (b) MB onto bentonite.

The mass transfer parameters for the adsorption of CV and MB onto bentonite at different adsorbent dosages are presented in Tables 4 and 6, respectively. The k_F values ranged from 9.27×10^{-3} to 17.76×10^{-3} cm s^{-1} for CV and from 2.00×10^{-3} to 3.22×10^{-3} cm s^{-1} for MB. It can be observed that the k_F values for CV were higher than the k_F values for MB. It has probably occurred because the MB has molecular size higher than CV, i.e. the MB dye has higher resistance to external mass transfer than the CV dye.

In the analyses of Tables 4 and 6, it can be noticed that values of D_s for CV (6.21×10^{-10} to 7.01×10^{-10} cm^2 s^{-1}) were higher than the values of MB (1.84×10^{-10} to 1.91×10^{-10} cm^2 s^{-1}). This tendency is explained again by the dyes molecular sizes. MB has larger molecule size than CV, thus, its transference within the adsorbent is slower, and thereby, the values of D_s are lower.

The values of D_s in Table 4 and 6 have revealed that D_s increased with q_e. This issue is probably explained due to the initial adsorption of dye molecules on sites, which demanded higher adsorption energy and few of the adsorbed molecules have sufficient energy to be desorbed from a site and diffuse to another adsorption site. After the sites with higher adsorption energy were occupied, the dye molecules were adsorbed on sites with lower adsorption energy and, hence, more dye molecules were desorbed and move from one site to another. This relationship between D_s and q_e can be interpreted with the following equation [23,41–42]:

$$D_s = D_{sq} \exp(-\alpha q_e) \quad (18)$$

The Equation (18) can be linearized and re-written in the following form:

$$\ln D_s = \ln D_{sq} - \alpha q_e \quad (19)$$

The parameters of Equation (19) were estimated by a least–squares method using MatLab® built–in routine *polyfit*, and the values were D_{sq} = 5.96 × 10^{-10} cm² s^{-1} and α = 0.00045 g mg^{-1} for CV and D_{sq} = 1.72 × 10^{-10} cm² s^{-1} and α = 0.0007 g mg^{-1} for MB. The tendency between q_e and D_s is graphed in Fig. 8. The linear relation satisfactorily fitted the experimental data for both dyes.

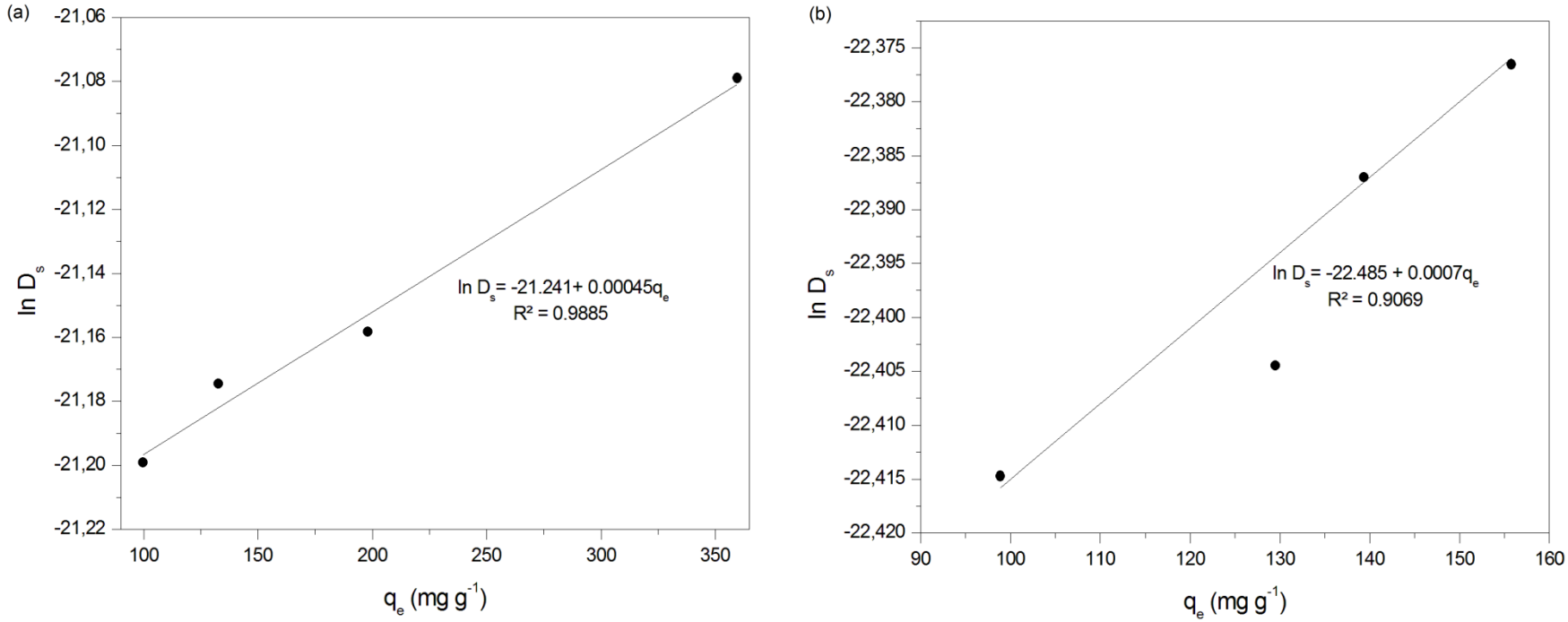

Fig. 8: Effect of the mass of bentonite adsorbed at equilibrium on D_s to (a) CV and (b) MB.

In Table 6 the D_p values ranged from 9.86×10^{-10} to 9.95×10^{-10} cm² s^{-1} for MB dye. These values are in accordance with the values reported in the literature for pore volume diffusion coefficient [20]. It can be remarked that the D_p values of MB were lower than CV (D_p = 5.64×10^{-7} cm² s^{-1}). It has occurred because the MB molecule has a greater resistance to mass transfer within the pore volume, since its molecular size is very close to the basal space of the adsorbent being exposed to the effects of wall drag and steric exclusion. Consequently, the contribution of the diffusion mechanism in the pore volume is higher in MB adsorption than in CV adsorption.

The dimensionless Biot number (*Bi*), which indicates the relative contribution of external mass transfer to intraparticle diffusion, was added in Table 4 and 6 to verify the influence of each mass transfer step on the dye adsorption. The Biot number is defined by the following equation [43].

$$Bi = \frac{k_F d_B C_{A0}}{2\rho_P D_{\text{int}} q_e} \tag{20}$$

According to the literature, a complete dominance of the external mass transfer exists for $Bi < 0.5$, while a considerable dominance of the intraparticle diffusion exists for $Bi > 10$ [43]. The *Bi* values obtained in this work ranged from 12.48 to 24.62 for CV and from 15.29 to 18.03 for MB; confirming that the intraparticle diffusion is the rate limiting step in the adsorption of both dyes onto bentonite.

5. Conclusion

In this work, diffusional mass transfer models were used to represent the adsorption of crystal violet (CV) and methylene blue (MB) dyes onto bentonite under different adsorbent dosages. The hindered diffusion effect was also considered. The equilibrium of the both systems was well represented by the Redlich–Peterson isotherm.

The results have indicated that the surface diffusion was much more important than pore volume diffusion in the adsorption rate of CV onto bentonite, contributing with more than 92.5 % of the total intraparticle diffusion regardless to the position and time. Considering the statistical tests and the graphical analyzes, both PVSDM and SDM models were able to predict

the phenomenon of adsorption of CV onto bentonite, using their respective estimated value of D_s.

In the adsorption of MB onto bentonite, it was necessary to consider the effect of hindered diffusion, which consisted of steric exclusion, drag effects and obstruction due to molecules adsorbed on the pore walls. It has been shown that this extra resistance occurred because the molecular size of the MB dye was very close to the basal space of the adsorbent. Thus, in this case, two parameters were estimated by nonlinear least squares and it was possible to conclude that the PVSDM model was the most adequate to explain the adsorption kinetics of MB onto bentonite. In addition, intraparticle diffusion was shown to be the control mechanism; that the pore volume and the surface diffusion represent, respectively, 20 and 80% of the global intraparticle diffusion.

It was observed that the higher the molecular size of the dyes, the higher the transfer resistance and consequently the lower the values of k_F, D_s and D_p. Therefore, the values of the diffusive parameters were higher for CV than for MB. Finally, the Biot number indicated that both dyes have adsorption limited by intraparticle diffusion.

Acknowledgement

The authors are grateful to Coordination for the Improvement of Higher Education Personnel (CAPES) for granting the scholarship to the first author.

References

[1] F. Güzel, H. Sayğili, G.A. Sayğili, F. Koyuncu, J. Ind. Chem. Eng. 20 (2014) 3375 –3386.

[2] B.C.S. Ferreira, F.S. Teodoro, A.B. Magesteb, L.F. Gil, R.P. Freitas, L.V.A. Gurgel, Ind. Crop.Prod. 65 (2015) 521–534.

[3] A.A. Oladipo, M. Gazi, J. Water Process Eng. 2 (2014) 43–52.

[4] S. Dardouri, J. Sghaier, J. Chem. Eng. (2017). doi.org/10.1016/j.cjche.2017.01.012

[5] A. Bhattacharjee, M. Ahmaruzzaman, T.B. Devi, J. Nath, J. Photoch. Photobio. A. 325 (2016) 116–124.

[6] G. Bayramoglu, B. Altintas, M.Y. Arica, Chem. Eng. J. 152 (2009) 339–346.

[7] D. Bharali, R.C. Deka, Colloid Surface A. 525 (2017) 64–76.

[8] A. Mittal, J. Mittal, A. Malviya, D. Kaur, V.K. Gupta, J. Colloid Interf. Sci. 343 (2010) 463–473.

[9] B. Yang, J. Zuo, X. Tang, F. Liu, X. Yu, X. Tang, H. Jiang, L. Gan, Ultrason. Sonochem. 21 (2014) 1310–1317.

[10] A.R. Khataee, G. Dehghan, A. Ebadi, M. Zarei, M. Pourhassan, Bioresource Technol. 101 (2010) 2252–2258.

[11] Y. Cheng, H. Lin, Z. Chen, M. Megharaj, R. Naidu, Ecotox. Environ. Safe. 83 (2012) 108–114.

[12] M. Angamuthu, G. Satishkumar, M.V. Landau, Micropor. Mesopor. Mat. 251 (2017) 58–68.

[13] G. Ovejero, A. Rodríguez, A. Vallet, J. García, Appl. Catalysis B–Environ. 125 (2012) 166–171.

[14] M. Wawrzkiewicz, M. Wisniewska, A. Wołowicz, V.M. Gun'ko, V.I. Zarko, Micropor. Mesopor. Mat. 250 (2017) 128–147.

[15] S. Arellano–Cárdenas, S. López–Cortez, M. Cornejo–Mazón, J.C, Mares–Gutiérrez, Appl. Surf. Sci. 280 (2013) 74–78.

[16] L. Yan, L. Qin, H. Yu, S. Li, R. Shan, B. Du, J. Mol. Liq. 211 (2015) 1074–1081.

[17] R. Leyva–Ramos, C.J. Geankoplis, Chem. Eng. Sci. 40 (5) (1985) 799–807.

[18] P.R. Souza, G.L. Dotto, N.P.G. Salau, Chem. Eng. Res. Des. 122 (2017) 298–307.

[19] P.R. Souza, G.L. Dotto, N.P.G. Salau, Submitted to J. Env. Chem. Eng. (2017)

[20] R. Leyva–Ramos, R. Ocampo–Perez, J. Mendoza–Barron, Chem. Eng. J. 183 (2012) 141–151.

[21] D.M. Ruthven, Principles of Adsorption and Adsorption Processes, John Wiley & Sons, New York, 1984.

[22] H. Qiu, L.L. Pan, Q.J. Zhang, W. Zhang, Q. Zhang, J. Zhejiang Univ. Sci. A. 10(5) (2009) 716–724.

[23] R. Ocampo–Perez, R. Leyva–Ramos, P. Alonso–Davila, J. Rivera–Utrilla, M. Sanches–Polo, Chem. Eng. J. 165 (2010) 133–141.

[24] I. Medved, R. Cerny, Micropor. Mesopor. Mat. 142 (2011) 405–422.

[25] T. Furusawa, J.M. Smith, Ind. Eng. Chem. Fund. 12 (1973) 197–203.

[26] C.R. Wilke, P. Chang, AIche. J. 1 (1995) 264–268.

[27] C. Valderrama, X. Gamisans, X. Heras, A.M. Farrán, J.L Cortina, J. Hazard. Mater. 157 (2008) 386–396.

[28] T.F. Coleman, Y. Li, SIAM. J. Optimiz. 6 (1996) 418−445.

[29] D. Heier, T. Blackstock, K. Stack, D. Richardson, T. Lewis, Colloid. Surf. A. 482 (2015) 213–221.

[30] M.D. Donohue, G.L. Aranovich, Adv. Colloid and Interfac. 76 (1998) 137–152.

[31] O. Redlich, D.L. Peterson, J. Chem. Phys. 63 (1959) 1024–1027.

[32] M. Schwaab, J.C. Pinto, Experimental Data Analysis I. Fundamentals of Statistics and Parameter Estimation, E−papers, Rio de Janeiro, 2007.

[33] C.N. Satterfield, C.K. Colton, W.H. Pitcher, AIChE J. 19 (1973) 628–635.

[34] R.E. Beck, J.S. Schultz, Biochim. Biophys. Acta. 255 (1972) 273–3003.

[35] J.L. Anderson, J.A. Quinn, Biophys. J. 14 (1974) 130–150.

[36] E.M. Renkin, J. Gen. Physiol. 38 (1954) 225–243.

[37] P.M. Bungay, H. Brenner, Int. J. Multiph. Flow 1 (1973) 25–33.

[38] P. Dechadilok, W.M. Deen, Ind. Eng. Chem. Res. 45 (2006) 6953–6959.

[39] J.J.L. Higdon, G.P. Muldowney, J. Fluid Mech. 298 (1995) 193–210.

[40] G.M. Mavrovouniotis, H. Brenner, J. Colloid Interface Sci. 124 (1988) 269–283.

[41] K.K.H. Choy, J.F. Porter, G. McKay, J. Chem. Technol. Biotechnol. 79 (2004) 1181–1188.

[42] A.H. Mollah, C.W. Robinson, Water Res. 30 (1996) 2907–2913.

[43] D.O. Cooney, Am. Inst. Chem. Eng. J. 39 (1993) 355–358.

6 DISCUSSÃO

Além da discussão de resultados presentes em cada um dos artigos que fazem parte dessa Dissertação, faz-se necessário também uma discussão global, a fim de relacionar os resultados obtidos com os objetivos previamente traçados.

De acordo com a revisão bibliográfica, a forma mais realista de prever a cinética de adsorção é através da utilização de modelos difusivos, uma vez que são baseados em pressupostos fenomenológicos, ou seja, seu desenvolvimento engloba as seguintes etapas consecutivas de transferência de massa: (i) transferência de massa externa, (ii) difusão intrapartícula e (iii) difusão nos sítios ativos. Conforme o mecanismo de difusão intrapartícula, três modelos podem ser propostos. O modelo PVSDM considera que a difusão intrapartícula ocorre devido à difusão superficial e a difusão no volume do poro. Já o modelo SDM considera que a difusão superficial é o único mecanismo na difusão intrapartícula enquanto que o modelo PVDM leva em conta apenas a difusão no volume do poro.

Frente à complexidade dos modelos difusionais, não se encontram na literatura os detalhes da solução numérica dos mesmos. Portanto, foi selecionada a técnica de aproximações por diferenças finitas para resolver o problema numérico.

O primeiro artigo aborda o escopo principal da pesquisa, no qual a solução pelo método de aproximações por diferenças finitas foi detalhado. Primeiramente, a região de interesse foi discretizada de maneira uniforme e constante. As derivadas em relação ao raio da partícula foram aproximadas por expressões algébricas e substituídas nas equações dos modelos. As aproximações de diferença central de segunda ordem para derivada primeira e segunda foram utilizadas no balanço de massa no interior da partícula do adsorvente. Além disso, para as condições de contorno no centro e no limite da partícula foram usados, respectivamente, as aproximações de diferenças progressivas e regressivas de segunda ordem. Após a transformação das equações diferenciais parciais em equações diferenciais ordinárias, um algoritmo em MatLab® foi desenvolvido e implementado. Ainda no primeiro artigo, a adsorção de verde malaquita em bentonita foi estudada através dos modelos difusivos e foi realizada a estimação dos parâmetros difusivos a partir do procedimento de mínimos quadrados não lineares, onde se concluiu que o modelo PVSDM foi o melhor para explicar a cinética de adsorção deste sistema.

O segundo trabalho é um complemento ao primeiro artigo. Em virtude de que no primeiro estudo foi observado um comportamento semelhante em alguns experimentos de

adsorção de verde malaquita e bentonita, um parâmetro global foi determinado por mínimos quadrados não lineares e testes estatísticos foram realizados para avaliar a concordância entre os dados preditos pelo modelo PVSDM e os dados experimentais.

No último trabalho, uma nova abordagem utilizando diferentes corantes foi realizada. A adsorção de cristal violeta e azul de metileno em bentonita foi modelada pelos modelos difusionais de acordo com a técnica desenvolvida no primeiro artigo. Considerando os testes estatísticos utilizados, além da minimização da função objetivo e das análises gráficas, a adsorção de cristal violeta em bentonita foi controlada pelo fenômeno de difusão superficial e a difusão no volume do poro pode ser desprezada. Entretanto, foi observado que os efeitos da difusão superficial e da difusão no volume do poro devem ser considerados na adsorção de azul de metileno em bentonita. Além disso, no caso da adsorção de azul de metileno a difusão impedida no poro precisou ser considerada uma vez que o tamanho molecular do corante foi semelhante ao tamanho do espaço basal do adsorvente.

Com isso, os objetivos propostos foram alcançados satisfatoriamente com relação ao ajuste dos modelos de transferência de massa difusionais e além do avanço relativo ao estudo da cinética de adsorção.

7 CONCLUSÃO

A partir deste estudo foi possível concluir que a técnica de aproximação por diferenças finitas aliada à estimação de parâmetros não lineares é uma ferramenta adequada para a solução numérica dos modelos de transferência de massa difusivo em sistemas de adsorção. Isso foi comprovado a partir dos ajustes satisfatórios da cinética de adsorção de verde malaquita, cristal violeta e azul de metileno em bentonita.

A caracterização da bentonita mostrou que o material possui as características necessárias para um bom adsorvente, isto é, elevada área superficial e presença de cavidades que permitem a adsorção. Além disso, apresenta bom desempenho em adsorver contaminantes catiônicos através da permuta catiônica.

O equilíbrio dos três sistemas de adsorção foi bem representado pela isoterma de Redlich-Peterson, indicando alta afinidade entre as moléculas dos corantes e os sítios acessíveis da bentonita.

Os primeiros dois artigos demonstraram, através de testes estatísticos e análises gráficas, que o modelo PVSDM é capaz de prever a cinética de adsorção do verde malaquita em bentonita para diferentes concentrações iniciais de corante. Os resultados ainda indicaram que a adsorção é controlada simultâneamente pela transferência de massa externa e pela difusão intrapartícula, sendo que nesse último as contribuições dos mecanismos de difusão superficial e de difusão no volume do poro devem ser considerados. Nota-se que para todas as concentrações inferiores a 300 mg L^{-1}, o parâmetro global $D_s = 7{,}73 \times 10^{-10}\ cm^2\ s^{-1}$ consegue prever a cinética de adsorção.

O terceiro artigo investigou a adsorção de cristal violeta e de azul de metileno em bentonita sob diferentes quantidades de adsorvente. Em relação ao cristal violeta, conclui-se que a difusão superficial representa mais que 92,5% do total da difusão intrapartícula, ou seja, a cinética de adsorção é limitada exclusivamente pelo mecanismo de difusão superficial, sendo possível desprezar o efeito da difusão no volume do poro e utilizar o modelo simplifiado SDM.

Já na adsorção de azul de metileno em bentonita foi necessário considerar uma resistência extra, a difusão impedida, isso porque o tamanho molecular do corante era muito próximo ao espaço basal da bentonita, aumentando a resistência dentro do poro. Ao incorporar esse novo parâmetro, os resultados indicaram que o modelo PVSDM é capaz de prever o comportamento cinético do sistema e que a difusão intrapartícula é o mecanismo limitante da adsorção, onde a contribuição da difusão superficial representa 80% e da difusão no volume do poro é igual a 20% do total da difusão intrpartícula.

De modo geral, foi possível concluir que os valores dos parâmetros difusivos são afetados pela concentração inicial de corante e a quantidade de adsorvente empregada. Portanto, quanto maior a concentração inicial de corante maior os valores dos coeficientes k_F e D_s, em contrapartida quanto maior a quantidade de adsorvente menores os valores de k_F e D_s. Além disso, o tamanho da molécula influência nos valores dos parâmetros difusivos, isto é, quanto maior a molécula maior é sua resistência frente à transferência de massa e como consequêcia menores são os valores dos parâmetros estimados.

Esse trabalho se encerra com a certeza de ter alcançado o objetivo de contribuir com o desenvolvimento de pesquisas nas áreas de modelagem de processos de adsorção, uma vez que todos os sistemas utilizados neste trabalho foram modelados e validados com dados experimentais e análises estatísticas e gráficas; sendo os resultados confiáveis para predizer os dados experimentais e, portanto, para descrever o comportamento geral do processo.

Como sugestões para trabalhos futuros, citam-se: (i) a implementação da técnica de aproximações por diferenças finitas para diferentes geometrias de adsorvente; (ii) a avaliação do coeficiente de difusão superficial como função da quantidade de massa adsorvida em cada intervalo de tempo; (iii) a avaliação da taxa global de adsorção considerando a variação no volume (inchamento) do adsorvente.

REFERÊNCIAS BIBLIOGRÁFICAS

ANIRUDHAN, T. S.; RAMACHANDRAN, M. Adsorptive removal of basic dyes from aqueous solutions by surfactant modified bentonite clay (organoclay): Kinetic and competitive adsorption isotherm, **Process Safety and Environmental Protection**, v. 95, p. 215–225, 2015.

BANERJEE, S. et al. Removal of Malachite Green, a hazardous dye from aqueous solutions using Avena sativa (oat) hull as a potential adsorbent, **Journal of Molecular Liquids**, v. 213, p. 162–172, 2016.

BAYRAMOGLU, G.; ALTINTAS, B.; ARICA, M. Y. Adsorption kinetics and thermodynamic parameters of cationic dyes from aqueous solutions by using a new strong cation–exchange resin, **Chemical Engineering Journal**, v. 152, p. 339–346, 2009.

BHATTACHARJEE, A. et al. Photodegradation of methyl violet 6B and methylene blue using tin–oxide nanoparticles (synthesized via a green route), **Journal of Photochemistry and Photobiology A: Chemistry**, v. 325, p. 116–124, 2016.

BLÁZQUEZ, G. et al. Equilibrium biosorption of lead (II) from aqueous solutions by solid waste from olive–oil production. **Chemical Engineering Journal**, v. 160, p. 615–622, 2010.

BORTOLUZZI, B. M. A. **Remoção dos corantes azul de metileno e cristal violeta de solução aquosa utilizando epicarpo (casca) de uva Niágara Rosada (*vitis labrusca*) como adsorvente**. 2015. 79 p. Dissertação (Mestrado em Engenharia) – Universidade Federal do Pampa, Bagé, 2015.

BULUT, E.; ÖZACAR, M., ŞENGIL, I. A. Adsorption of malachite green onto bentonite: Equilibrium and kinetic studies and process design, **Microporous and Mesoporous Materials**, v. 115, p. 234–246, 2008.

COONEY, D. O. Comparison of simple adsorber breakthrough curve method with exact solution, **AIChE Journal**, v. 39, p. 355–358, 1993.

CRINI, G.; BADOT, P.M. Application of chitosan, a natural aminopolysaccharide, for dye removal from aqueous solutions by adsorption processes using batch studies: A review of recent literature. **Progress in Polymer Science**, v. 33, p. 399–447, 2008.

DARDOURI, S.; SGHAIER, J. A comparative study of adsorption and regeneration with different agricultural wastes as adsorbents for the removal of methylene blue from aqueous solution, **Chinese Journal of Chemical Engineering**, Available online 25 April 2017.

DAVIS, M. E. **Numerical methods and modeling for chemical engineers**. New York: Wiley, 1984.

DEMIRBAS, A. Agricultural based activated carbons for the removal of dyes from aqueous solutions: A review, **Journal of Hazardous Materials**, v. 167, p. 1–9, 2009.

DONOHUE, M. D.; ARANOVICH, G. L. Classification of Gibbs adsorption isotherms. **Advances in Colloid and Interface Science**, v. 76, p. 137–152, 1998.

DOTTO, G. L. et al. Remoção dos Corantes Azul brilhante, Amarelo Crepúsculo e Amarelo Tartrazina de Soluções Aquosas Utilizando Carvão Ativado, Terra Ativada, Terra Diatomácea, Quitina e Quitosana: Estudos de Equilíbrio e Termodinâmica. **Química Nova**, v. 34, p. 1193–1199, 2011.

DOTTO, G. L. et al. Surface modification of chitin using ultrasound–assisted and supercritical CO2 technologies for cobalt adsorption, **Journal of Hazardous Materials**, v. 295, p. 29–36, 2015.

EDGAR, T. F.; HIMMELBLAU, D. M. **Optimization of chemical processes**. New York: McGraw–Hill, 1989.

EL QADA, E. N.; ALLEN, S. J.; WALKER, G. M. Adsorption of basic dyes from aqueous solutions onto activated carbon, **Chemical Engineering Journal**, v. 135, p. 174–184, 2008.

FERREIRA, B. C. S. et al. Application of a new carboxylate–functionalized sugarcane bagasse for adsorptive removal of crystal violet from aqueous solution: Kinetic, equilibrium and thermodynamic studies, **Industrial Crops and Products**, v. 65, p. 521–534, 2015.

FREUNDLICH, H. Over the adsorption in solution. **Journal Physical Chemistry**, v. 57, p. 385–470, 1906.

GHASEMI, M. et al., Microwave–assisted synthesis of tetraethylenepentamine functionalizes active carbon with high adsorption capacity for Malachite green dye, **Journal of Molecular Liquids**, v. 213, p. 317–325, 2016.

GRASEGGER, G. et al. A solution method for autonomous first–order algebraic partial differential equations, **Journal of Computational and Applied Mathematics**, v. 300, p. 119–133, 2016.

GUPTA, V.K.; SUHAS. Application of low–cost adsorbents for dye removal: A review, **Journal of Environmental Management**, v. 90, p. 2313–2342, 2009.

GÜZEL, F. et al. Decolorisation of aqueous crystal violet solution by a new nanoporous carbon: Equilibrium and kinetic approach, **Journal of Industrial and Engineering Chemistry**, v. 20, p. 3375–3386, 2014.

HO, Y. S.; MCKAY, G. Kinetic models for the sorption of dye from aqueous solution by wood. **Process Safety Environmental Protection**, v. 76, p. 183–191, 1998.

JAURIS, I. M. et al. Adsorption of acridine orange and methylene blue synthetic dyes and anthracene on single wall carbon nanotubes: A first principle approach, **Computational and Theoretical Chemistry**, v. 1076, p. 42–50, 2016.

LAGERGREN, S. About the theory of so–called adsorption of soluble substances**. Kungliga Svenska Vetenskapsakademiens Handlingar**, v. 24, p. 1–39, 1898.

LANGMUIR, I. The adsorption of gases on plane surfaces of glass, mica and platinum. **Journal of the American Chemical Society**, v. 40, p. 1361–1403, 1918.

LEYVA–RAMOS, R.; GEANKOPLIS, C. J. Model simulation and analysis of surface diffusion of liquids in porous solids, **Chemical Engineering Journal**, v. 40, p. 799–807, 1985.

LIN, K. A.; LEE, W. Highly efficient removal of Malachite green from water by magnetic reduced grapheme oxide/zeolitic imidazolate framework self–assembled nanocomposite, **Applied Surface Science**, v. 36, p. 114–121, 2016.

MAKHOUKHI, B.; DJAB, M.; DIDI, M. A. Adsorption of Telon dyes onto bis–imidazolium modified bentonite in aqueous solutions, **Journal of Environmental Chemical Engineering**, v. 3, p. 1384–1392, 2015.

MCCABE, W. L.; SMITH, J. C.; HARRIOT, P. **Unit Operations of Chemical Engeneering**. 4ª ed., New York: McGraw–Hill, 1985.

MELO, K. J. M.; Aplicação do método das diferenças finitas explícito na solução da equação do calor para o caso transiente e unidimensional. 2011. 46 p. Monografia (Graduação em Ciência e Tecnologia) – Universidade Federal Rural Do Semi–Árido, Angicos, 2011.

MITTAL, A. et al. Adsorption of hazardous dye crystal violet from waste water by waste materials, **Journal of Colloid Interface Science**, v. 343, p.463–473, 2010.

OCAMPO–PEREZ, R. et al. Modeling adsorption rate of pyridine onto granular activated carbon, **Chemical Engineering Journal**, v. 165, p. 133–141, 2010.

PAVAN, F. A. et al. Formosa papaya seed powder (FPSP): Preparation, characterization and application as an alternative adsorbent for the removal of crystal violet from aqueous phase, **Journal of Environmental Chemical Engineering**, v. 2, p. 230–238, 2014.

QIU, H. et al. Critical review in adsorption kinetic models, **Journal of Zhejiang University Science A**, v. 10, p. 716–724, 2009.

REDLICH, O.; PETERSON, D. L. A useful adsorption isotherm, **Journal of Chemical Physics**, v. 63, p. 1024–1027, 1959.

RUTHVEN, D. M. **Principles of Adsorption and Adsorption Processes**. John Wiley & Sons. New York, 1984.

SABNA, V.; THAMPI, S. G.; CHANDRAKARAN, S. Adsorption of crystal violet onto functionalized multi–walled carbon nanotubes: Equilibrium and kinetic studies, **Ecotoxicology and Environmental Safety**, v. 134, p. 390–397, 2016.

SCHIESSER, W.E. **The numerical method of lines: integration of partial differential equations**. San Diego: Academic Press, 1991.

SCHWAAB, M. **Desenvolvimento e implementação de novas técnicas de estimação de parâmetros e planejamento seqüencial de experimentos**. 2007. 182 p. Tese (Doutorado em Engenharia Química) – Universidade Federal do Rio de Janeiro, Rio de Janeiro, 2007.

SCHWAAB, M.; PINTO, J. C. **Análise de dados experimentais I: Fundamentos de estatística e estimação de parâmetros**, Rio de Janeiro: E−papers, 2007.

SRINIVASAN, A.; VIRARAGHAVAN, T. Decolorization of dye wastewaters by biosorbents: A review, **Journal of Environmental Management**, v. 91, p. 1915–1929, 2010.

SRIVASTAVA, S.; SINHA, R.; ROY, D. Toxicological effects of malachite green, **Aquatic Toxicology**, v. 66, p. 319–329, 2004.

SUZUKI, M. **Adsorption Engineering**, Tokyo: Kodansha, 1990.

YAN, L. et al. Adsorption of acid dyes from aqueous solution by CTMAB modified bentonite: Kinetic and isotherm modeling, **Journal of Molecular Liquids**, v. 211, p. 1074–1081, 2015.

YANG, P. et al. Screening of freshwater fungi for decolorizing multiple synthetic dyes, **Brazilian Journal of Microbiology**, 2016.

ANEXO A – APROXIMAÇÃO DE PRIMEIRA ORDEM POR DIFERENÇAS FINITAS

Diferença	**Aproximação**
Diferença progressiva para derivada de 1ª ordem	$\frac{df(x_i)}{dx} = \frac{f(x_{i+1}) - f(x_i)}{h}$
Diferença progressiva para derivada de 2ª ordem	$\frac{d^2 f(x_i)}{dx^2} = \frac{f(x_i) - 2f(x_{i+1}) + f(x_{i+2})}{h^2}$
Diferença regressiva para derivada de 1ª ordem	$\frac{df(x_i)}{dx} = \frac{f(x_i) - f(x_{i-1})}{h}$
Diferença regressiva para derivada de 2ª ordem	$\frac{d^2 f(x_i)}{dx^2} = \frac{f(x_i) - 2f(x_{i-1}) + f(x_{i-2})}{h^2}$

Fonte: SCHIESSER, 1991.

ANEXO B – APROXIMAÇÃO DE SEGUNDA ORDEM POR DIFERENÇAS FINITAS

Diferença	**Aproximação**
Diferença progressiva para derivada de 1ª ordem	$\frac{df(x_i)}{dx} = \frac{-3f(x_i)+4f(x_{i+1})-f(x_{i+2})}{2h}$
Diferença progressiva para derivada de 2ª ordem	$\frac{d^2f(x_i)}{dx^2} = \frac{2f(x_i)-5f(x_{i+1})+4f(x_{i+2})-f(x_{i+3})}{h^2}$
Diferença central para derivada de 1ª ordem	$\frac{df(x_i)}{dx} = \frac{f(x_{i+1})-f(x_{i-1})}{2h}$
Diferença central para derivada de 2ª ordem	$\frac{d^2f(x_i)}{dx^2} = \frac{f(x_{i+1})-2f(x_i)+f(x_{i-1})}{h^2}$
Diferença regressiva para derivada de 1ª ordem	$\frac{df(x_i)}{dx} = \frac{3f(x_i)-4f(x_{i-1})+f(x_{i-2})}{2h}$
Diferença regressiva para derivada de 2ª ordem	$\frac{d^2f(x_i)}{dx^2} = \frac{2f(x_i)-5f(x_{i-1})+4f(x_{i-2})-f(x_{i-3})}{h^2}$

Fonte: SCHIESSER, 1991.